SUPPORTING INFORMATION FOR

Reactivity of Rhodium(I) complexes bearing nitrogen containing ligands toward CH_3I: Synthesis and full characterization of neutral *cis*-[Rh(X)(CO)$_2$(L)] and acetyl [RhI(μ-I)(COMe)(CO)(L)]$_2$ complexes; Kinetic studies

Romain J. Adcock, Duc Hanh Nguyen*, Sonia Ladeira, Carole Le Berre, Philippe Serp and Philippe Kalck*

Laboratoire de Chimie de Coordination UPR CNRS 8241, composante ENSIACET, Université de Toulouse UPS-INP-LCC 4 allée Emile Monso BP 44362, 31030 Toulouse Cedex 4, France,

Corresponding authors:duc.nguyen@ensiacet.fr ; Philippe.Kalck@ensiacet.fr

S.I-1: FT-IR SPECTRA OF 3 AND 4 IN CH_2Cl_2

Figure 1. FT-IR spectrum of **3a** at 298 K in CH_2Cl_2.

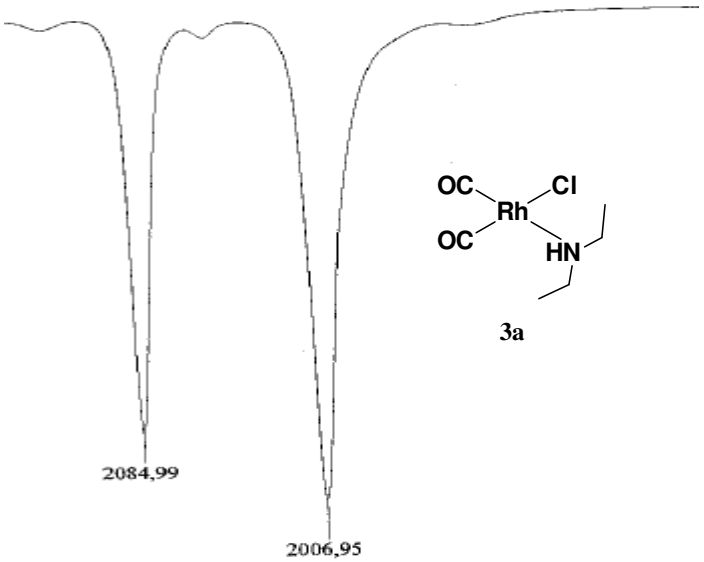

Figure 2. FT-IR spectrum of **3b** at 298 K in CH_2Cl_2.

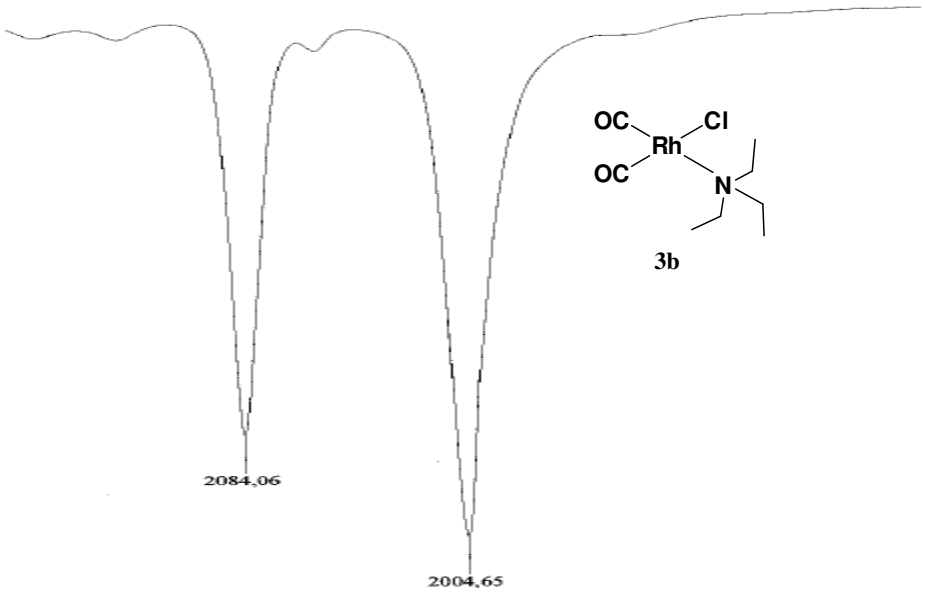

Figure 3. FT-IR spectrum of **3d** at 298 K in CH_2Cl_2.

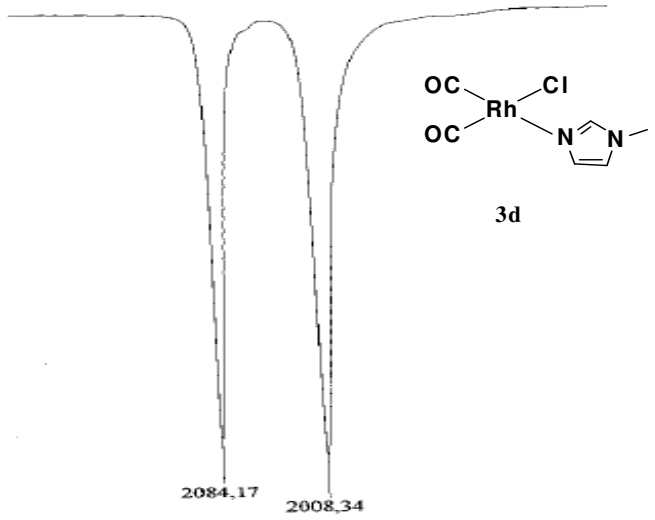

Figure 4. FT-IR spectrum of **3e** at 298 K in CH_2Cl_2.

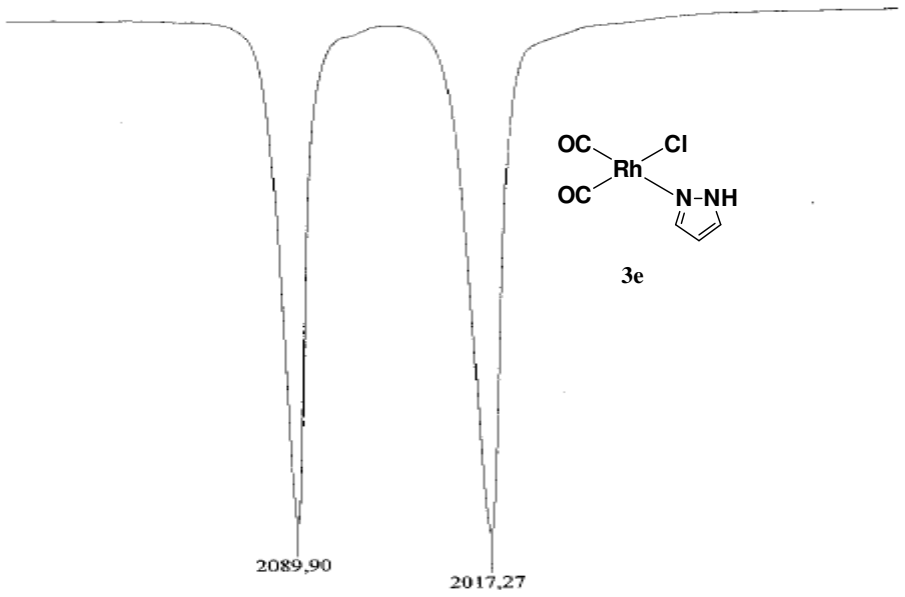

Figure 5. FT-IR spectrum of **3f** at 298 K in CH_2Cl_2.

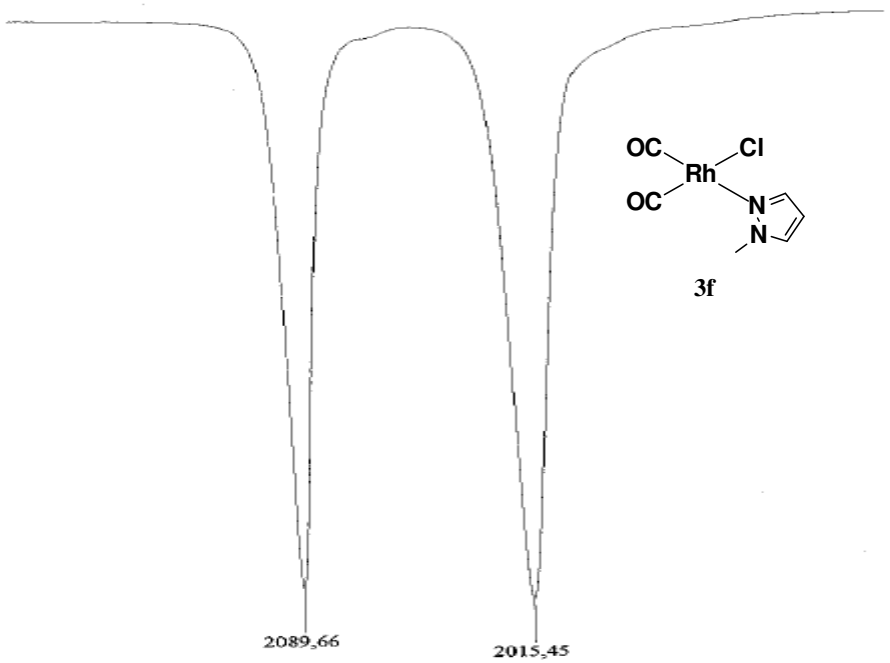

Figure 6. FT-IR spectrum of **4a** at 298 K in CH_2Cl_2.

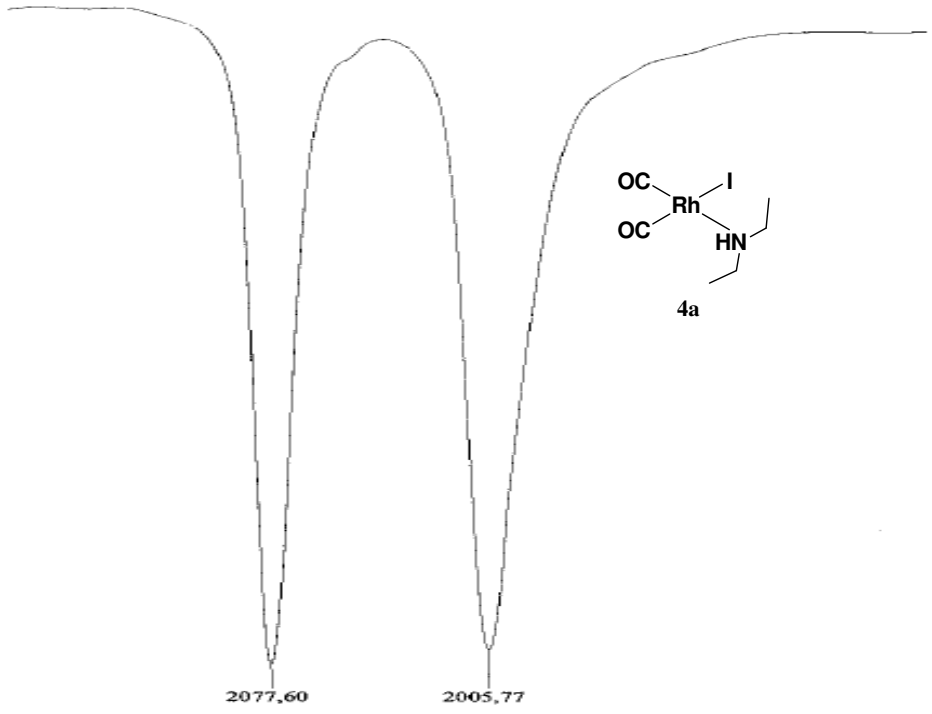

Figure 7. FT-IR spectrum of **4b** at 298 K in CH_2Cl_2.

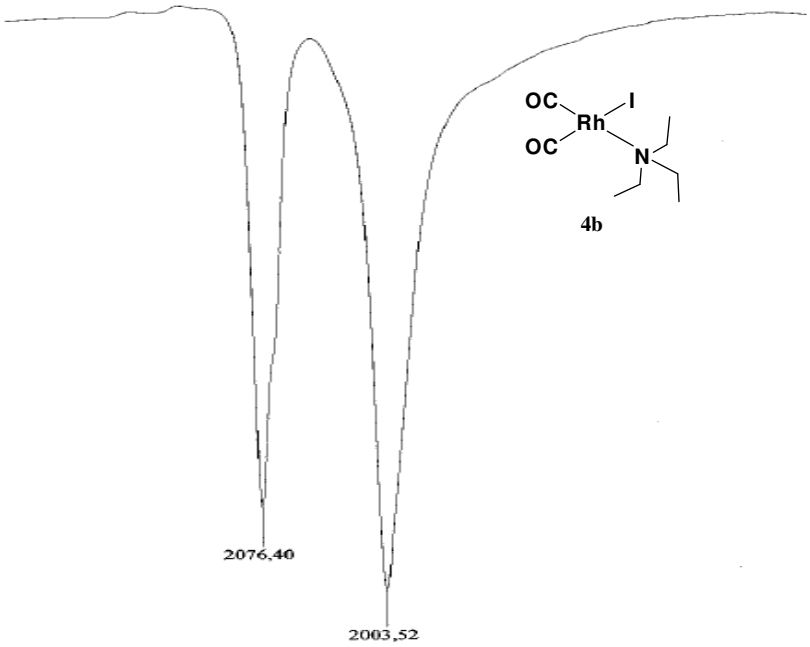

Figure 8. FT-IR spectrum of **4c** at 298 K in CH_2Cl_2.

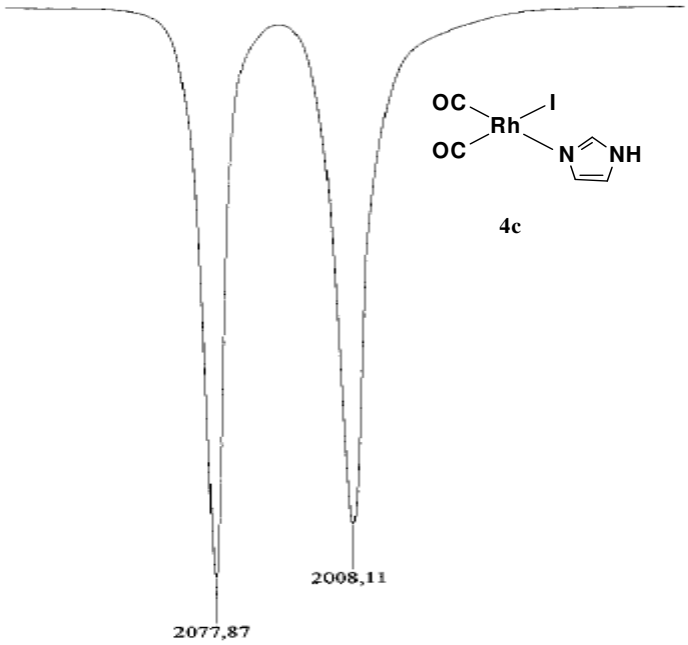

Figure 9. FT-IR spectrum of **4d** at 298 K in CH_2Cl_2.

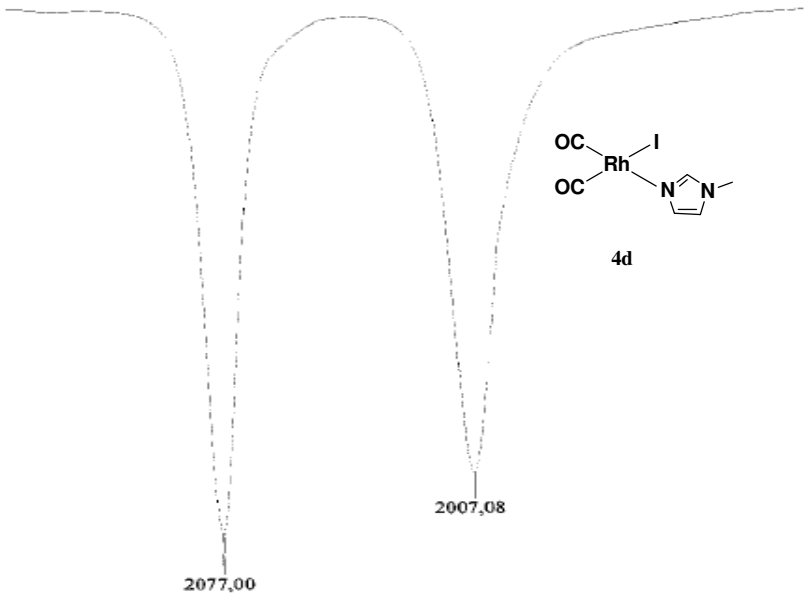

Figure 10. FT-IR spectrum of **4e** at 298 K in CH_2Cl_2.

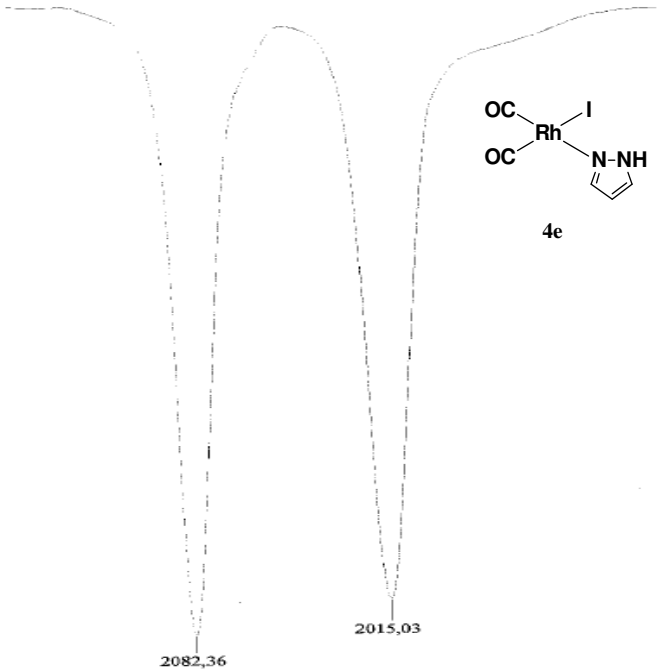

Figure 11. FT-IR spectrum of **4f** at 298 K in CH_2Cl_2.

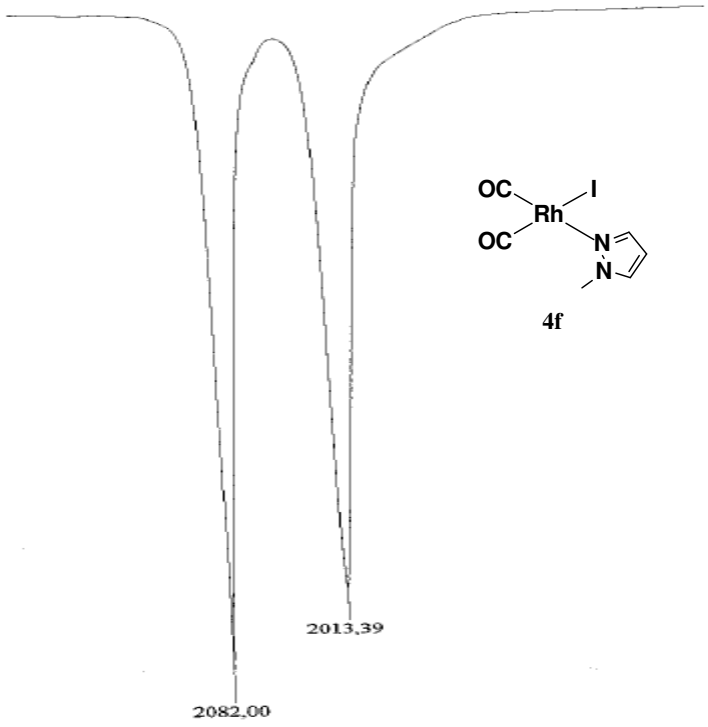

Figure 12. FT-IR spectrum of **4g** at 298 K in CH_2Cl_2.

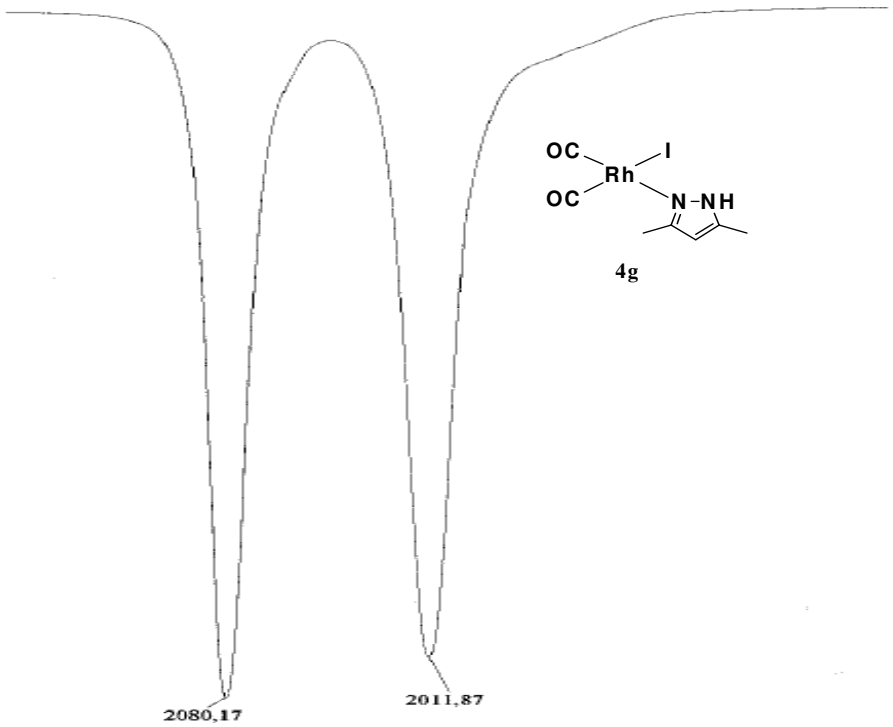

Figure 13. FT-IR spectrum of **4h** at 298 K in CH_2Cl_2.

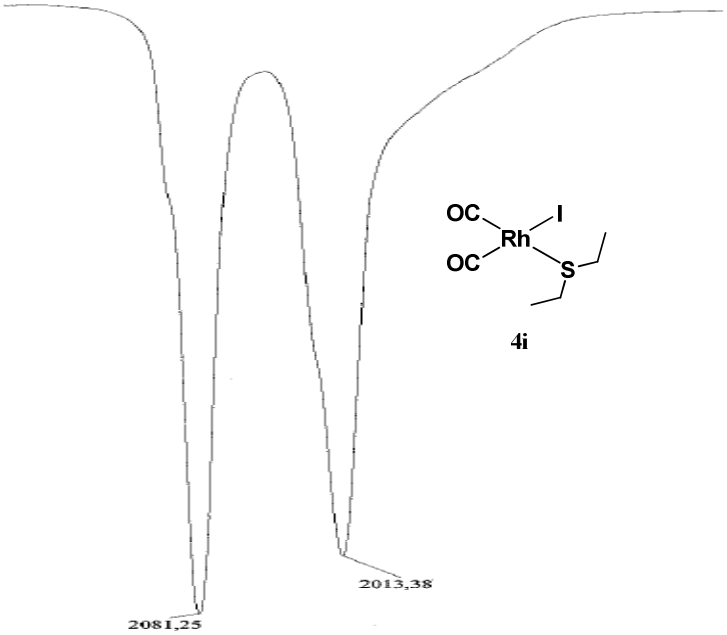

S.I-2: FT-IR SPECTRA OF 6 IN CH_2Cl_2

Figure 1. FT-IR spectrum of **5** at 298 K in CH_2Cl_2. (Poor solubility in CH_2Cl_2).

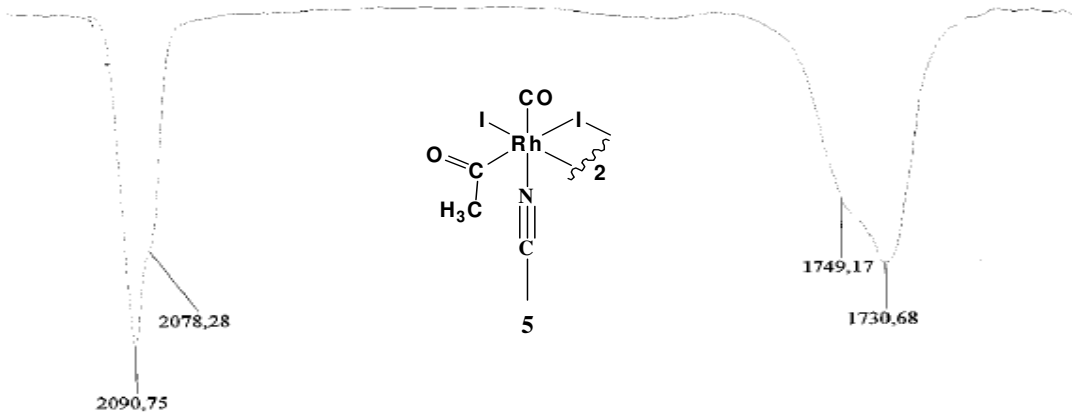

Figure 2. FT-IR spectrum of **6a** at 298 K in CH_2Cl_2.

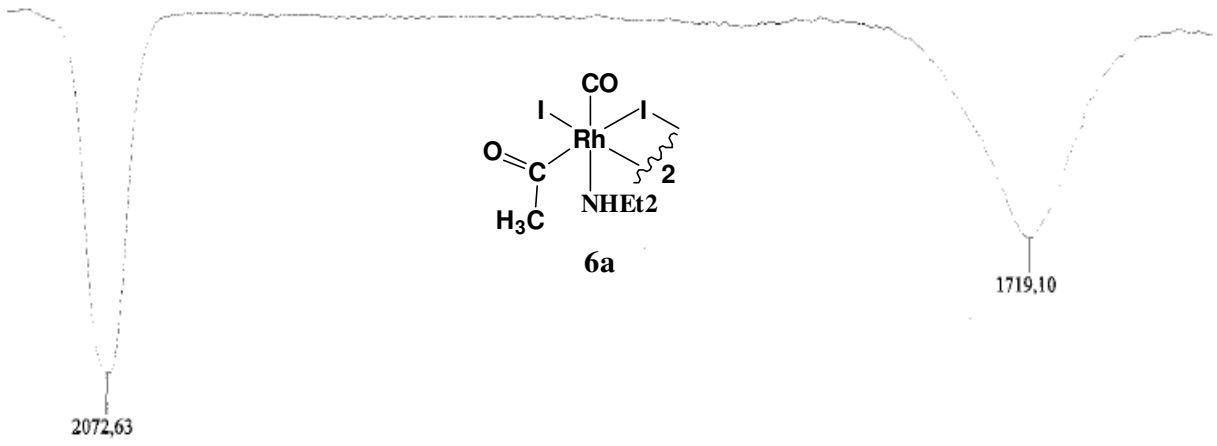

Figure 3. FT-IR spectrum of **6a** at 298 K in CH_3I.

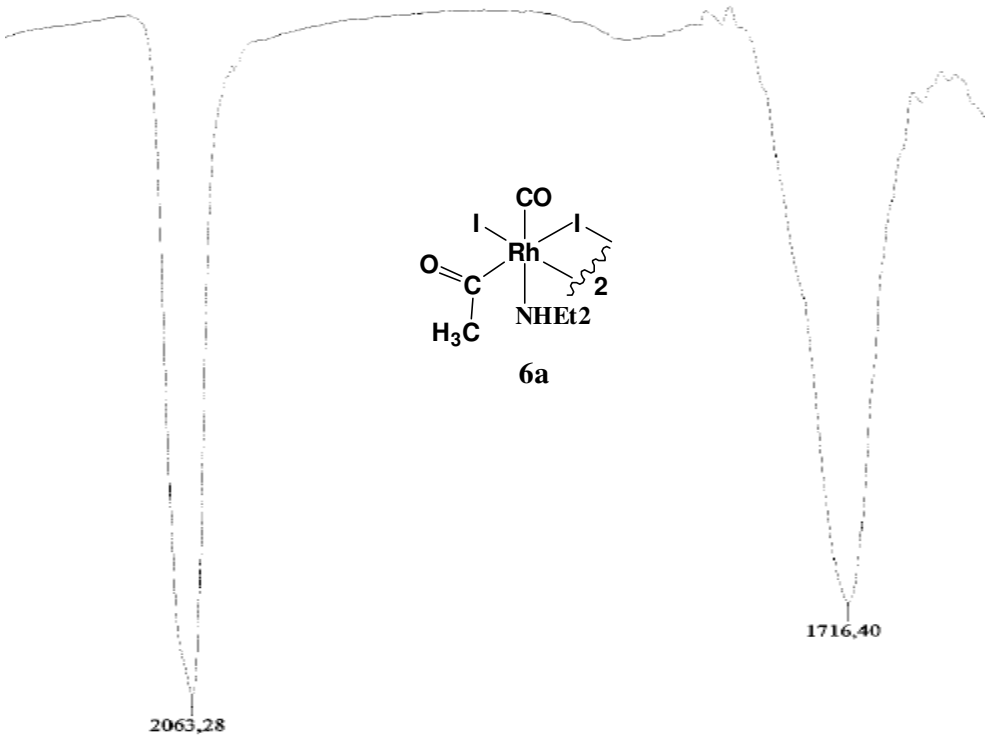

Figure 4. FT-IR spectrum of **6c** at 298 K in CH_2Cl_2.

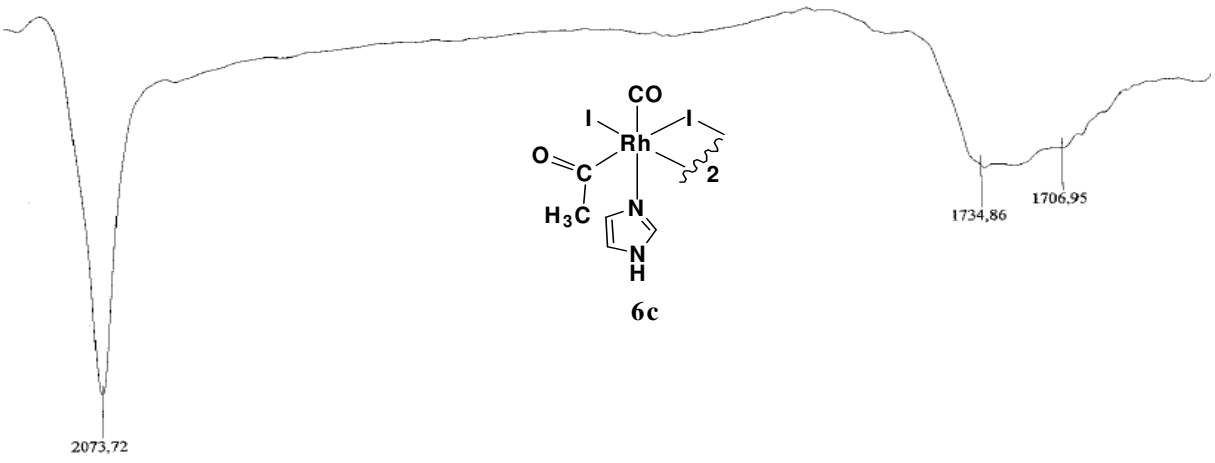

Figure 5. FT-IR spectrum of **6c** at 298 K in CH_3I.

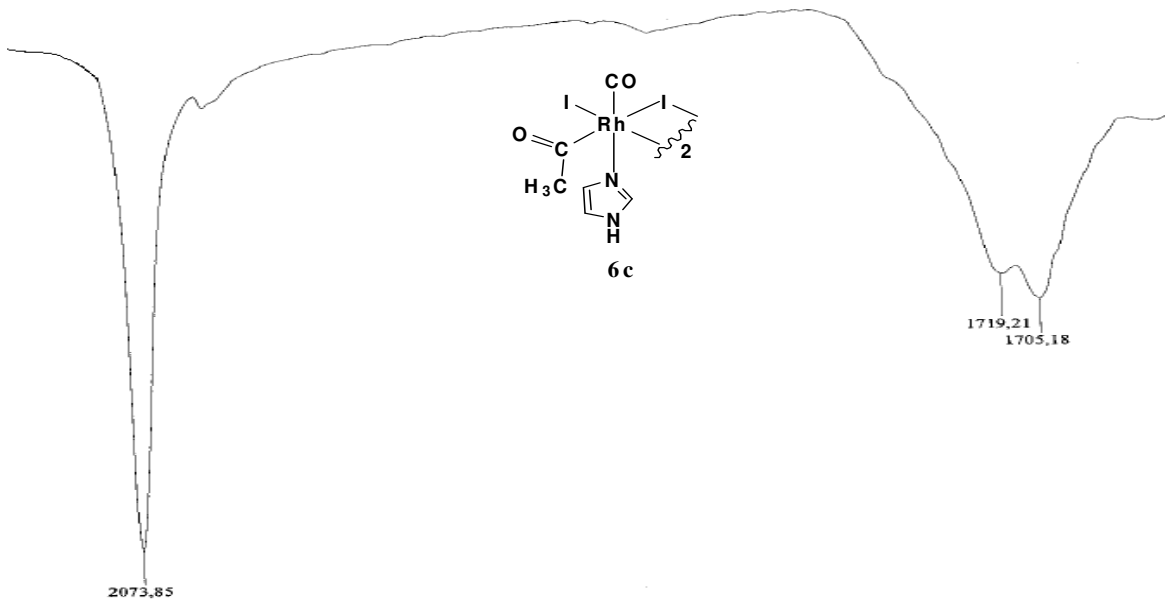

Figure 6. FT-IR spectrum of **6d** at 298 K in CH_2Cl_2.

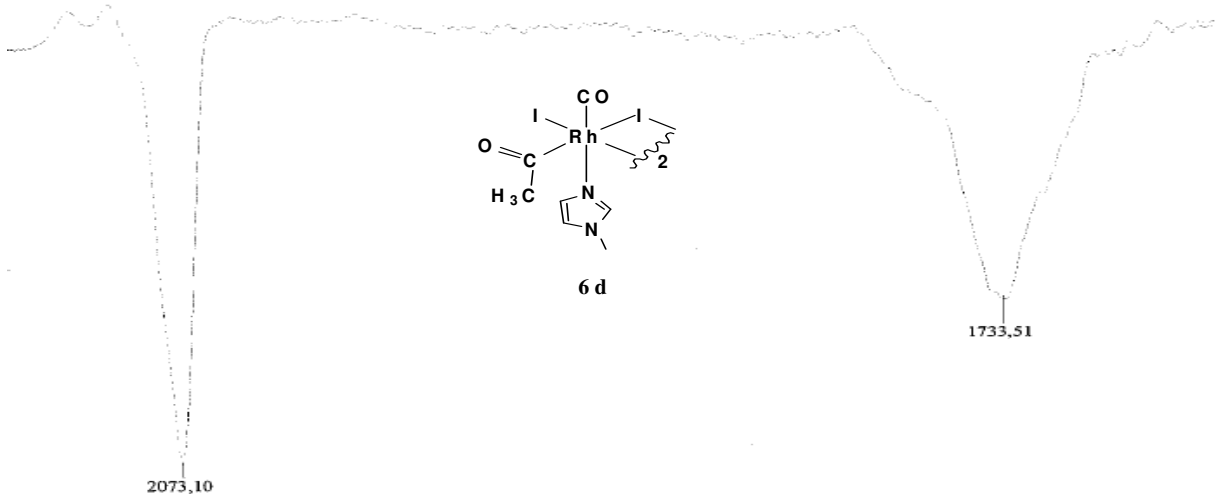

Figure 7. FT-IR spectrum of **6d** at 298 K in CH_3I.

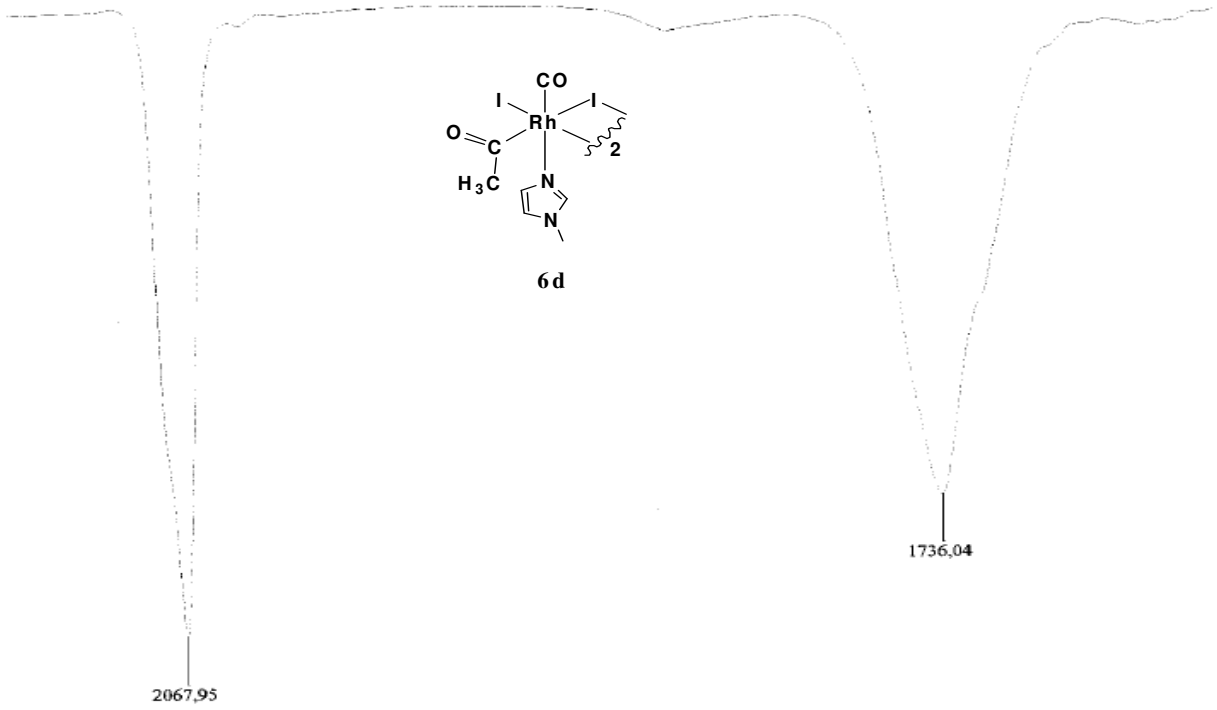

Figure 8. FT-IR spectrum of **6e** at 298 K in CH_2Cl_2.

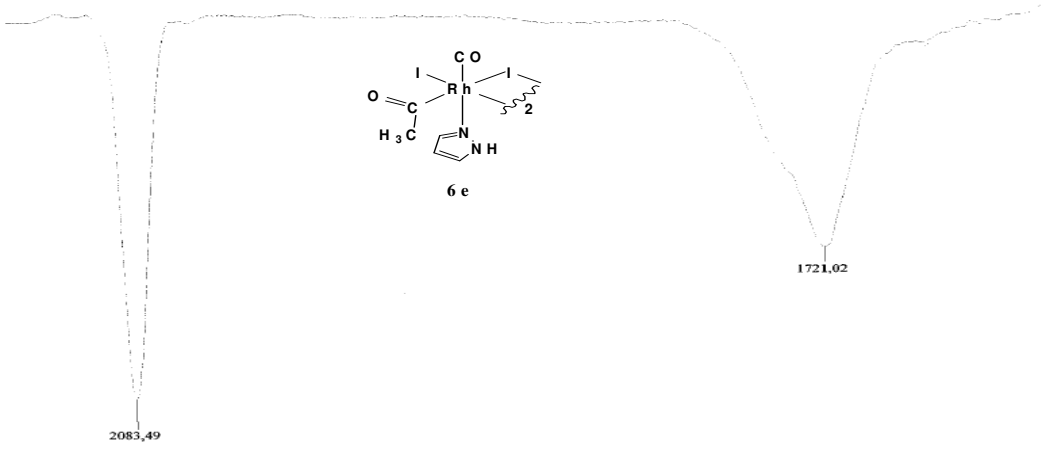

Figure 9. FT-IR spectrum of **6e** at 298 K in CH_3I.

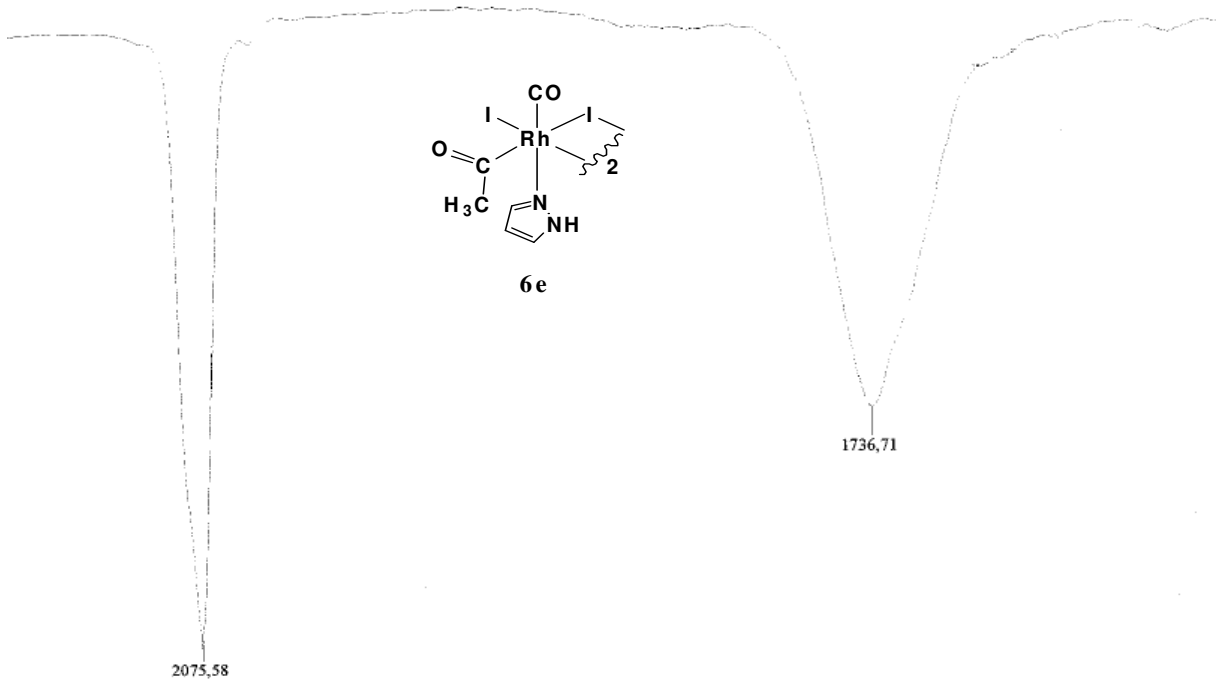

Figure 10. FT-IR spectrum of **6f** at 298 K in CH_2Cl_2.

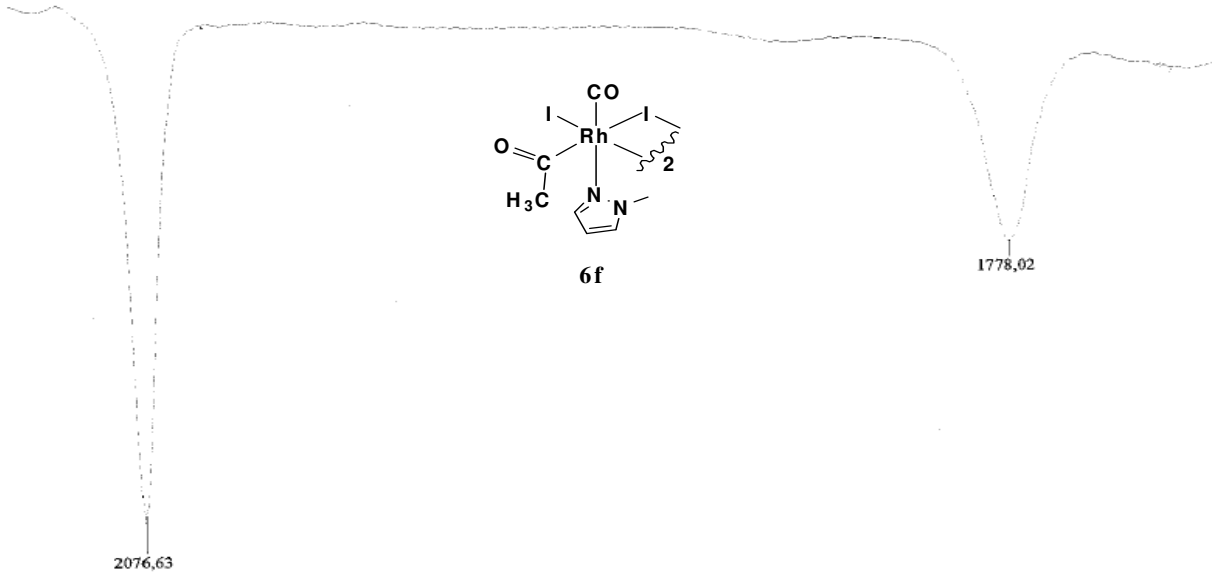

Figure 11. FT-IR spectrum of **6f** at 298 K in CH_3I.

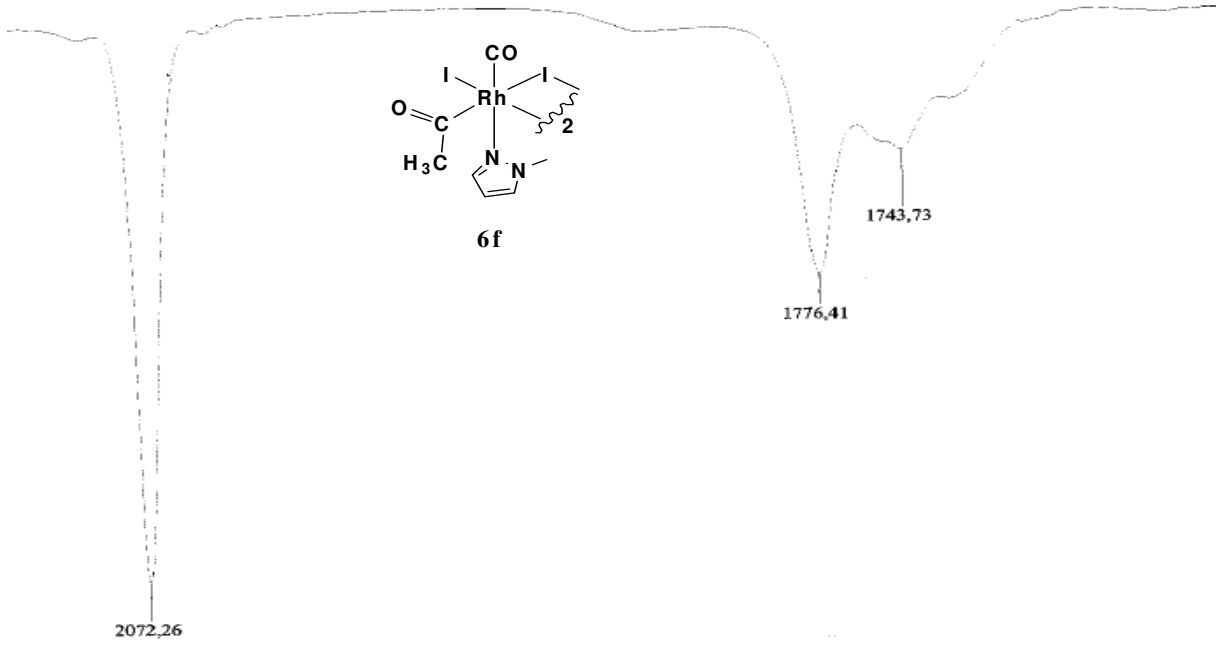

Figure 12. FT-IR spectrum of **6g** at 298 K in CH_2Cl_2.

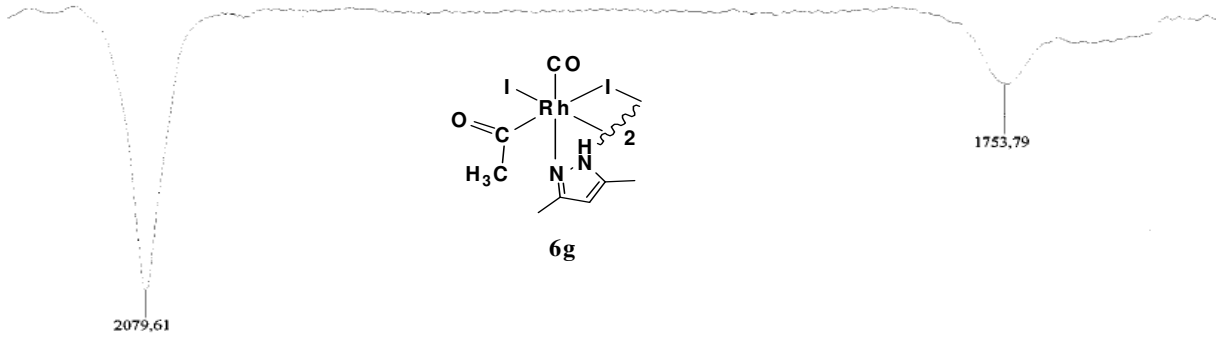

Figure 13. FT-IR spectrum of **6g** at 298 K in CH_3I.

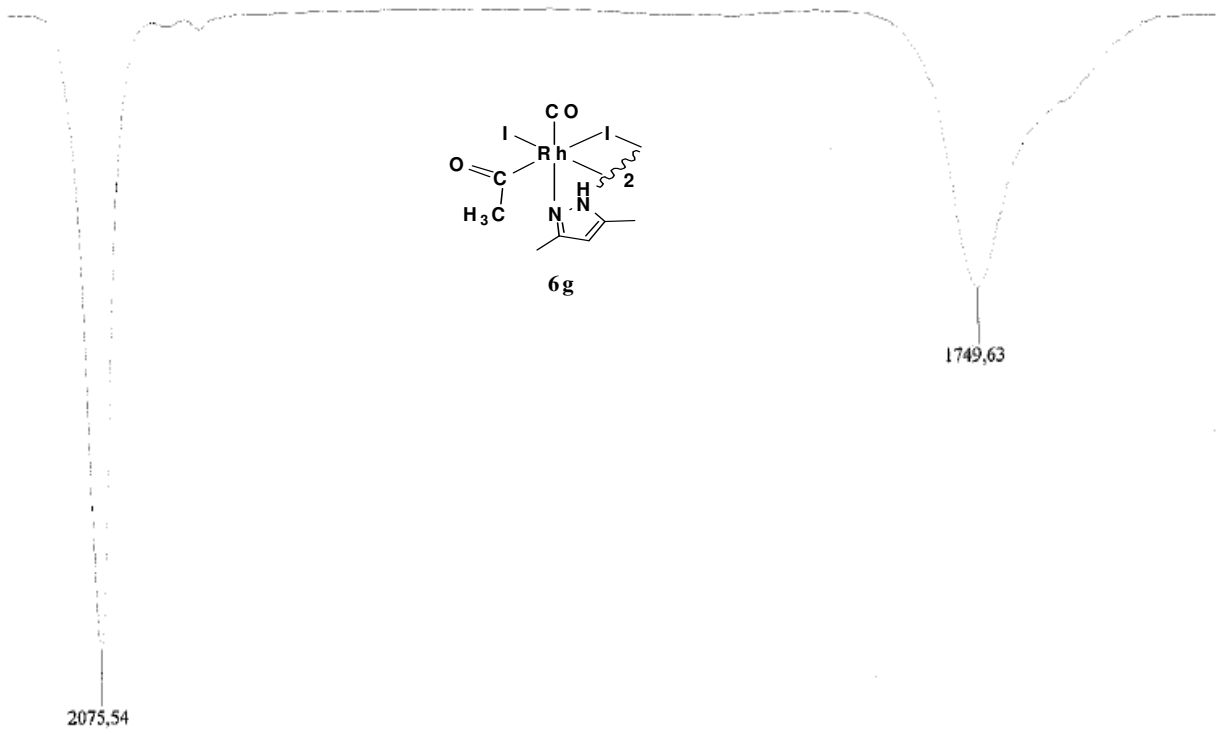

Figure 14. FT-IR spectrum of **7d** at 298 K in CH_2Cl_2.

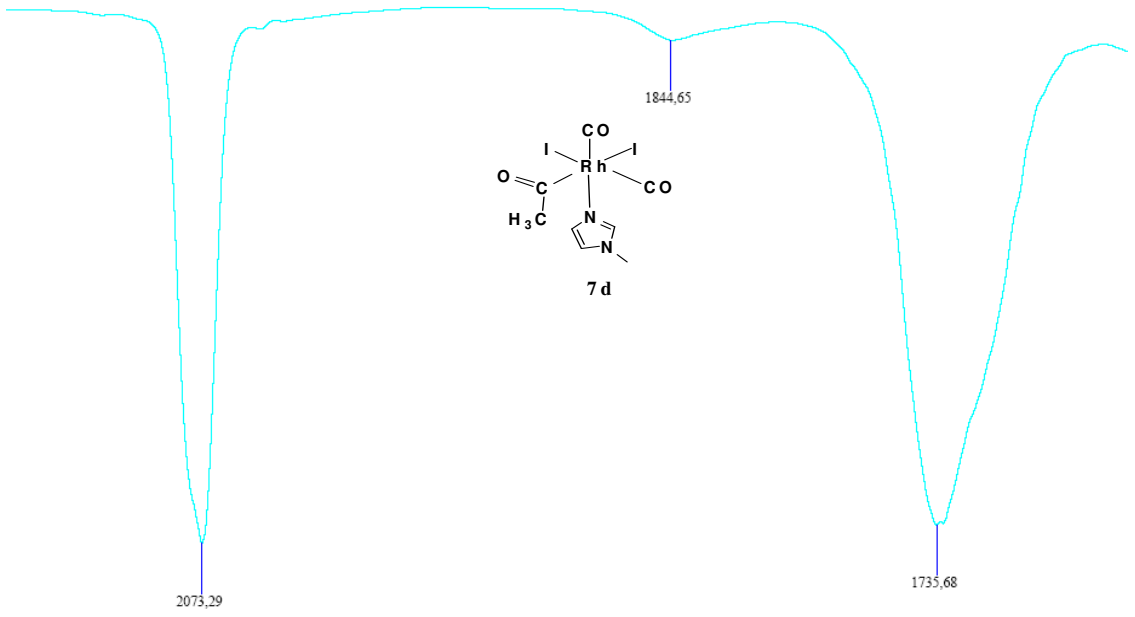

Figure 15. FT-IR spectrum of **8e** at 298 K in CH_2Cl_2.

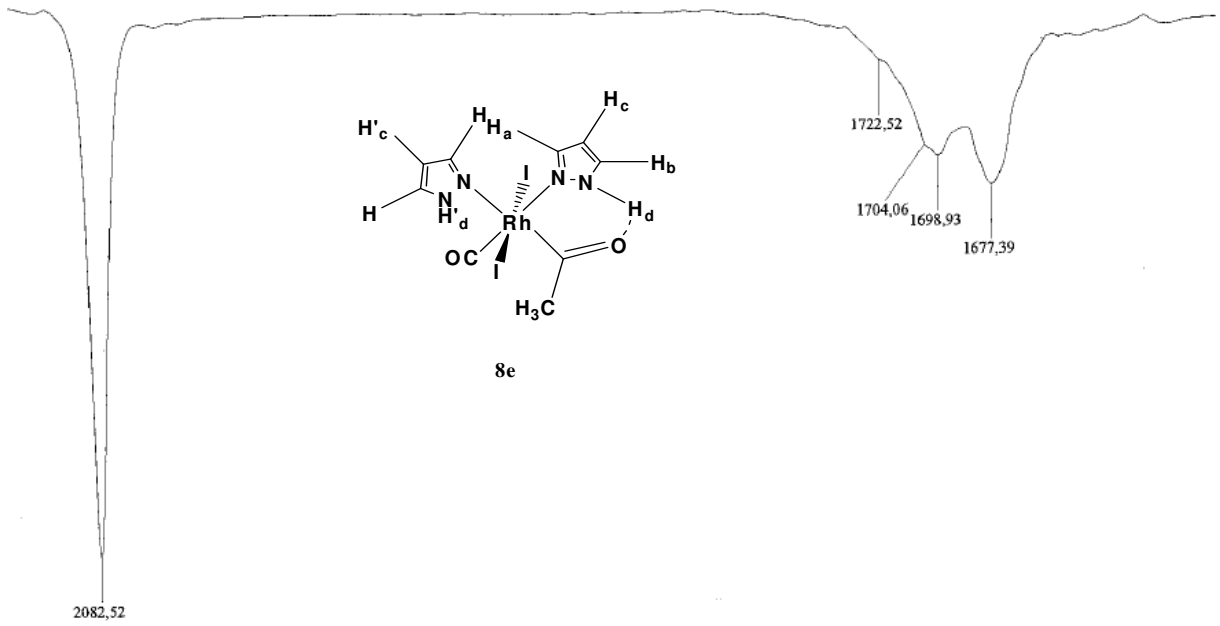

S.I-3: ATR-IR SPECTRA

ATR-IR Figure 1. Spectrum of **3a** at 298 K.

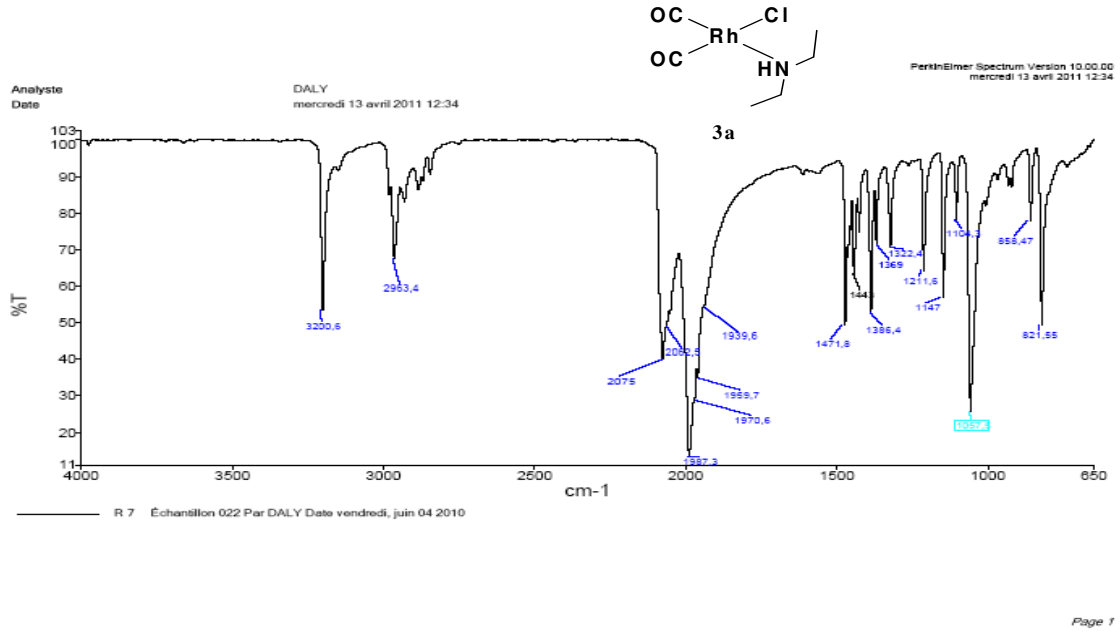

ATR-IR Figure 2. Spectrum of **3d** at 298 K.

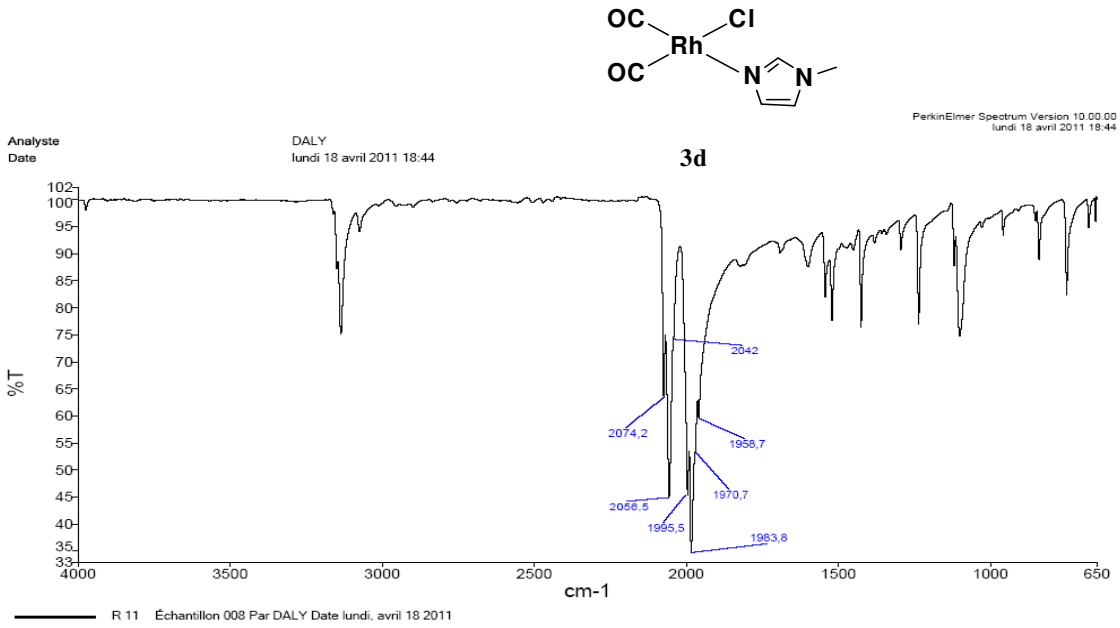

ATR-IR Figure 3. Spectrum of **3e** at 298 K.

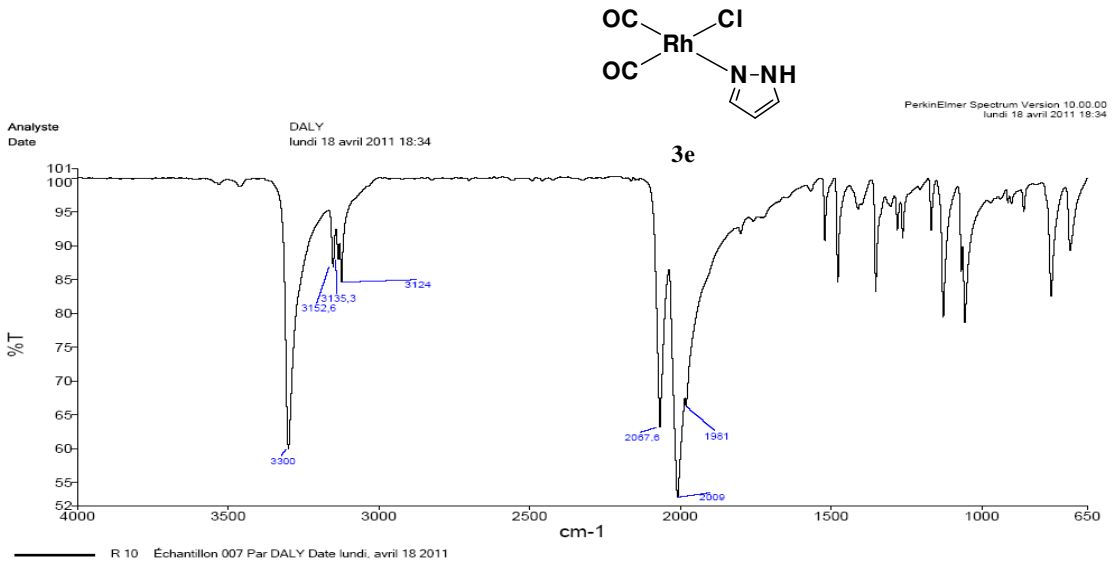

ATR-IR Figure 4. Spectrum of **3f** at 298 K.

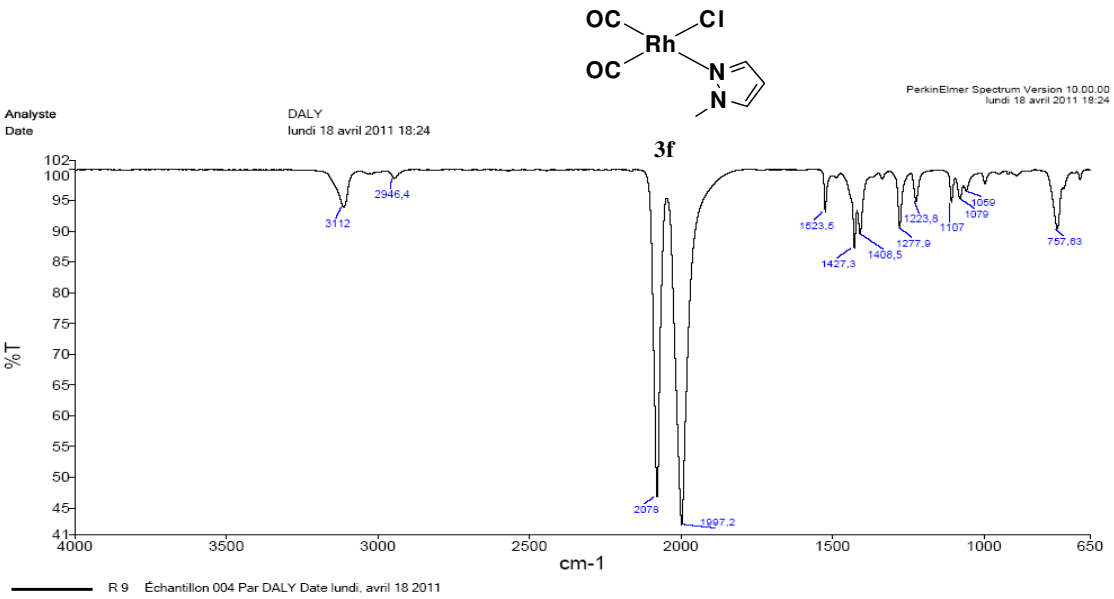

ATR-IR Figure 5. Spectrum of **4a** at 298 K.

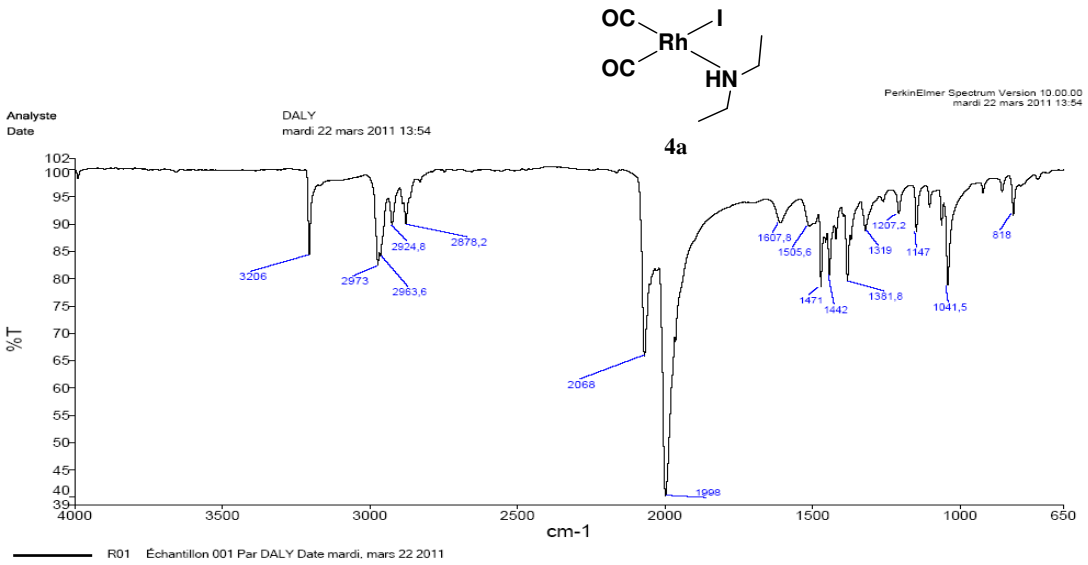

ATR-IR Figure 6. Spectrum of **4c** at 298 K.

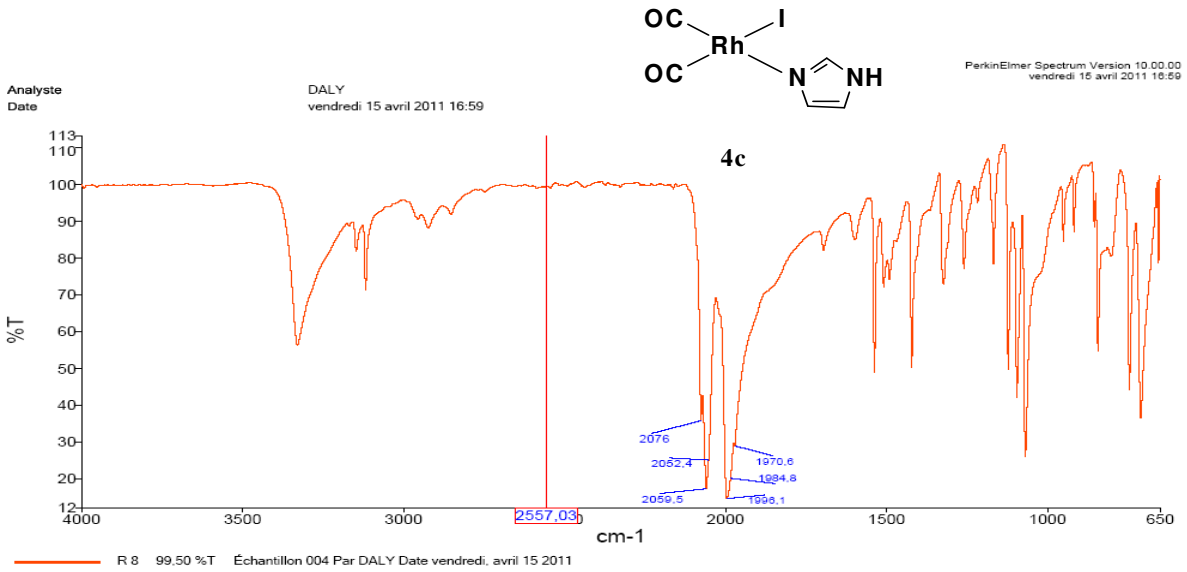

ATR-IR Figure 7. Spectrum of **4d** at 298 K.

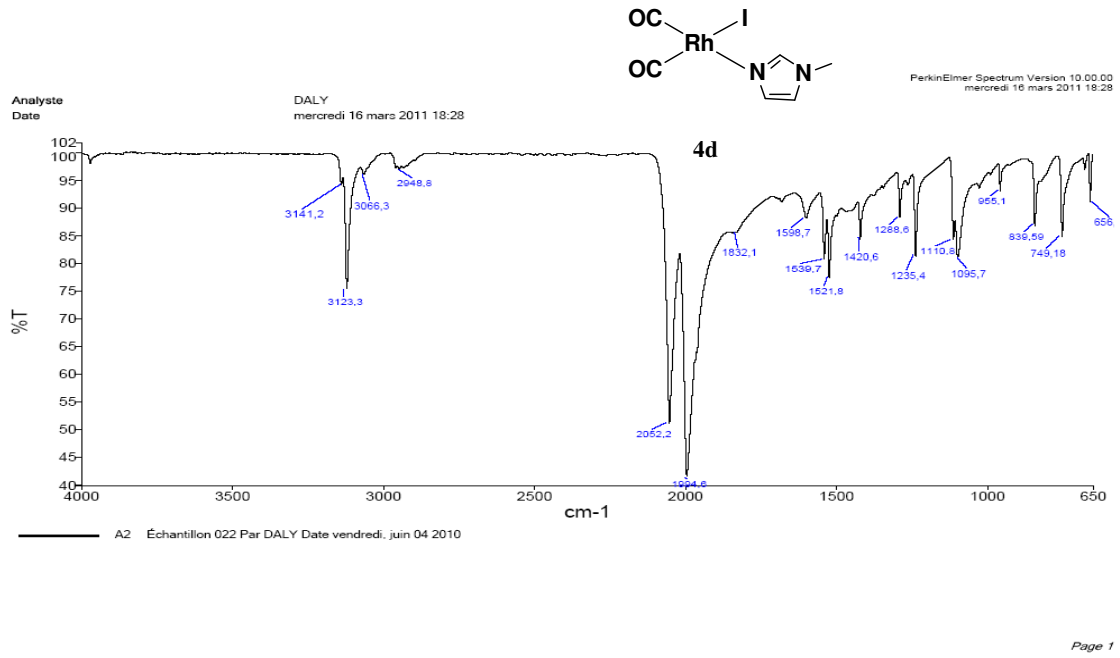

ATR-IR Figure 8. Spectrum of **4e** at 298 K.

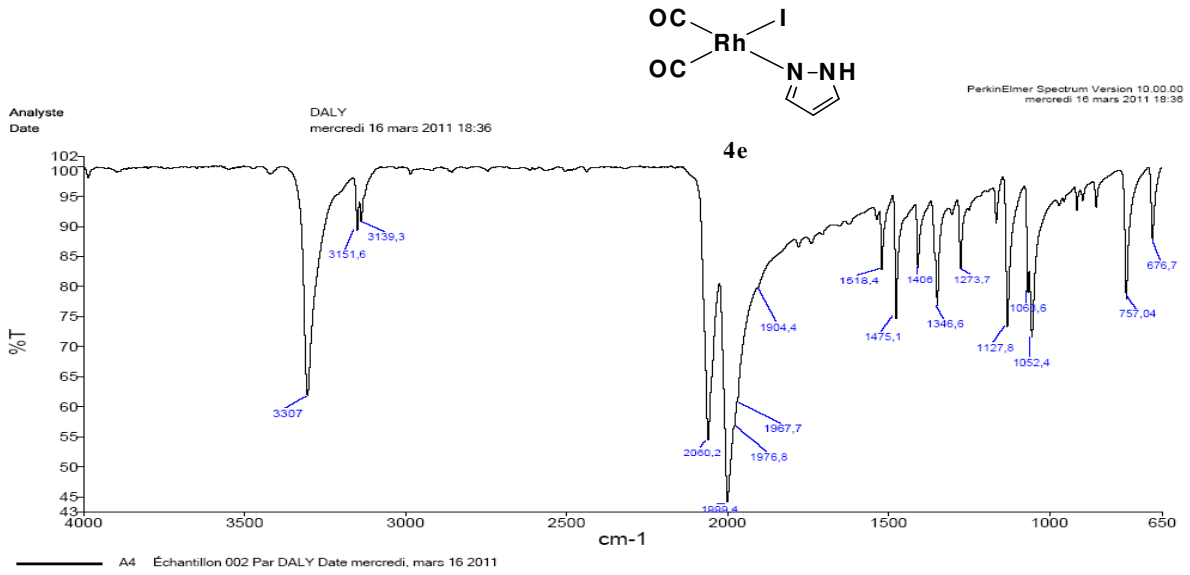

ATR-IR Figure 9. Spectrum of **4f** at 298 K.

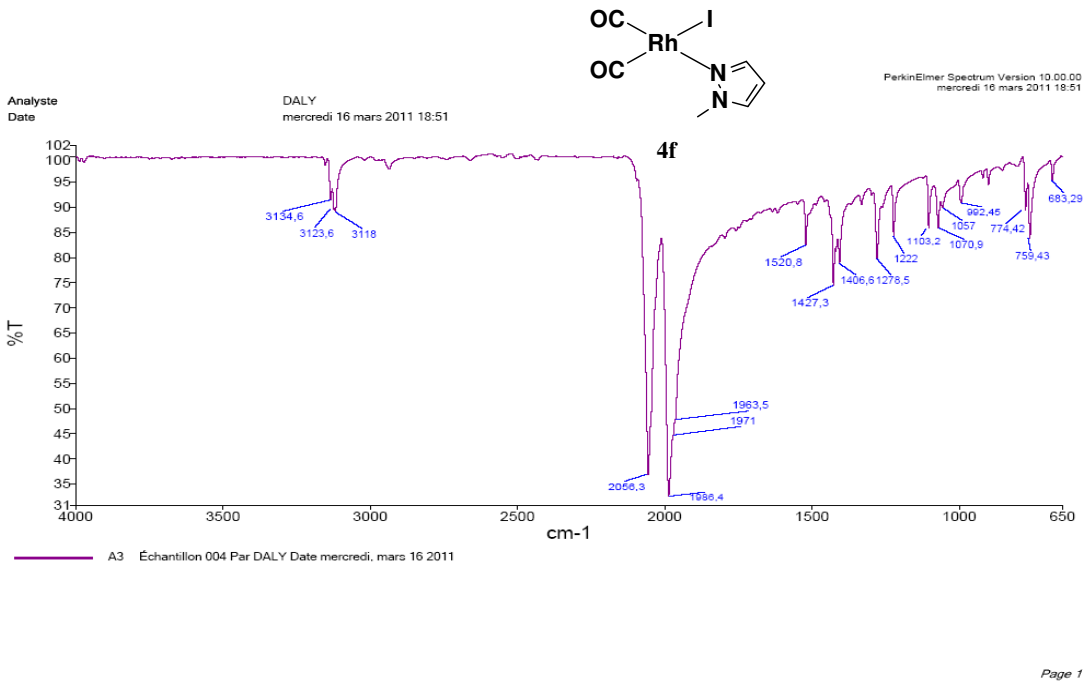

ATR-IR Figure 10. Spectrum of **4g** at 298 K.

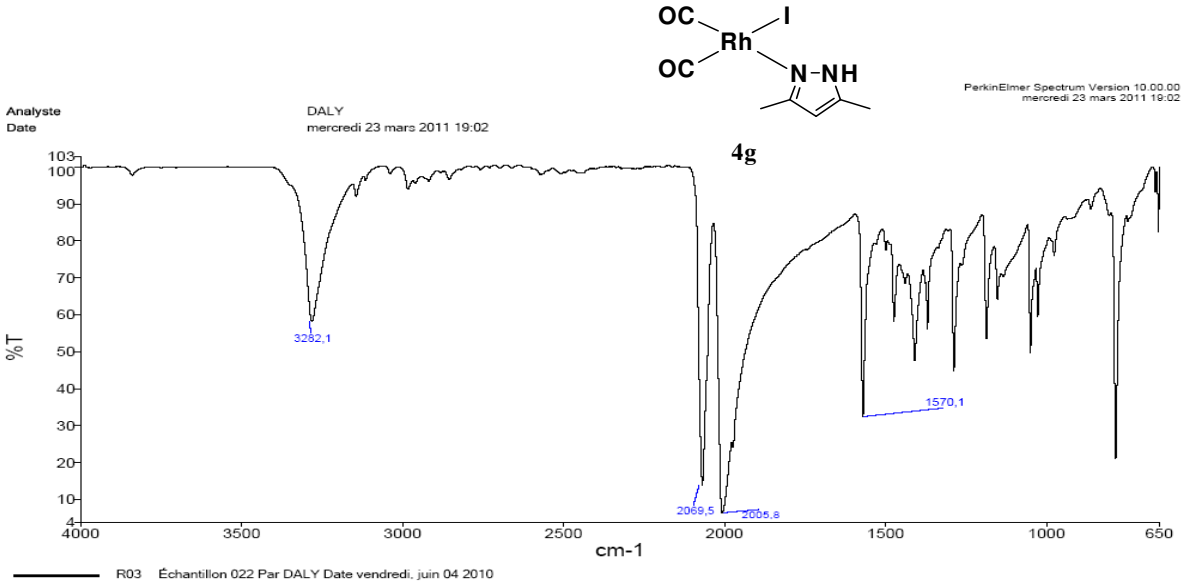

S.I-4: NMR DATA / SELECTED Rh(I) NMR SPECTRA

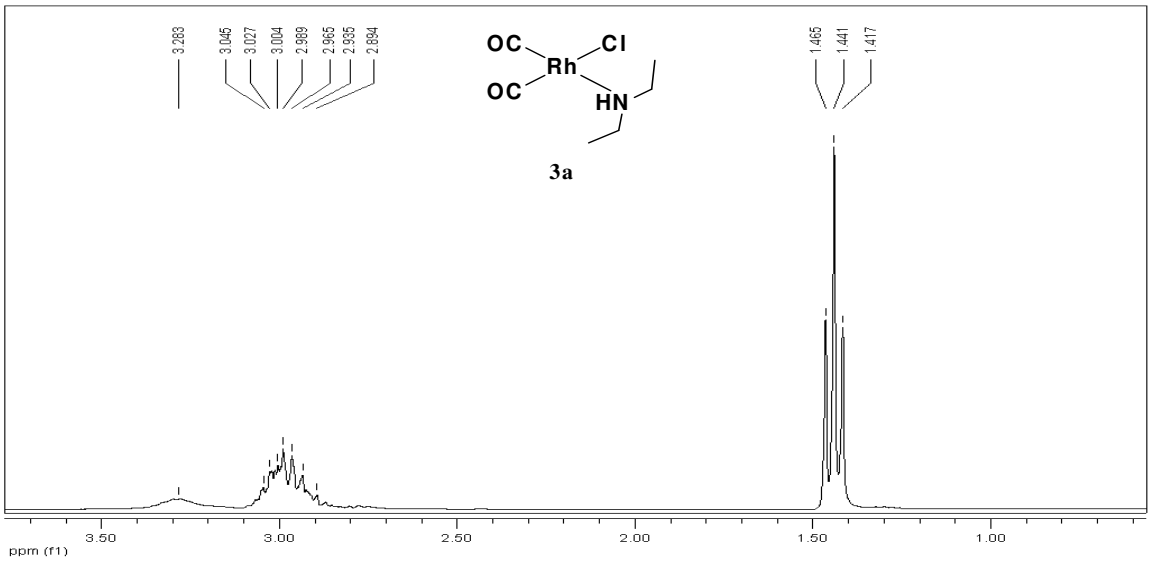

Figure 1. ^{1}H NMR spectrum of **3a** at 298 K in CD_2Cl_2.

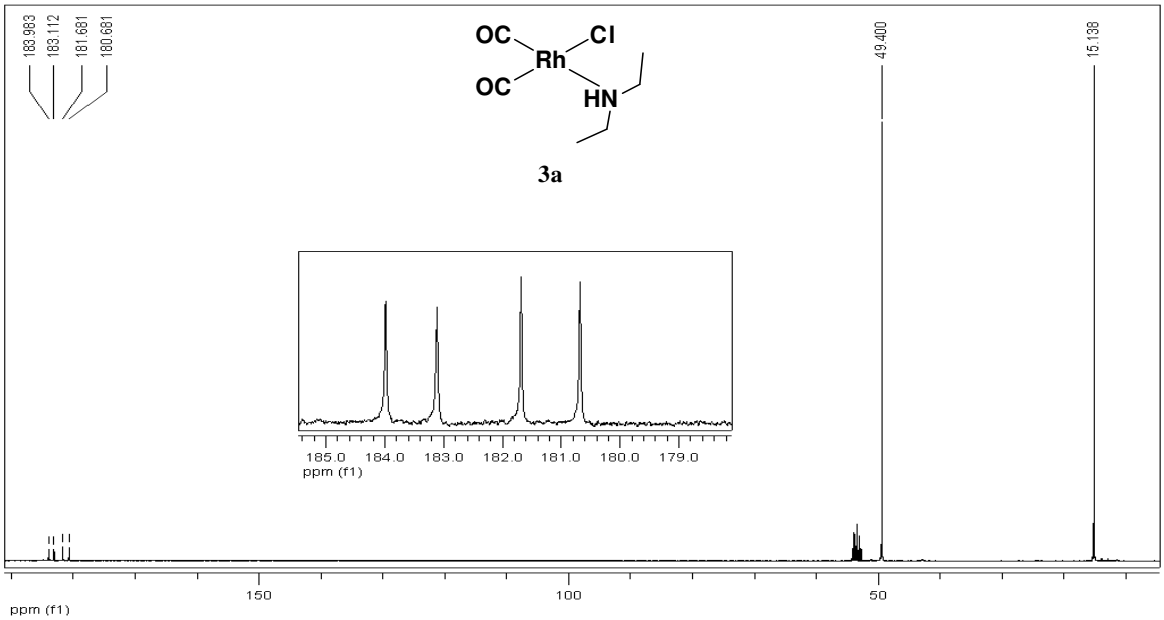

Figure 2. ^{13}C{^{1}H} NMR spectrum of **3a** at 298 K in CD_2Cl_2.

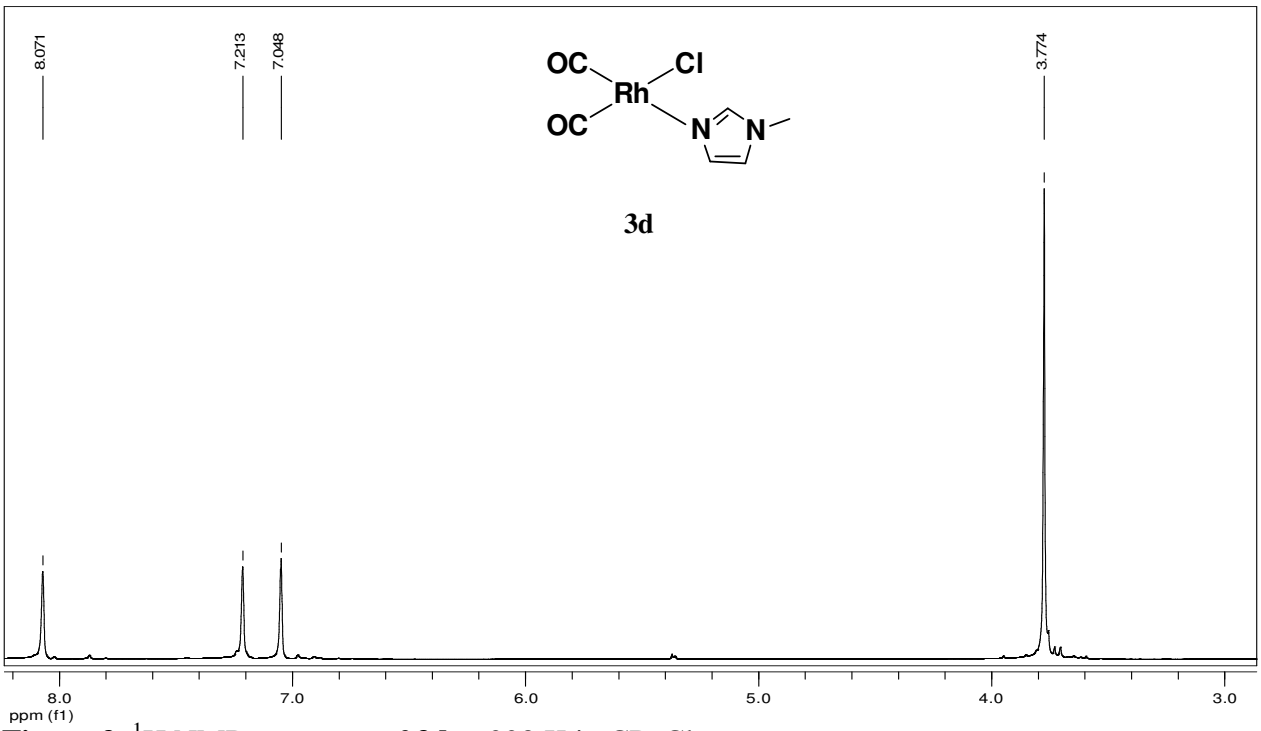

Figure 3. ^{1}H NMR spectrum of **3d** at 298 K in CD_2Cl_2.

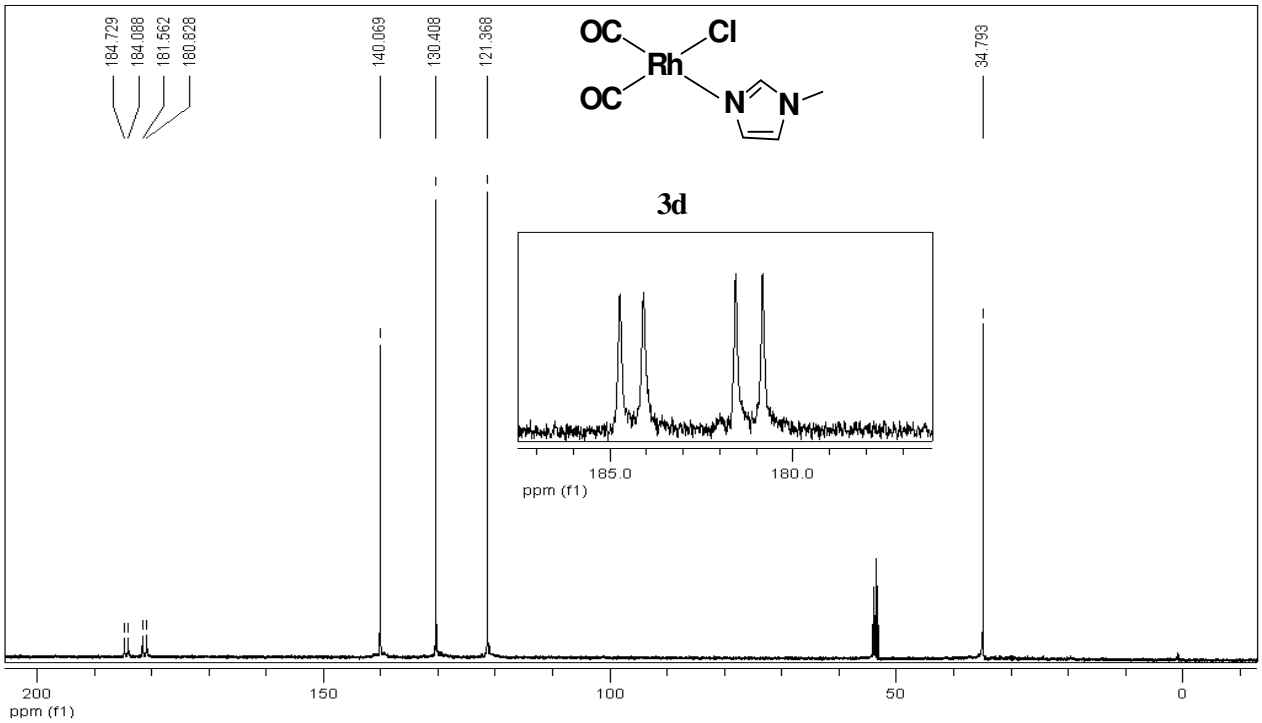

Figure 4. ^{13}C{^{1}H} NMR spectrum of **3d** at 298 K in CD_2Cl_2.

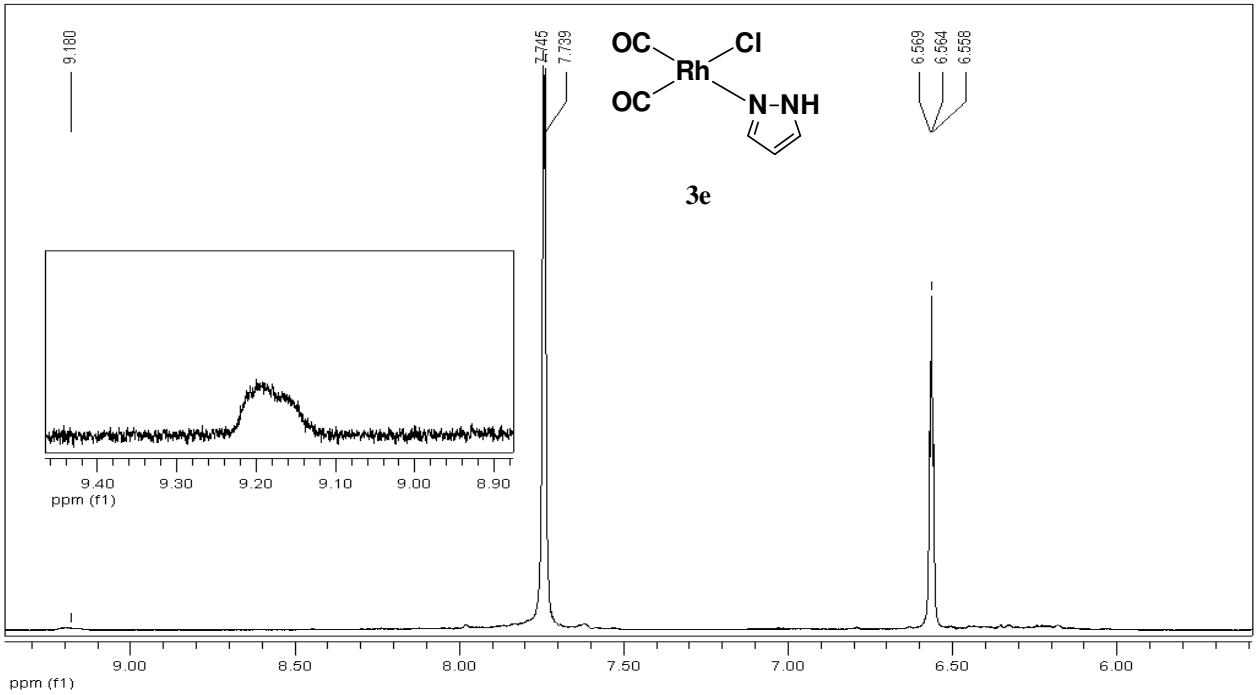

Figure 5. ^{1}H NMR spectrum of **3e** at 298 K in CD_2Cl_2.

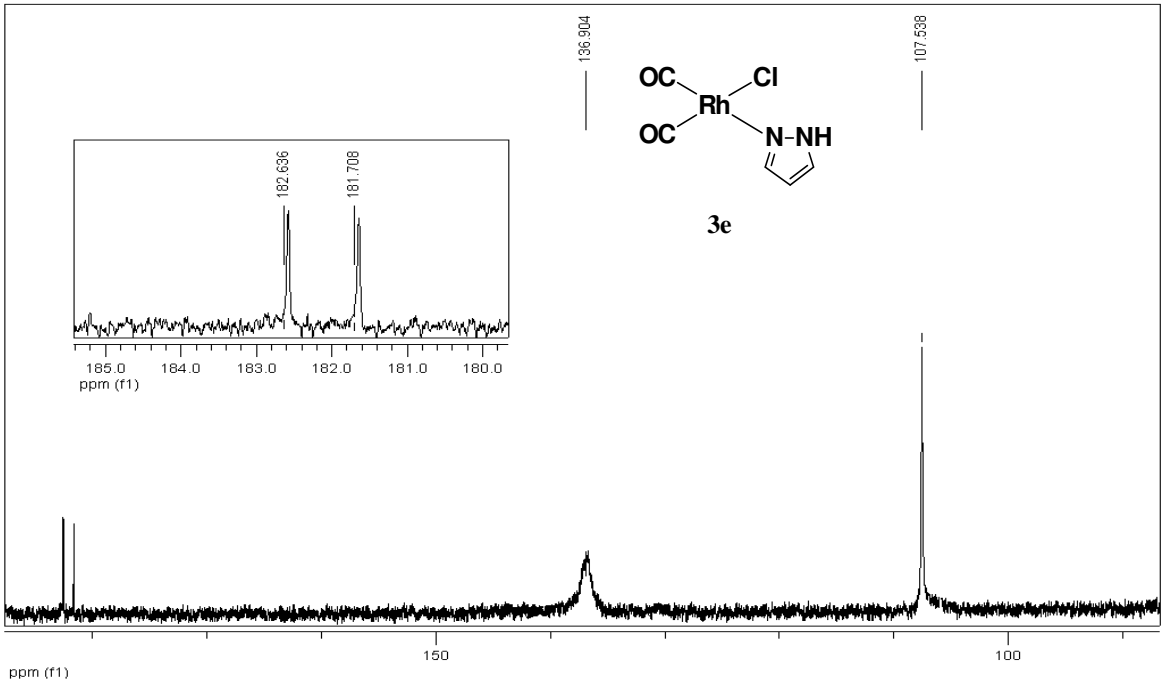

Figure 6. ^{13}C{^{1}H} NMR spectrum of **3e** at 298 K in CD_2Cl_2.

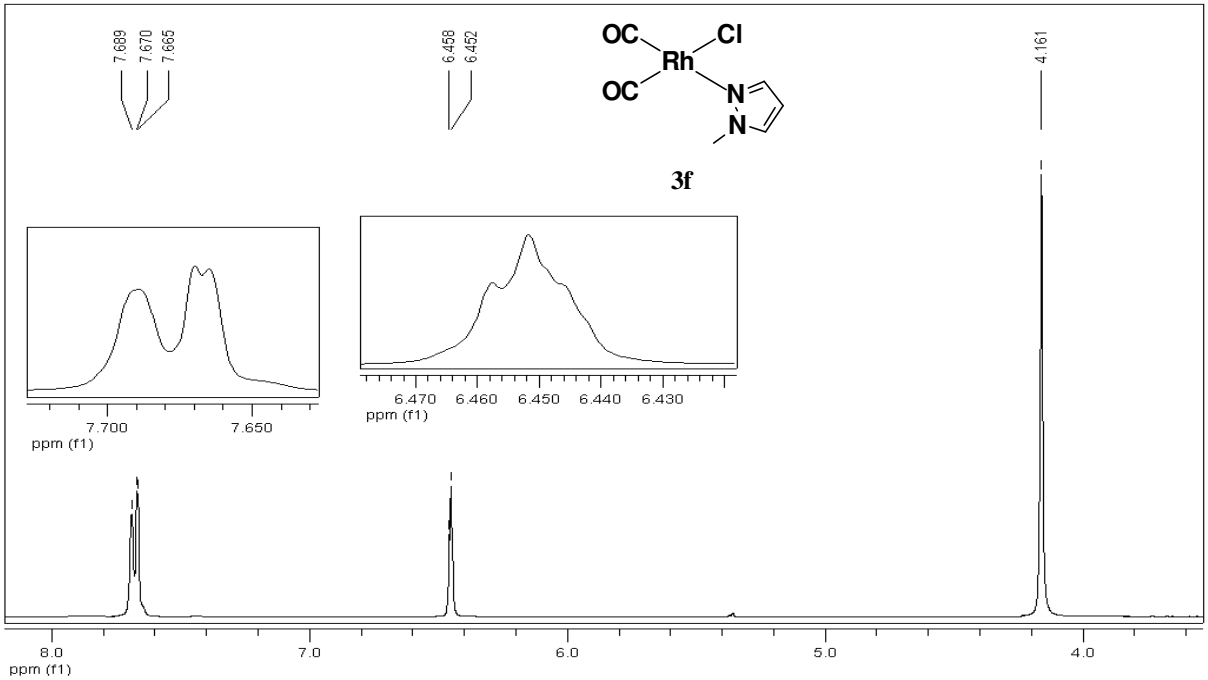

Figure 7. ^{1}H NMR spectrum of **3f** at 298 K in CD_2Cl_2.

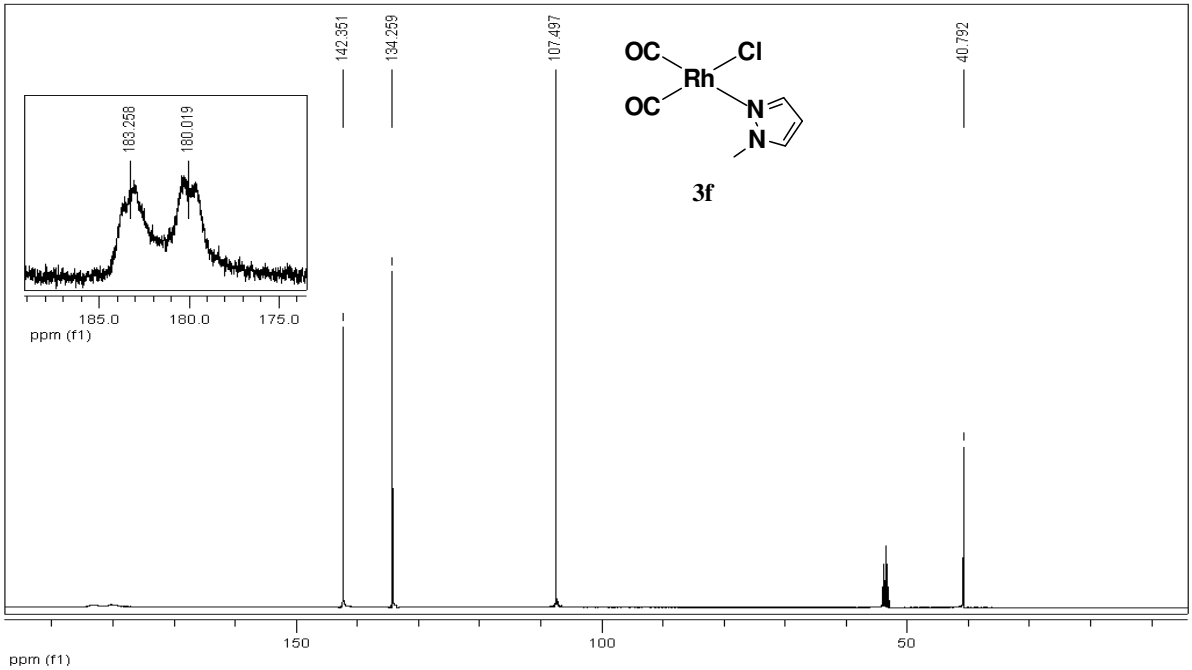

Figure 8. ^{13}C{^{1}H} NMR spectrum of **3f** at 298 K in CD_2Cl_2.

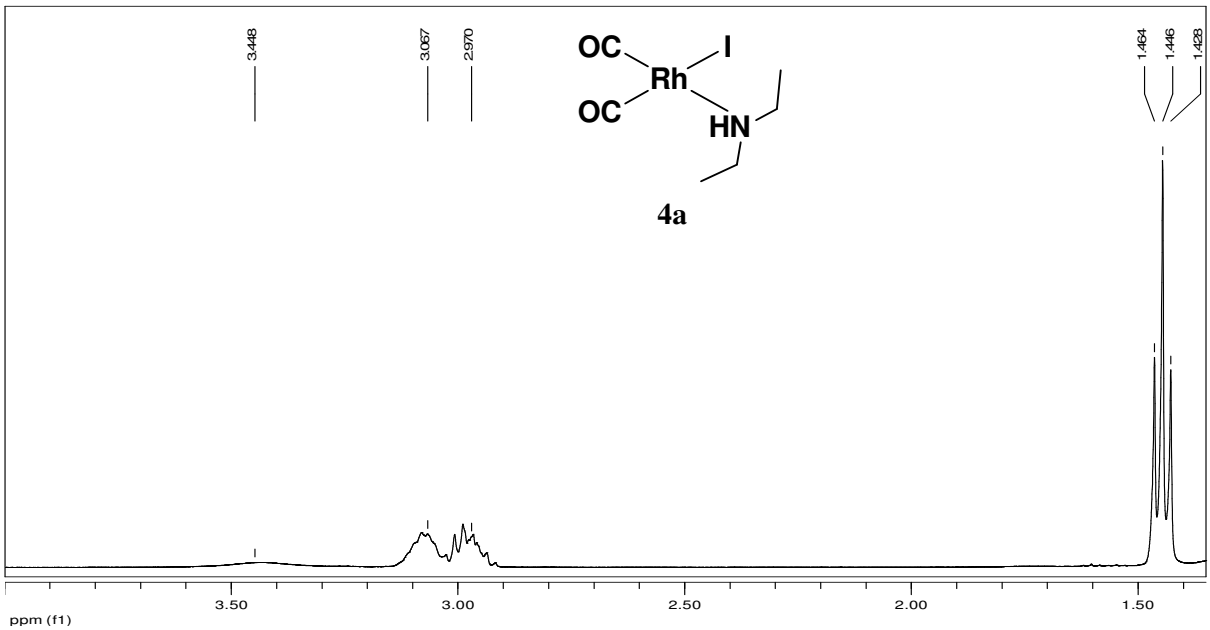

Figure 9. ^{1}H NMR spectrum of **4a** at 298 K in CD_2Cl_2.

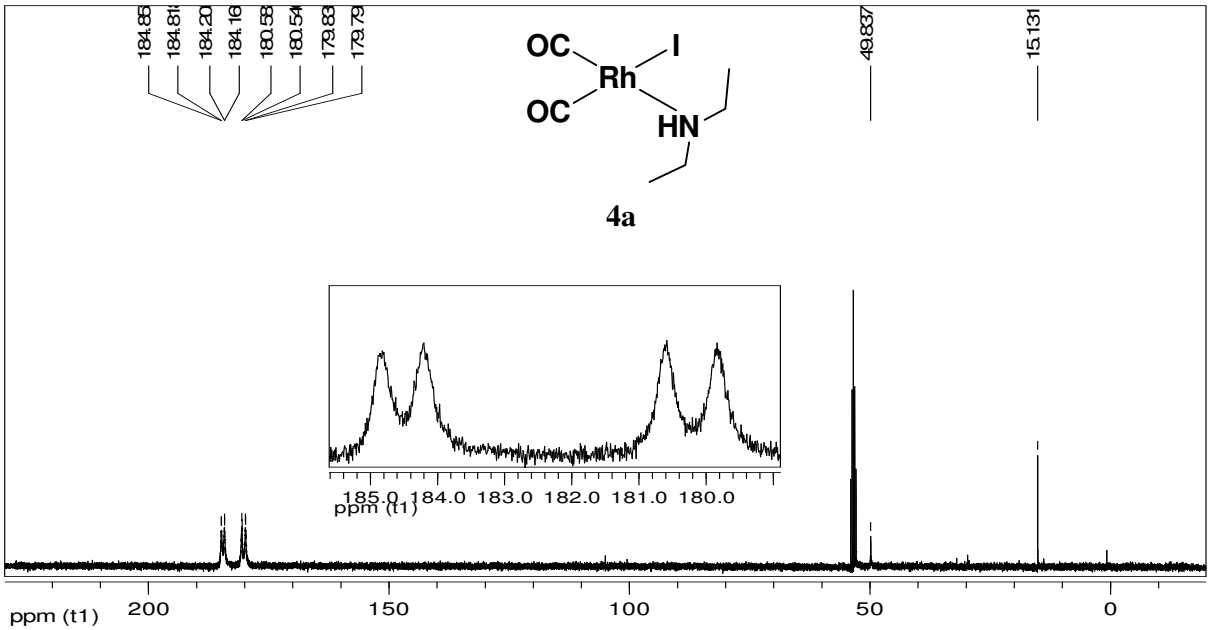

Figure 10. ^{13}C{^{1}H} NMR spectrum of **4a** at 298 K in CD_2Cl_2.

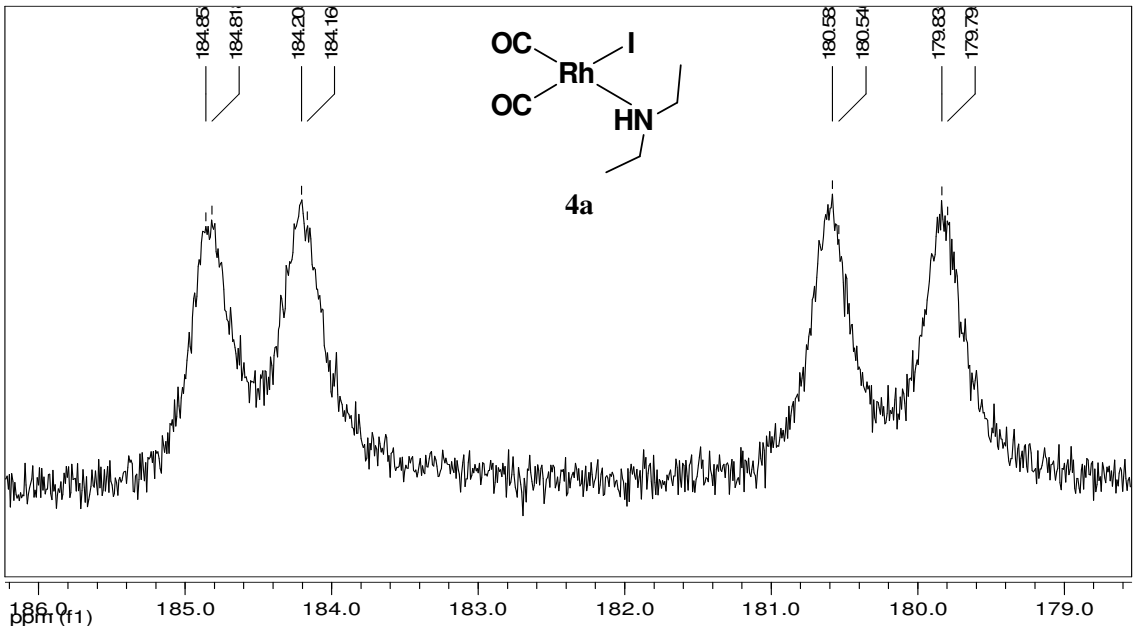

Figure 11. $^{13}C\{^{1}H\}$ NMR spectrum of **4a** at 298 K in CD_2Cl_2 in the carbonyl region. No dynamic ligand-exchange occurs. Two double doublets are represented: $^{2}J_{13CO\text{-}13CO}$ ~ 4 Hz.

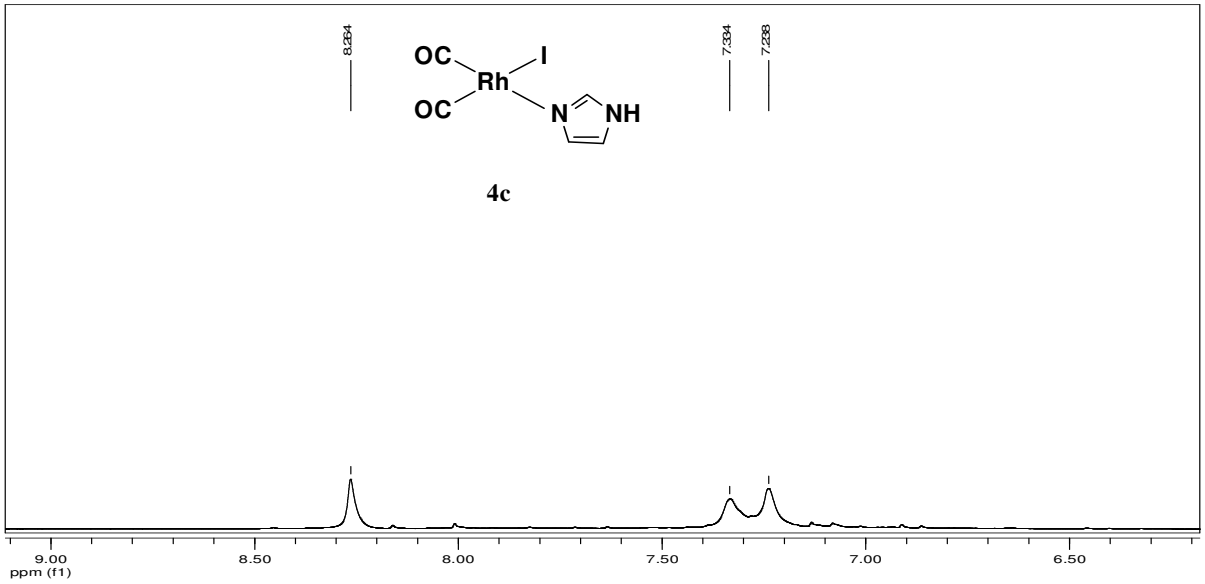

Figure 12. ^{1}H NMR spectrum of **4c** at 298 K in CD_3OD. (N-*H* signal was not detected).

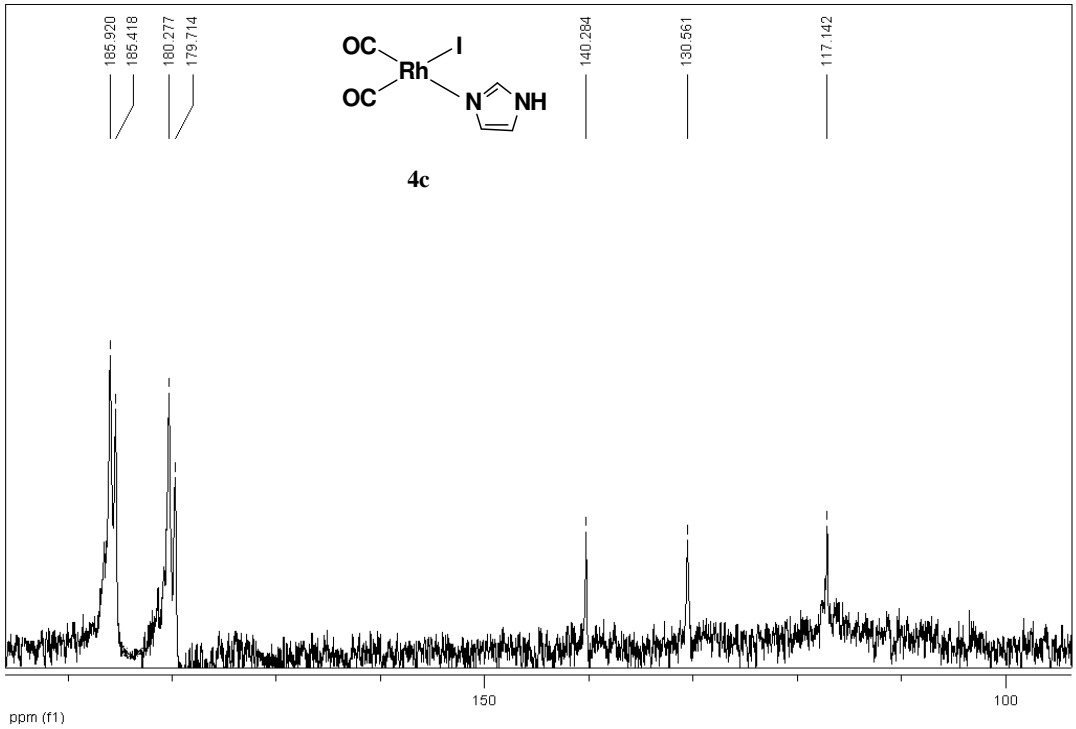

Figure 13. $^{13}C\{^{1}H\}$ NMR spectrum of **4c** at 298 K in CD_3OD.

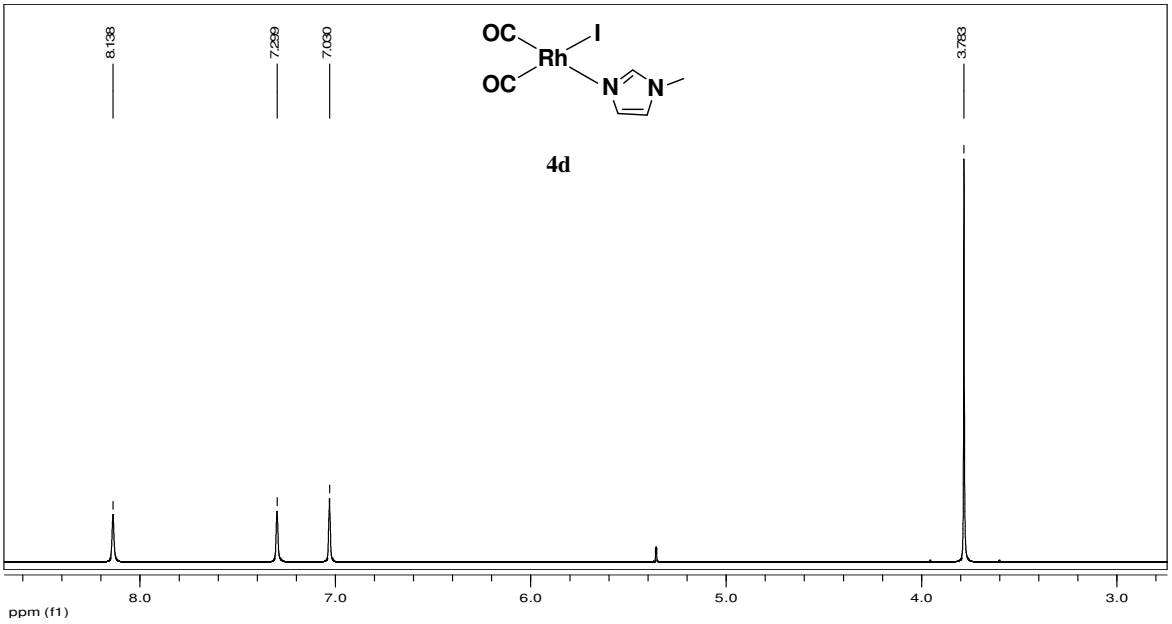

Figure 14. ^{1}H NMR spectrum of **4d** at 298 K in CD_2Cl_2.

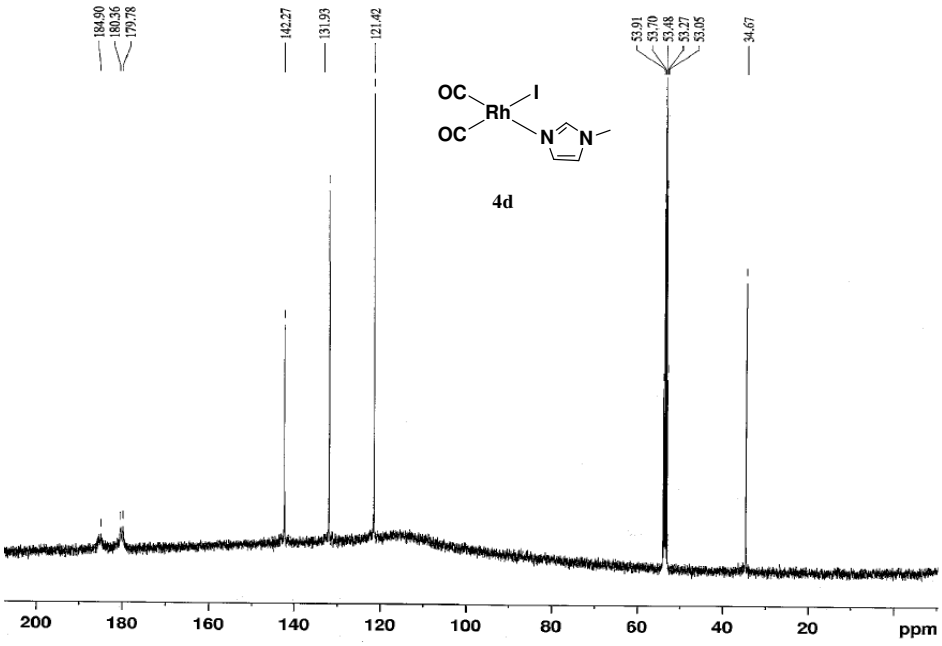

Figure 15. $^{13}C\{^{1}H\}$ NMR spectrum of **4d** at 298 K in CD_2Cl_2.

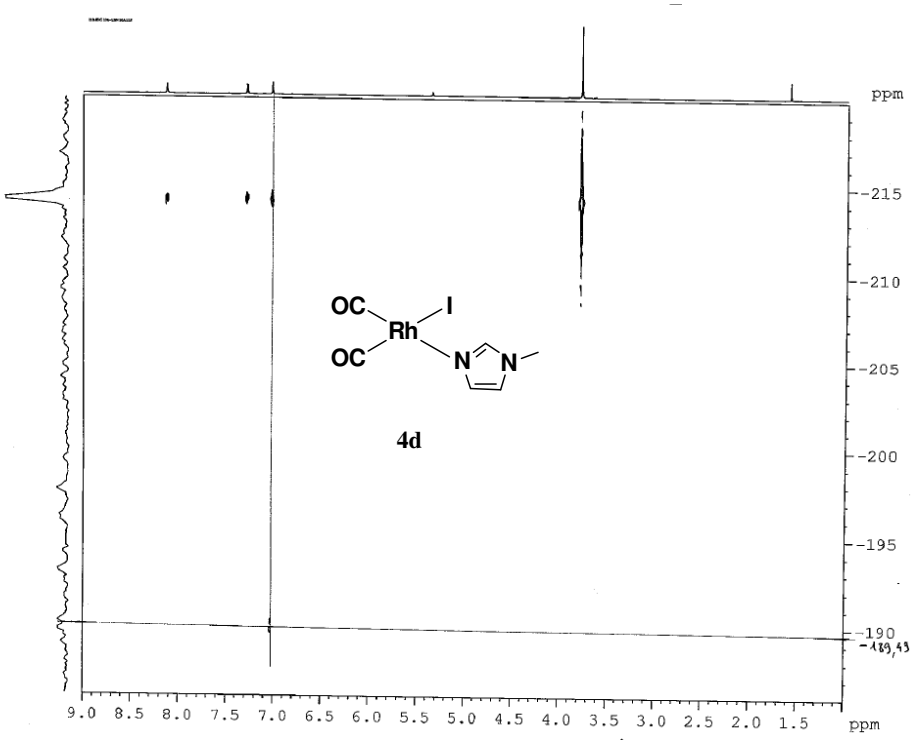

Figure 16. 2D (^{1}H-^{15}N) HMBC NMR spectrum of **4d** at 298 K in CD_2Cl_2.

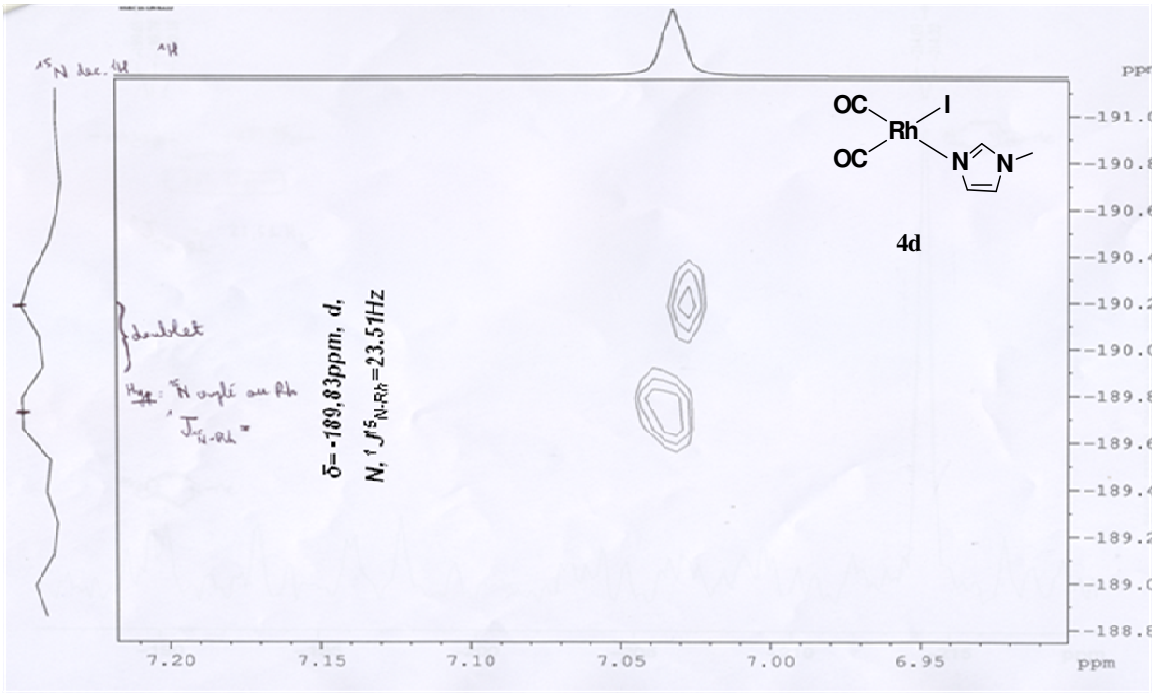

Figure 17. Zoomed 2D (^{1}H-^{15}N) HMBC NMR spectrum of **4d** at 298 K in CD_2Cl_2.

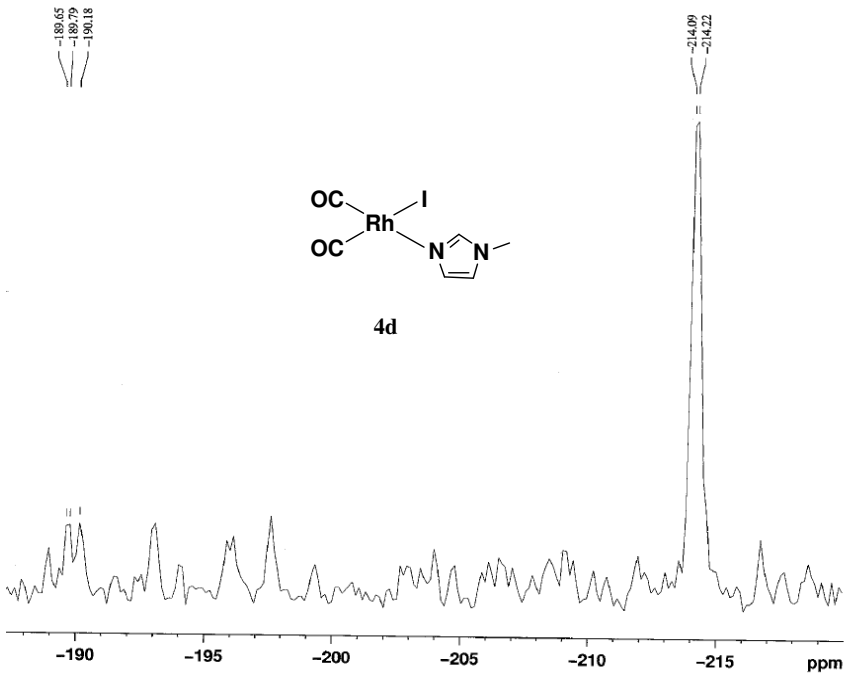

Figure 18. 2D (^{1}H-^{15}N) HMBC NMR: ^{15}N projection spectrum of **4d** at 298 K in CD_2Cl_2.

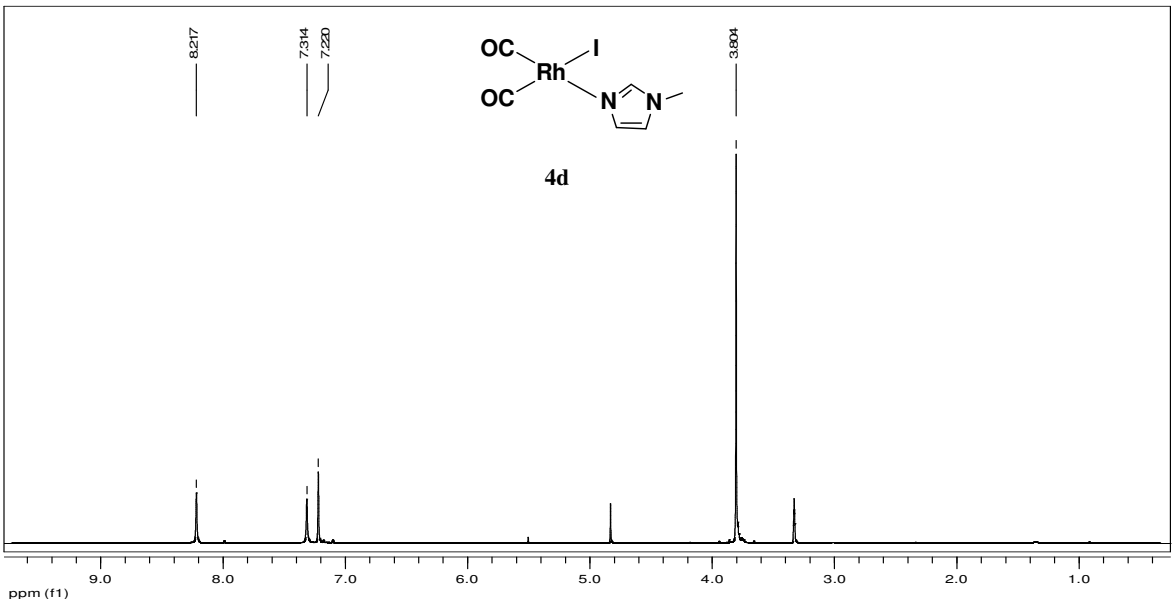

Figure 19. ^{1}H NMR spectrum of **4d** at 298 K in CD_3OD.

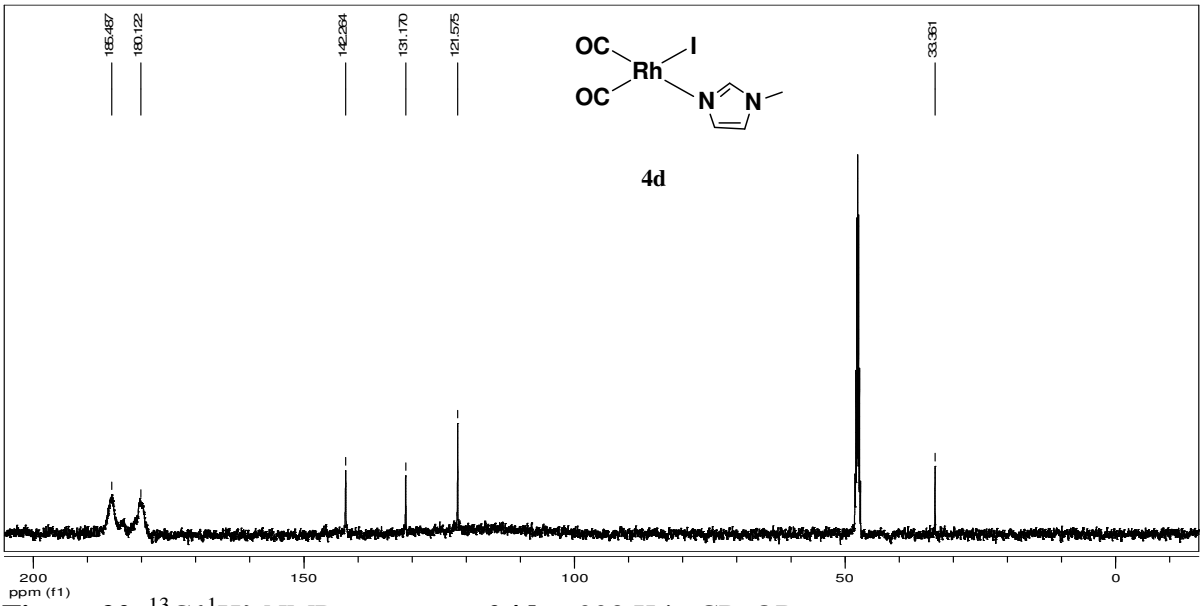

Figure 20. ^{13}C{^{1}H} NMR spectrum of **4d** at 298 K in CD_3OD.

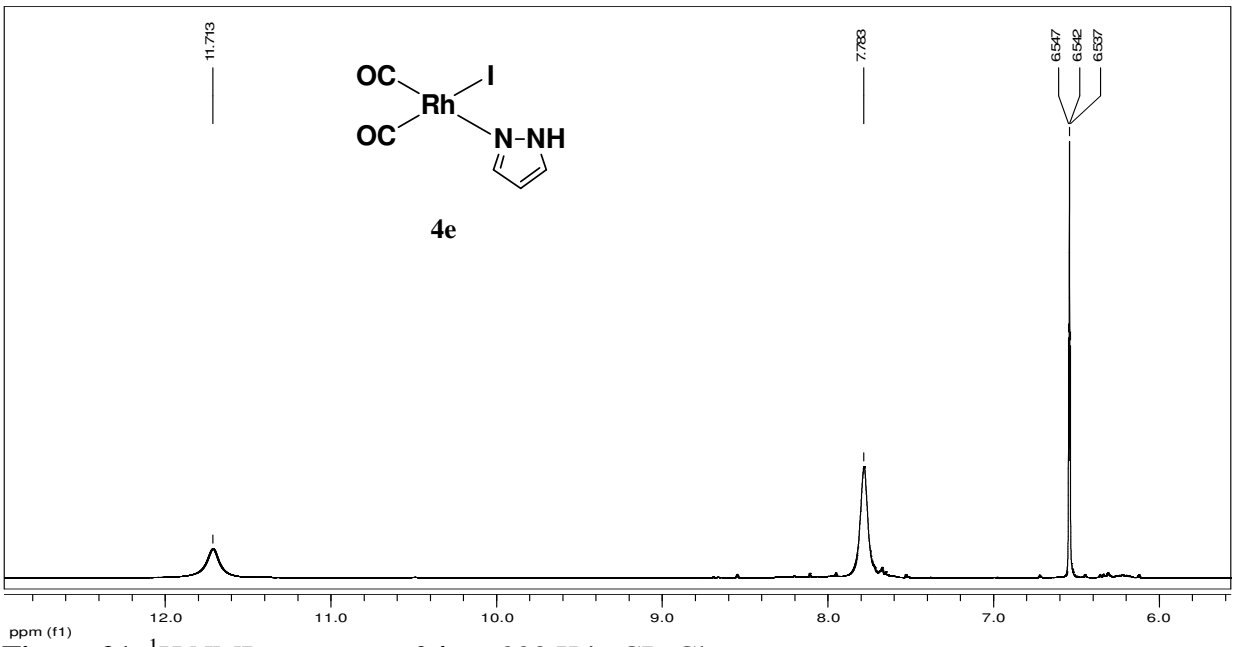

Figure 21. ^{1}H NMR spectrum of **4e** at 298 K in CD_2Cl_2.

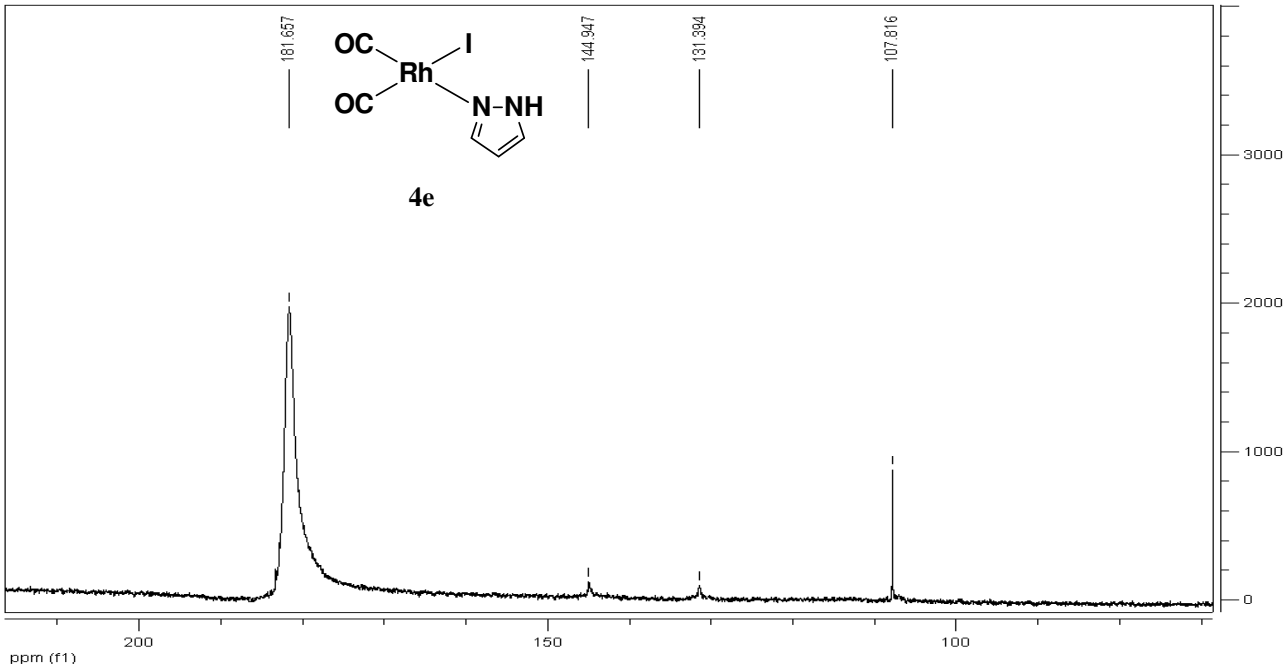

Figure 22. ^{13}C{^{1}H} NMR spectrum of **4e** at 298 K in CD_2Cl_2.

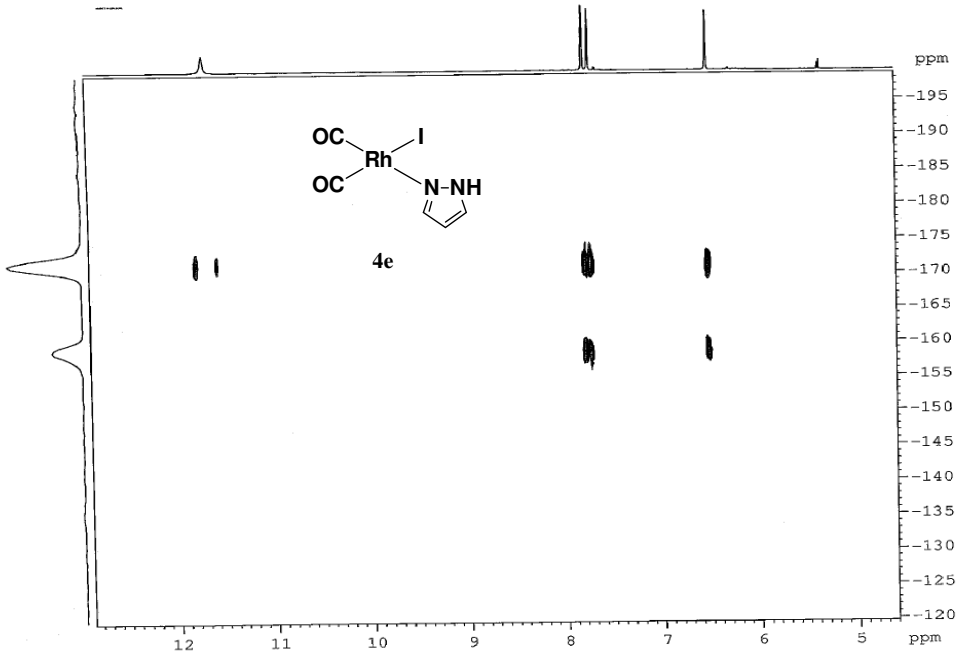

Figure 23. 2D (^{1}H-^{15}N) HMBC NMR spectrum of **4e** at 250 K in CD_2Cl_2.

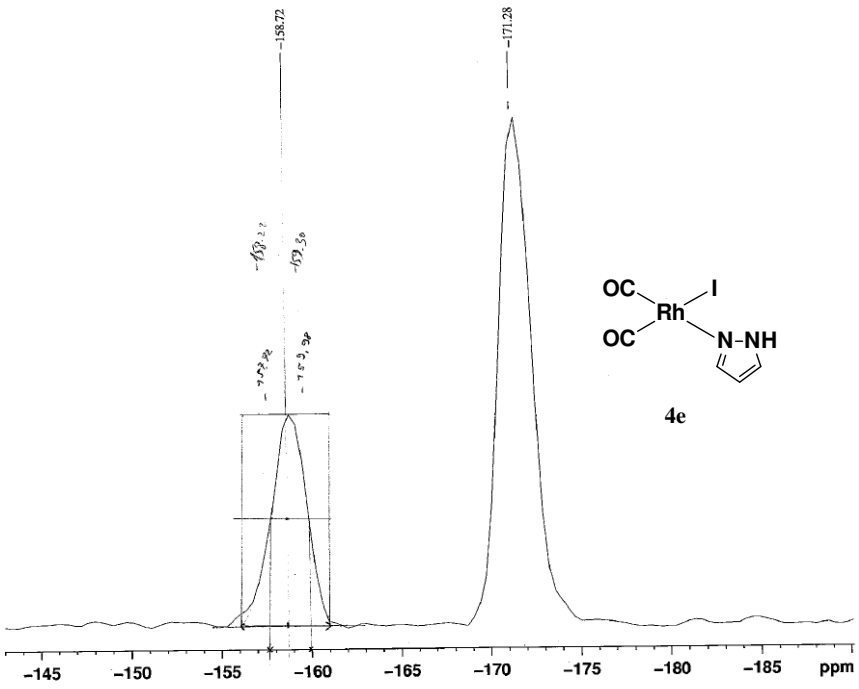

Figure 24. 2D (^{1}H-^{15}N) HMBC NMR: ^{15}N projection spectrum of **4e** at 250 K in CD_2Cl_2.

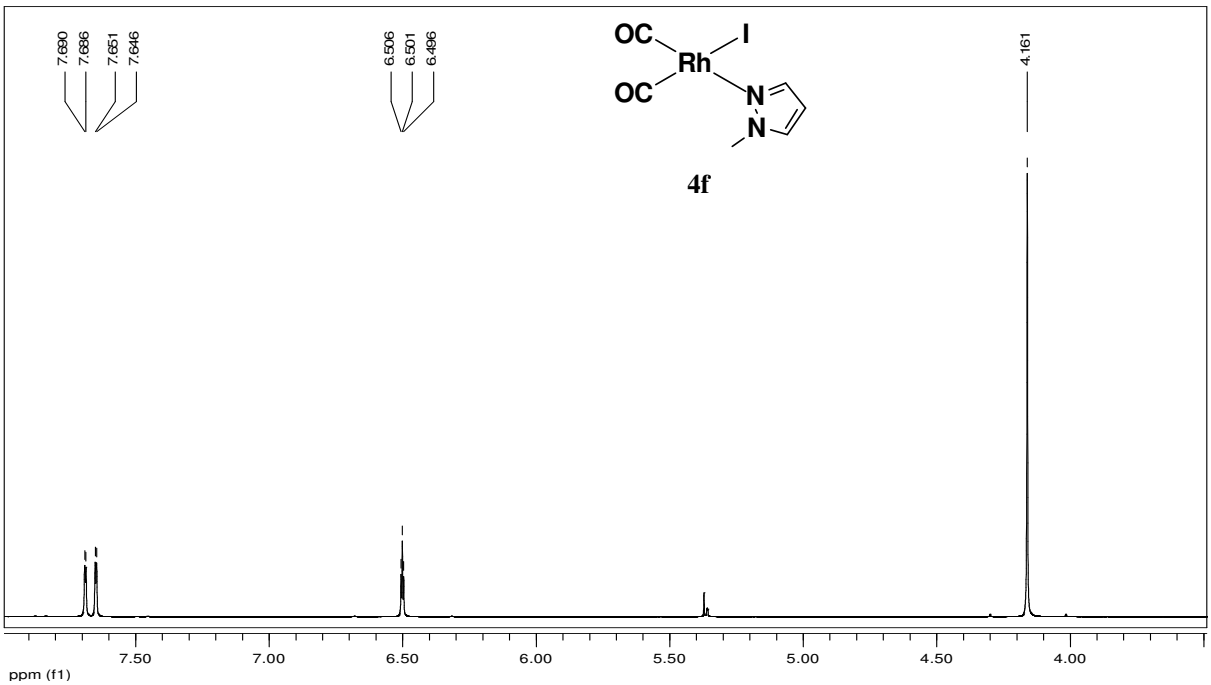

Figure 25. ^{1}H NMR spectrum of **4f** at 298 K in CD_2Cl_2.

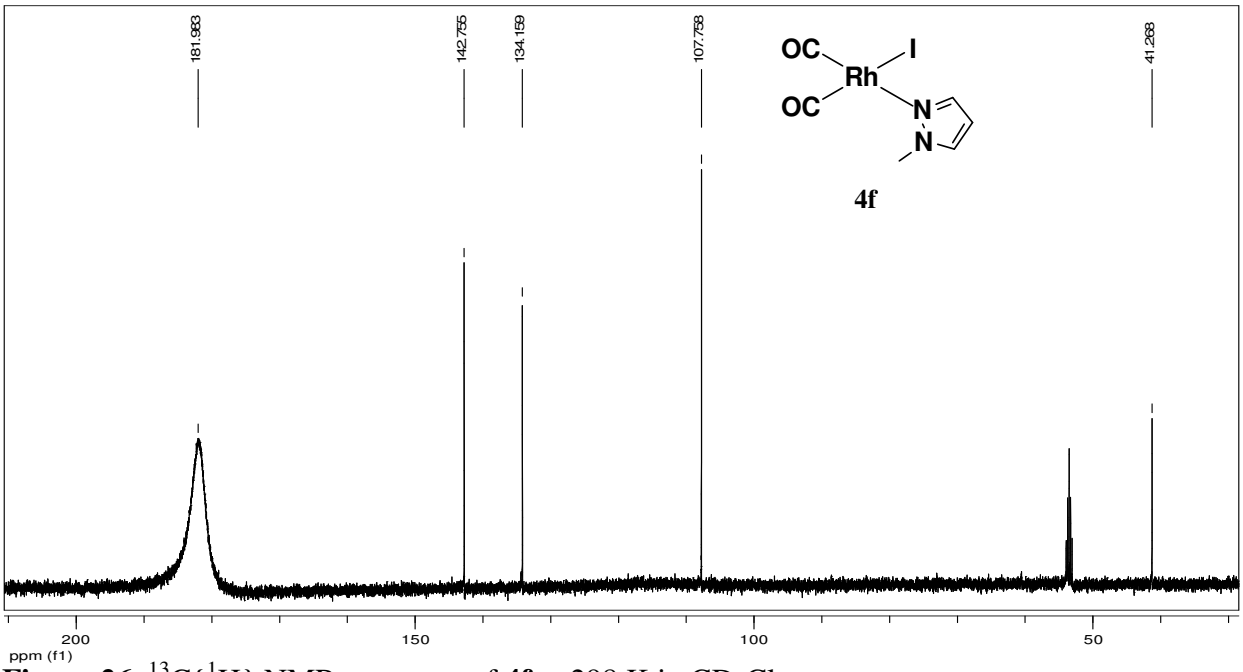

Figure 26. ^{13}C{^{1}H} NMR spectrum of **4f** at 298 K in CD_2Cl_2.

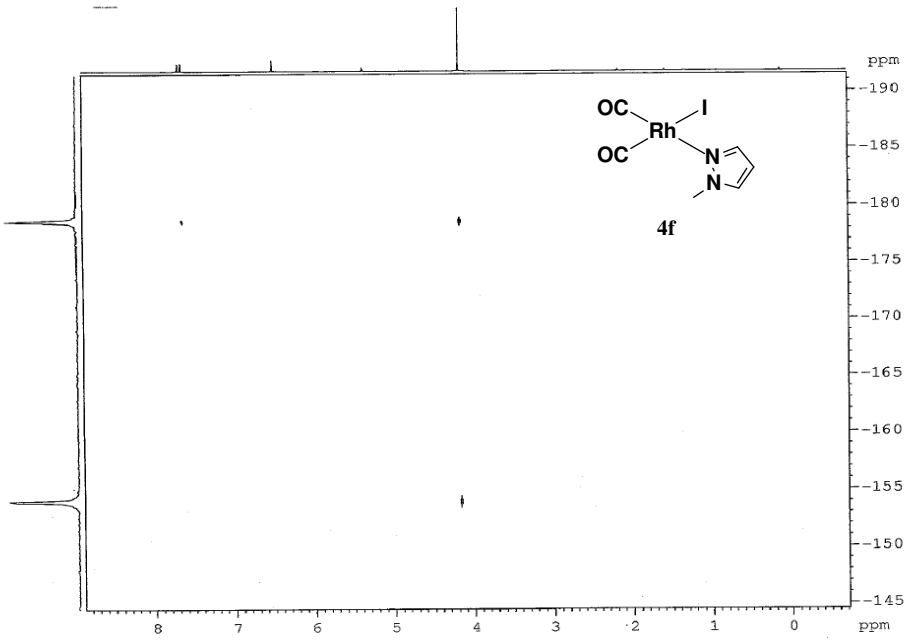

Figure 27. 2D (^{1}H-^{15}N) HMBC NMR spectrum of **4f** at 298 K in CD_2Cl_2.

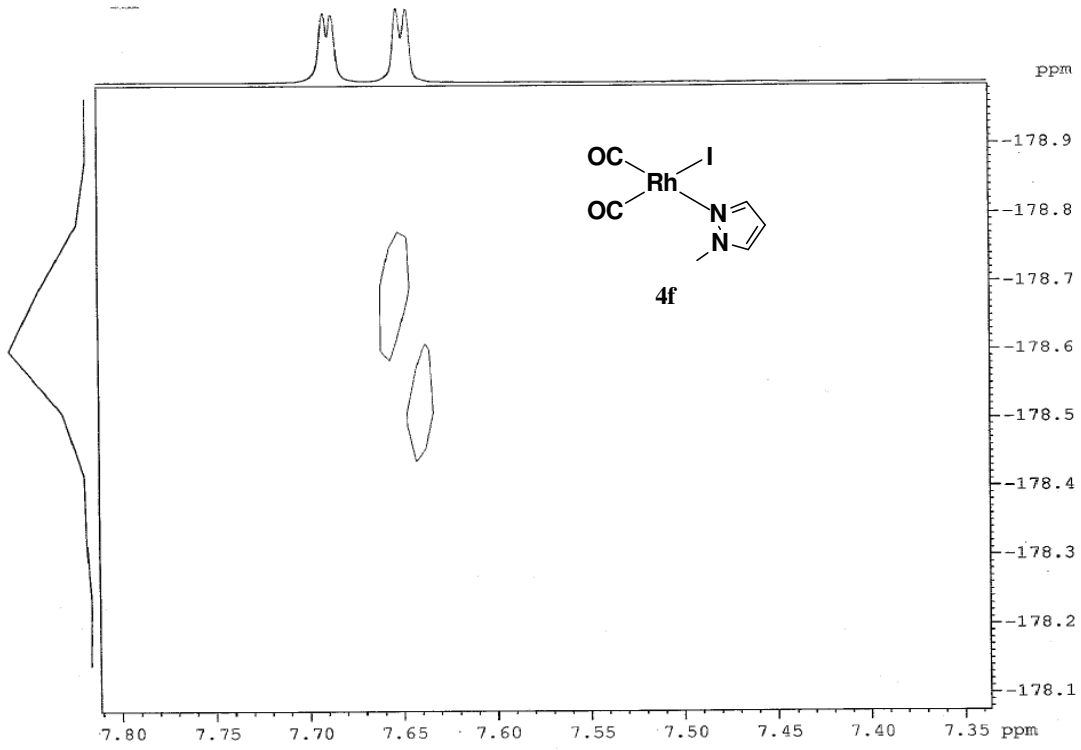

Figure 28. Zoomed 2D (^{1}H-^{15}N) HMBC NMR spectrum of **4f** at 298 K in CD_2Cl_2.

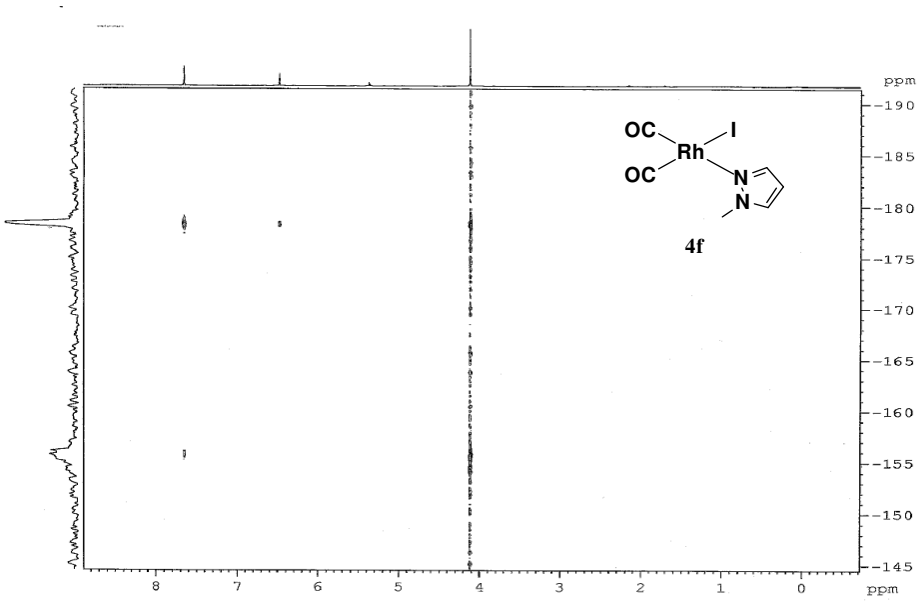

Figure 29. 2D (^{1}H-^{15}N) HMBC NMR spectrum of **4f** at 230 K in CD_2Cl_2.

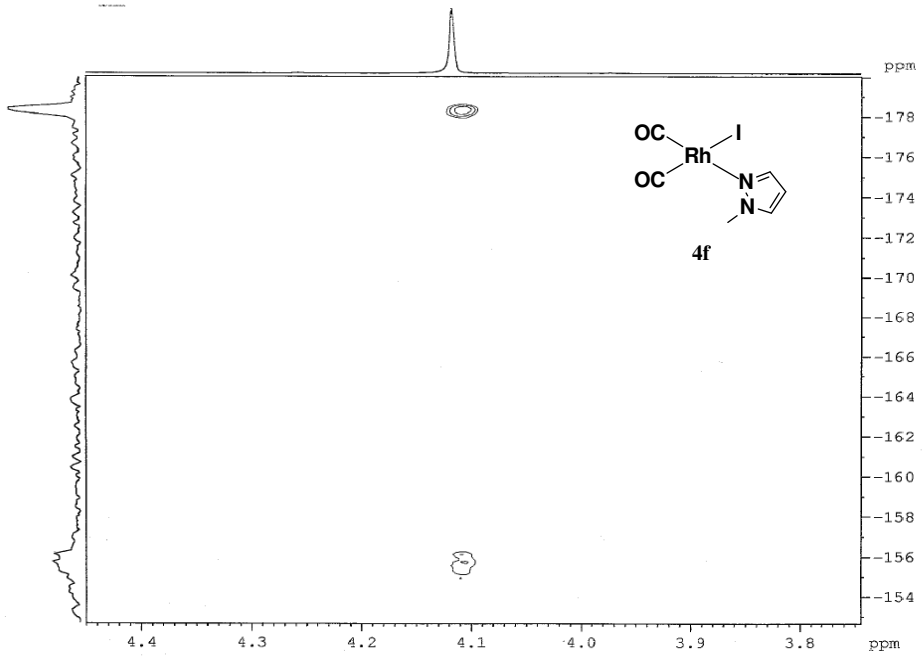

Figure 30. Zoomed 2D (^{1}H-^{15}N) HMBC NMR spectrum of **4f** at 230 K in CD_2Cl_2.

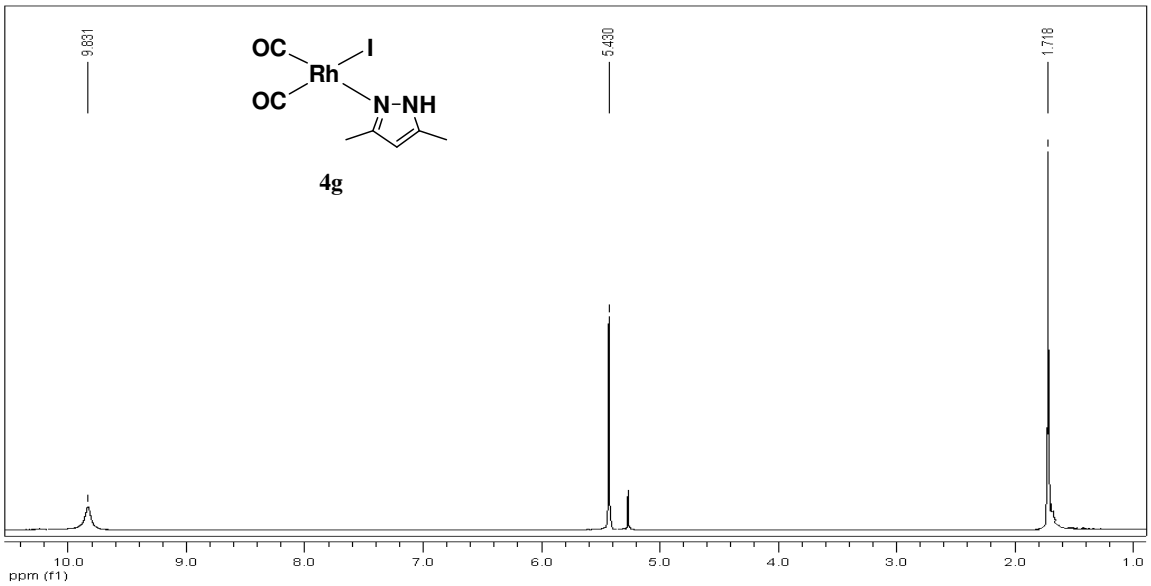

Figure 31. ^{1}H NMR spectrum of **4g** at 298 K in CD_2Cl_2.

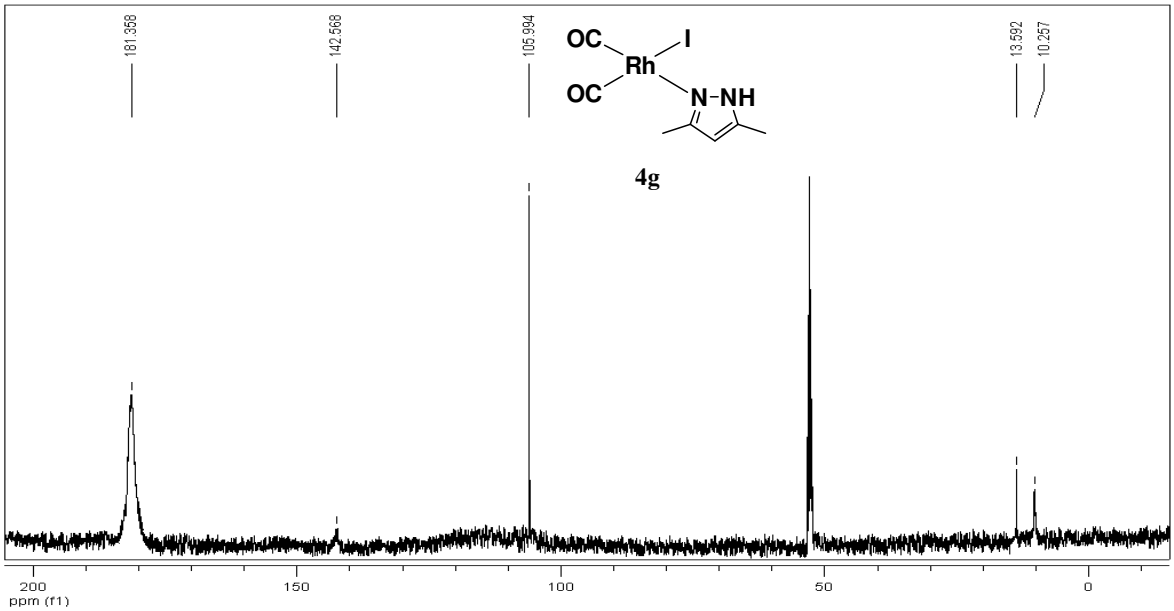

Figure 32. ^{13}C{^{1}H} NMR spectrum of **4g** at 298 K in CD_2Cl_2.

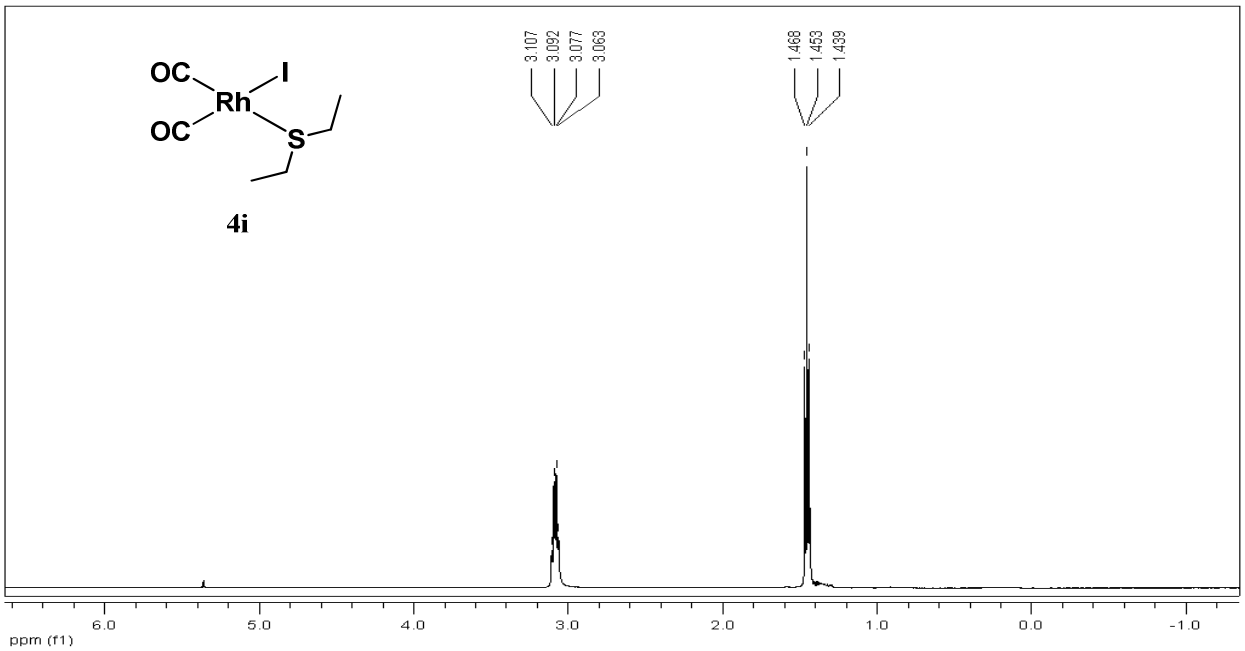

Figure 33. ^{1}H NMR spectrum of **4h** at 298 K in CD_2Cl_2.

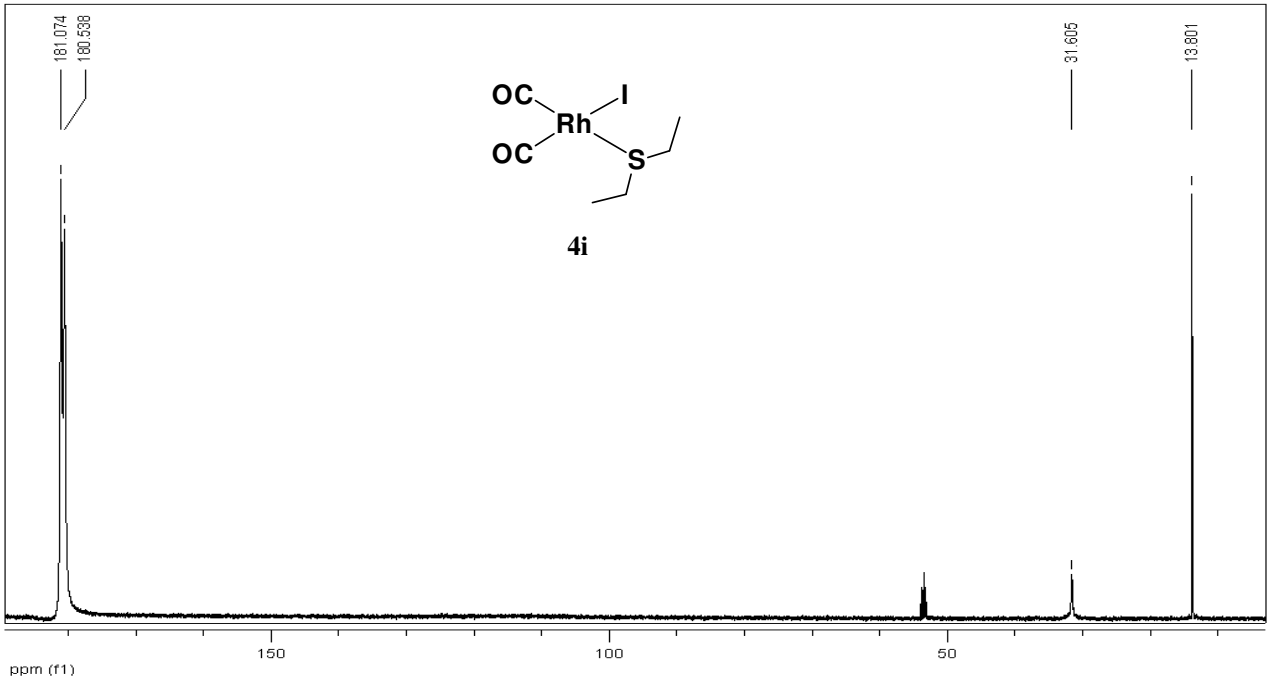

Figure 34. ^{13}C{^{1}H} NMR spectrum of **4i** at 298 K in CD_2Cl_2.

S.I-5: SELECTED VT-NMR SPECTRA

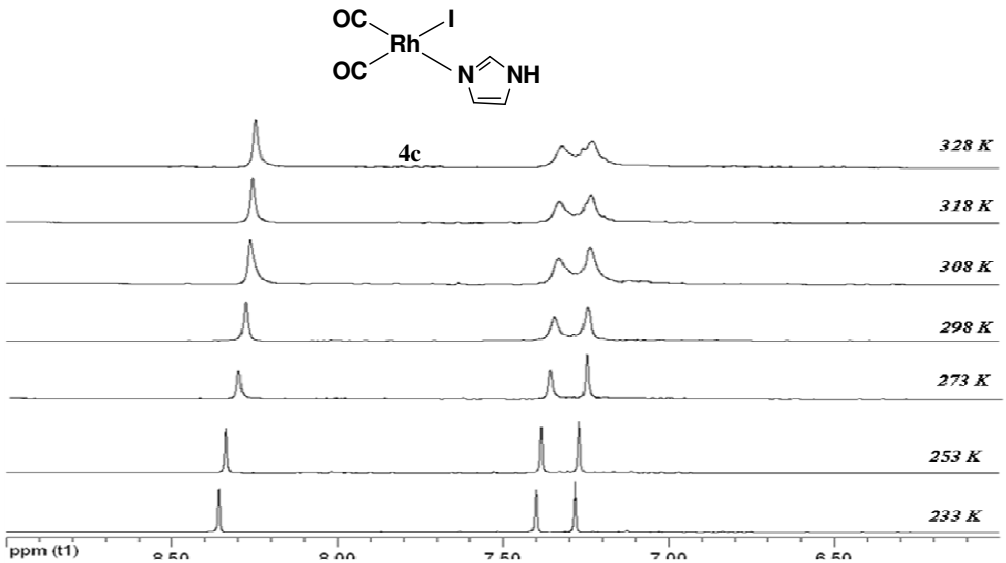

Figure 1. ^{1}H VT-NMR stacked spectra of **4c** in the 7.00-8.50 ppm region in CD_3OD.

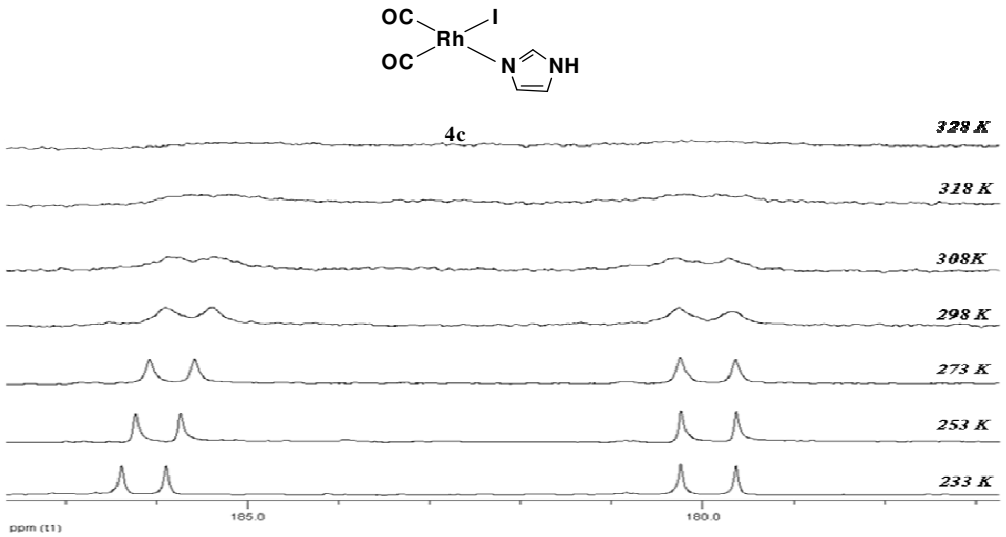

Figure 2. $^{13}C\{^{1}H\}$ VT-NMR stacked spectra of **4c** in the carbonyl region in CD_3OD.

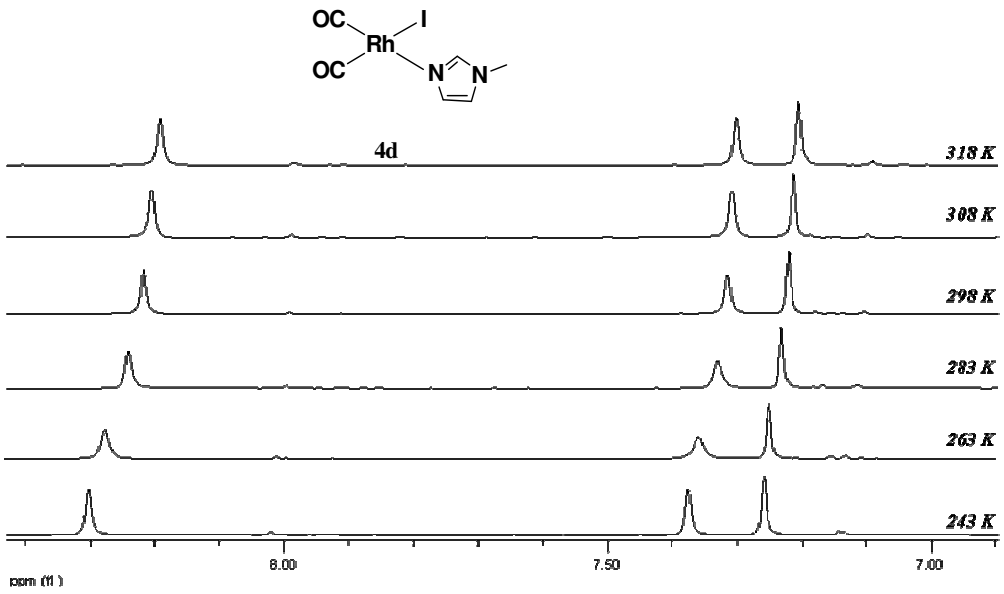

Figure 3. ^{1}H VT-NMR stacked spectra of **4d** in the 7.00-8.50 ppm region in CD_3OD.

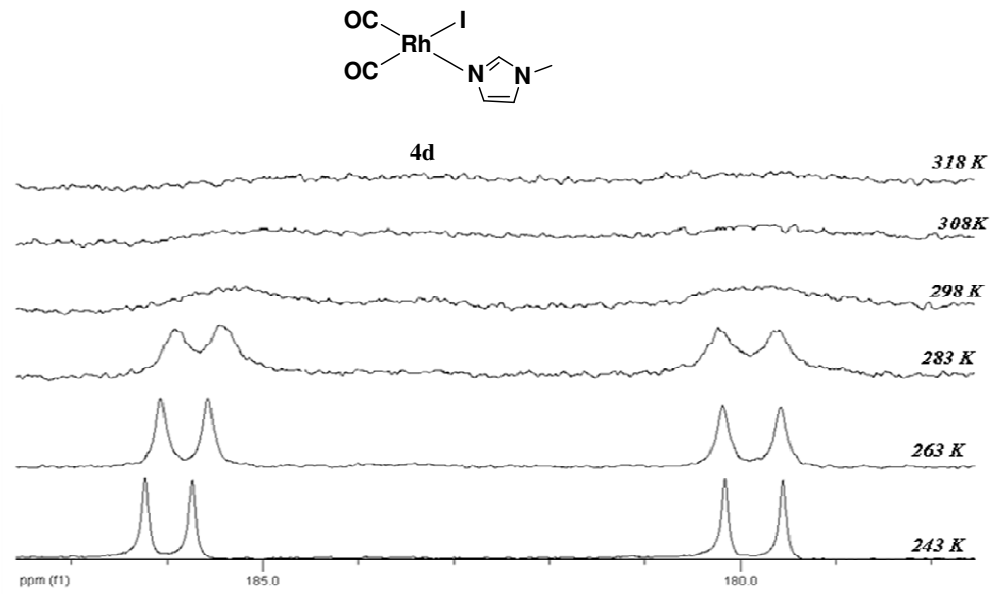

Figure 4. ^{13}C{^{1}H} VT-NMR stacked spectra of **4d** in the carbonyl region in CD_3OD.

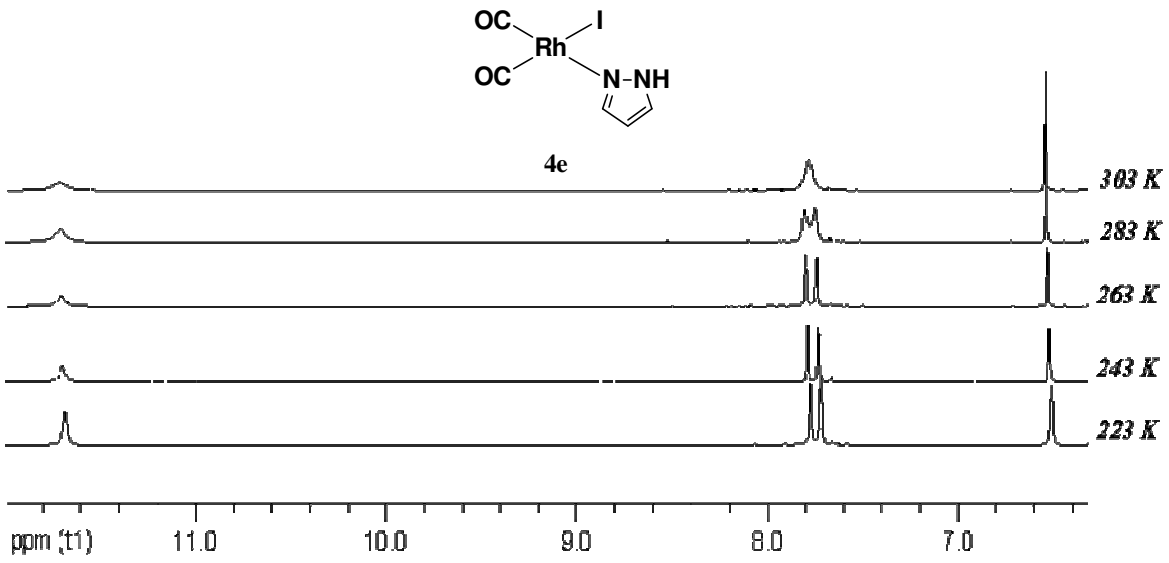

Figure 5. ^{1}H VT-NMR stacked spectra of **4e** in the 6.00-12.00 ppm region in CD_2Cl_2.

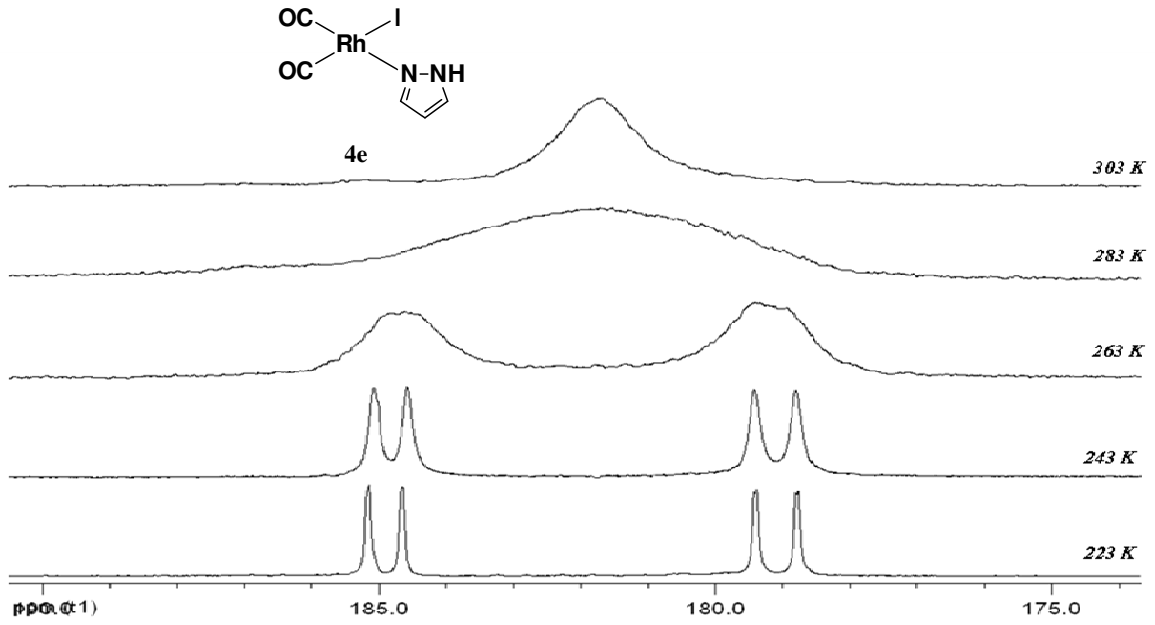

Figure 6. ^{13}C{^{1}H} VT-NMR stacked spectra of **4e** in the carbonyl region in CD_2Cl_2.

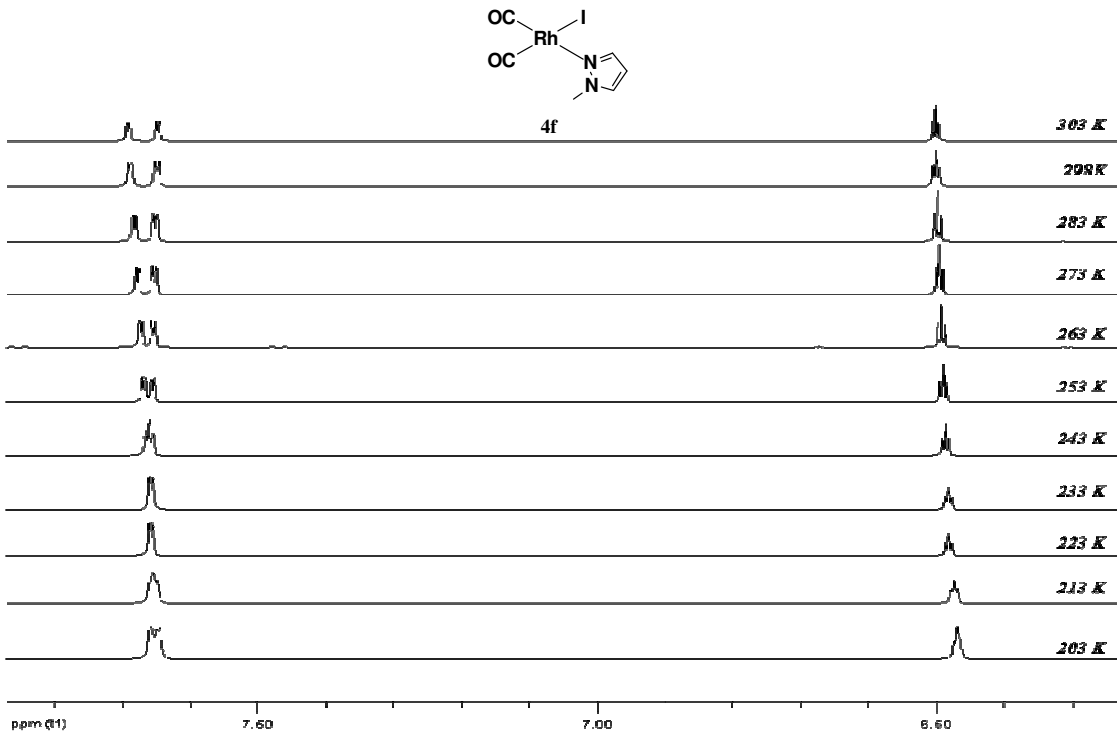

Figure 7. ^{1}H VT-NMR stacked spectra of **4f** in the 6.00-7.80 ppm region in CD_2Cl_2.

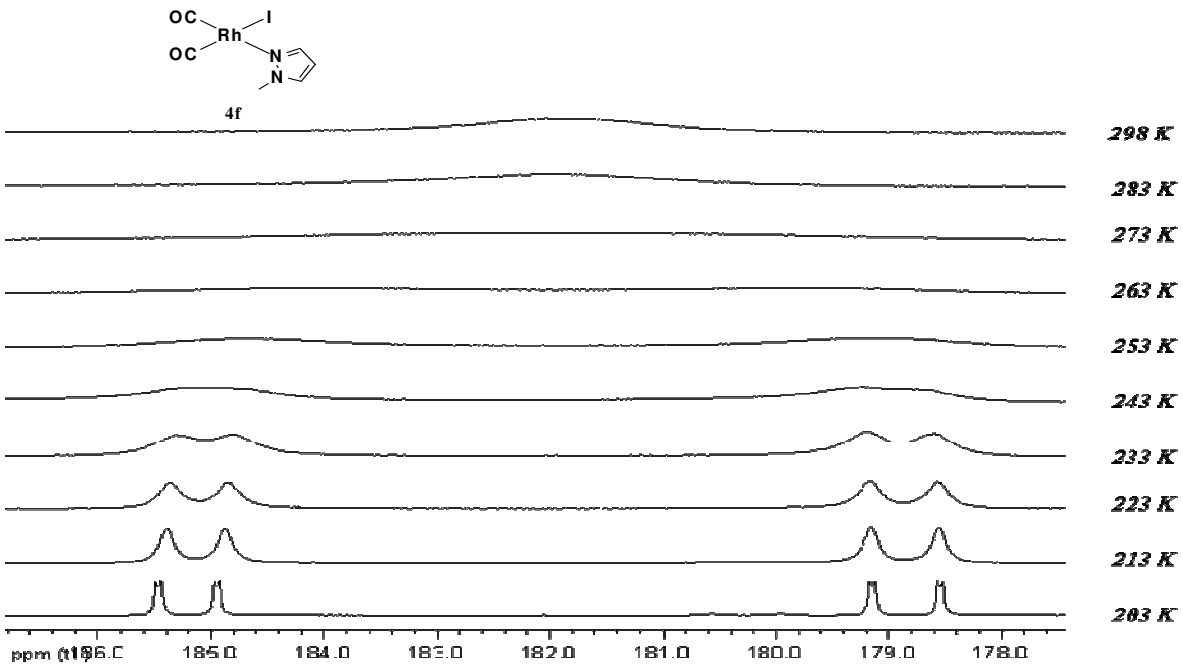

Figure 8. ^{13}C{^{1}H} VT-NMR stacked spectra of **4f** in the carbonyl region in CD_2Cl_2.

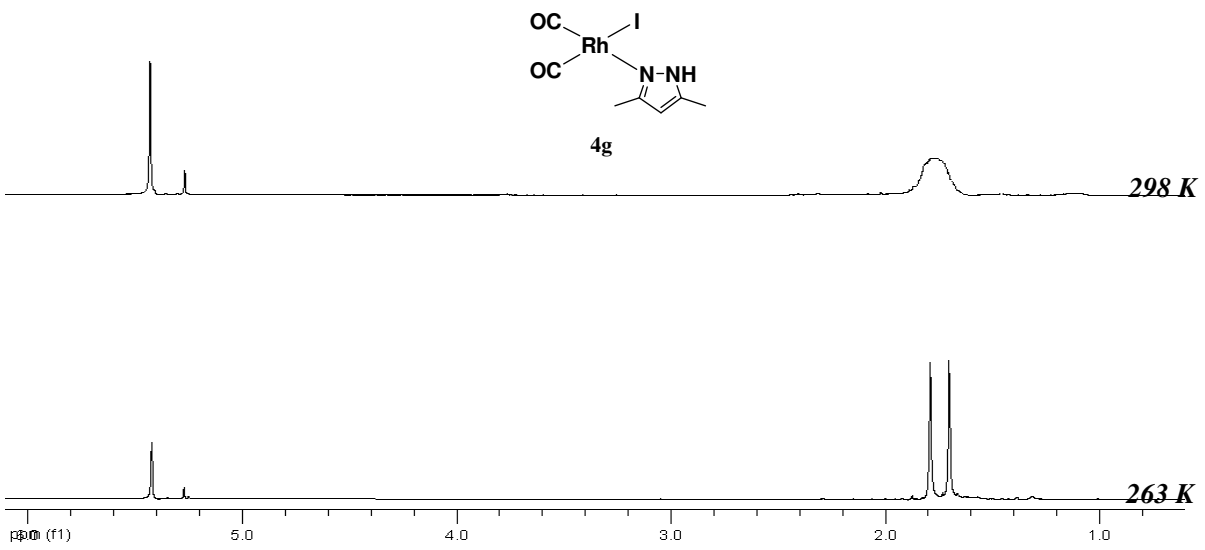

Figure 9. ^{1}H VT-NMR spectra of **4g** in the 1.00-6.00 ppm region in CD_2Cl_2.

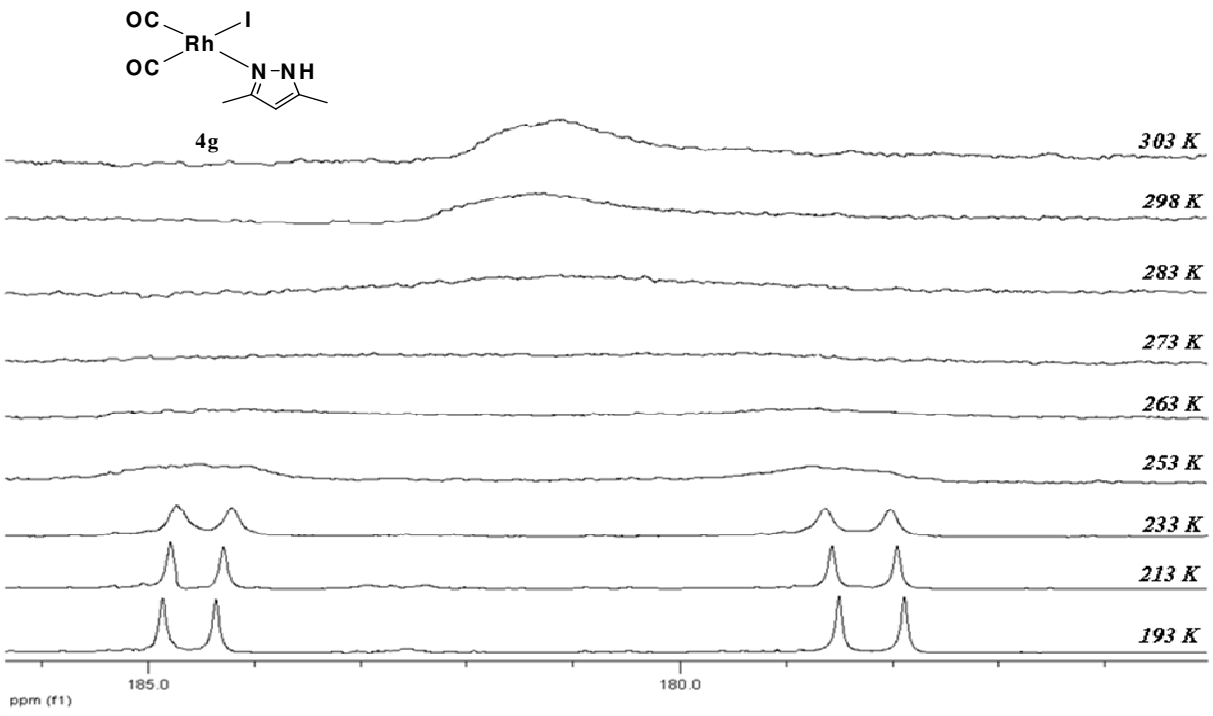

Figure 10. ^{13}C{^{1}H} VT-NMR stacked spectra of **4g** in the carbonyl region in CD_2Cl_2.

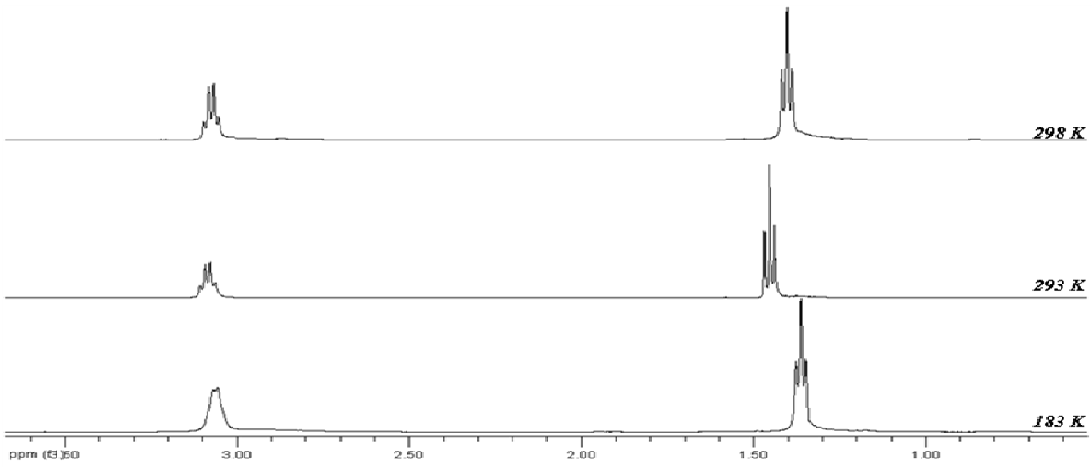

Figure 11. ^{1}H VT-NMR stacked spectra of **4h** in the 1.00-3.50 ppm region in CD_2Cl_2.

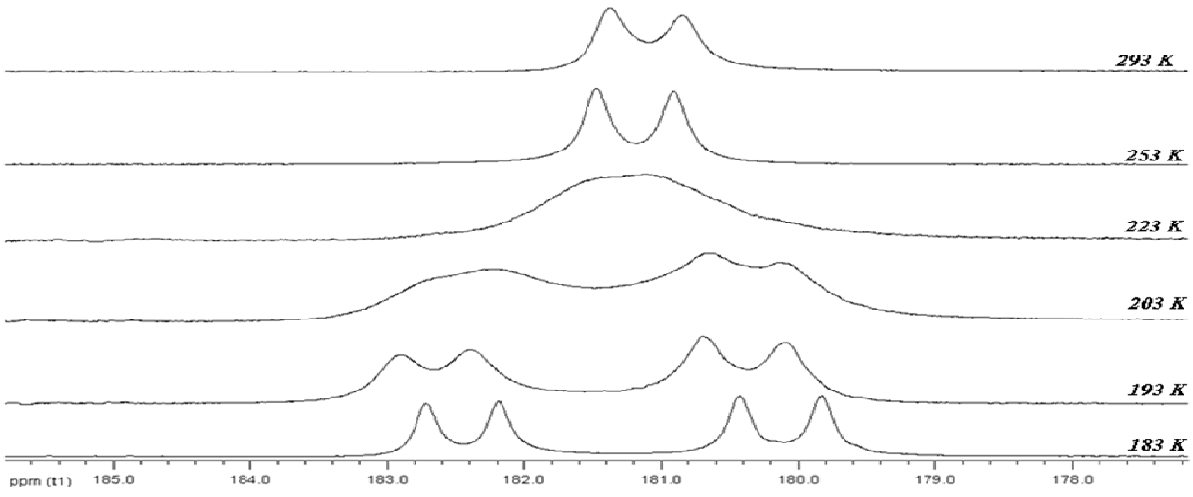

Figure 12. ^{13}C{^{1}H} VT-NMR stacked spectra of **4h** in the carbonyl region in CD_2Cl_2.

S.I-6: SELECTED Rh(III) NMR SPECTRA

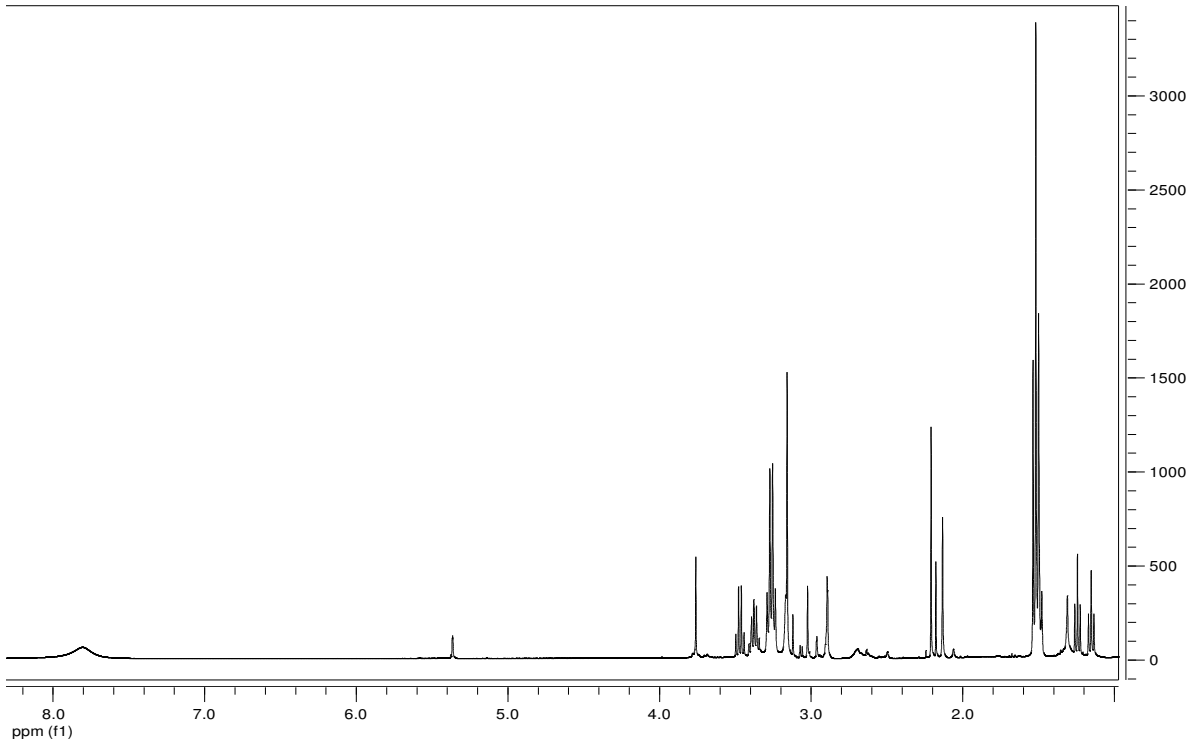

Figure 1. ^{1}H NMR spectrum of crude products resulting from CH_3I oxidative addition to **4a** at 298 K in CD_2Cl_2.

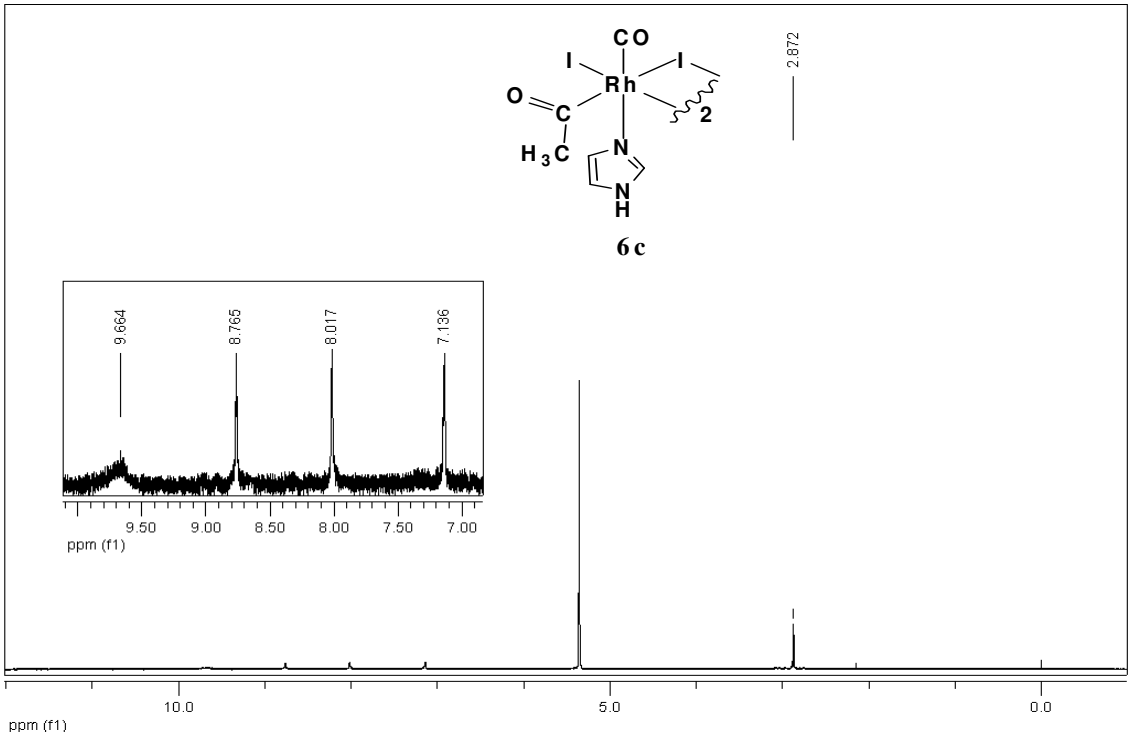

Figure 2. ^{1}H NMR spectrum of **6c** (poorly soluble) in the -1.00-12.00 ppm region at 298 K in CD_2Cl_2.

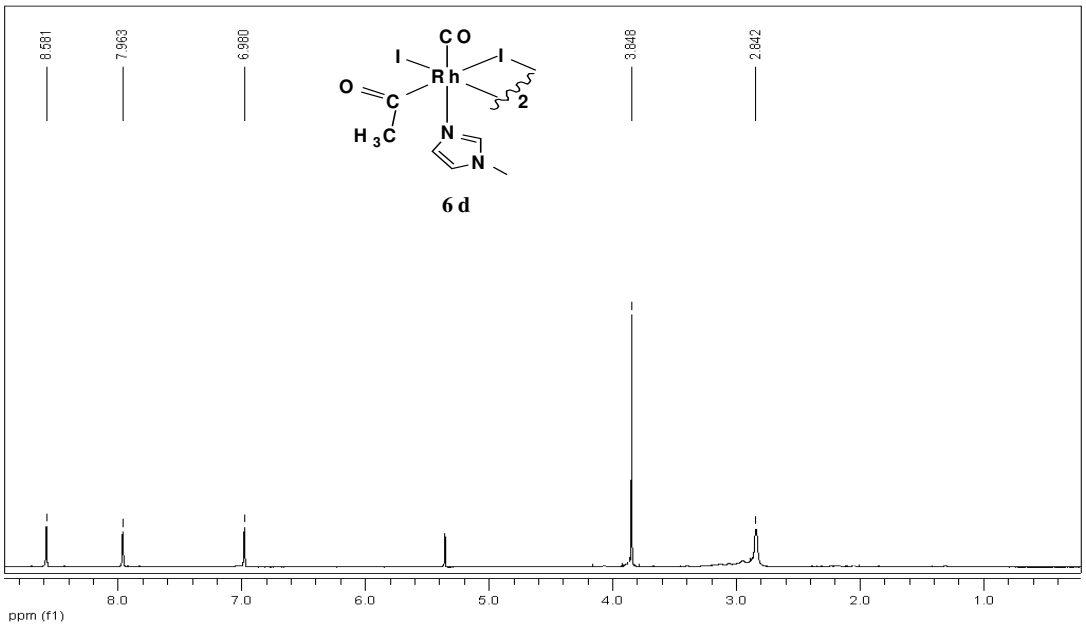

Figure 3. ^{1}H NMR spectrum of **6d** in the 1.00-9.00 ppm region at 298 K in CD_2Cl_2.

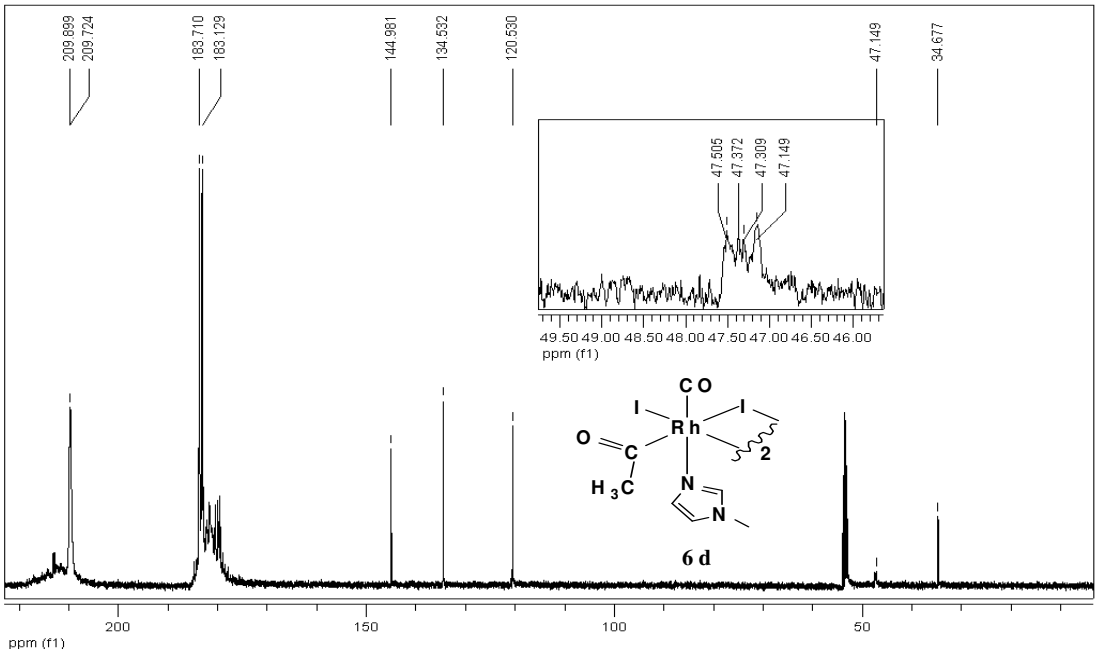

Figure 4. $^{13}C\{^{1}H\}$ NMR spectrum of **6d** at 298 K in CD_2Cl_2.

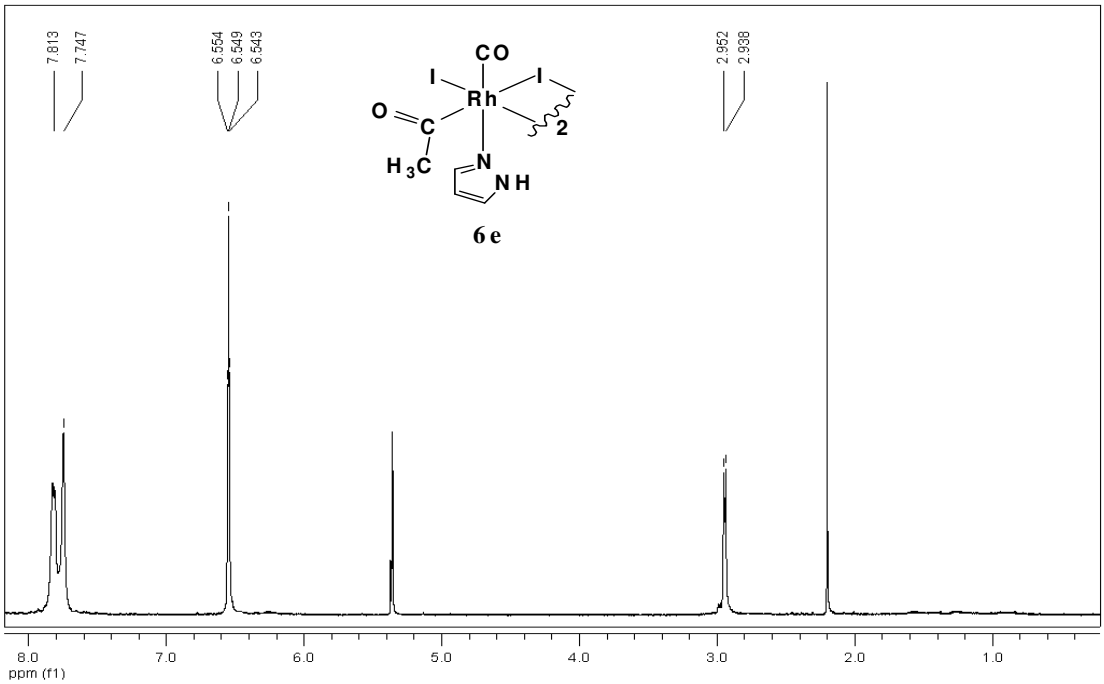

Figure 5. ^{1}H NMR spectrum of **6e** in the 1.00-8.00 ppm region at 298 K in CD_2Cl_2. δ (N-*H*) was omitted for clarity.

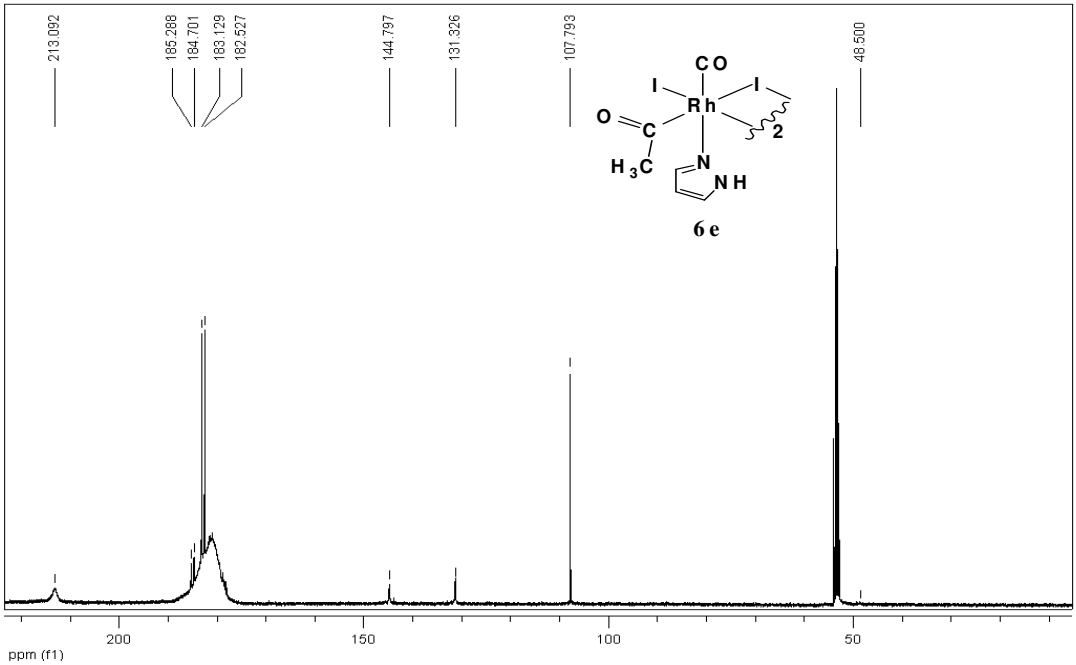

Figure 6. $^{13}C\{^{1}H\}$ NMR spectrum of **6e** at 298 K in CD_2Cl_2. $-CH_3CO$ signal was hardly detected.

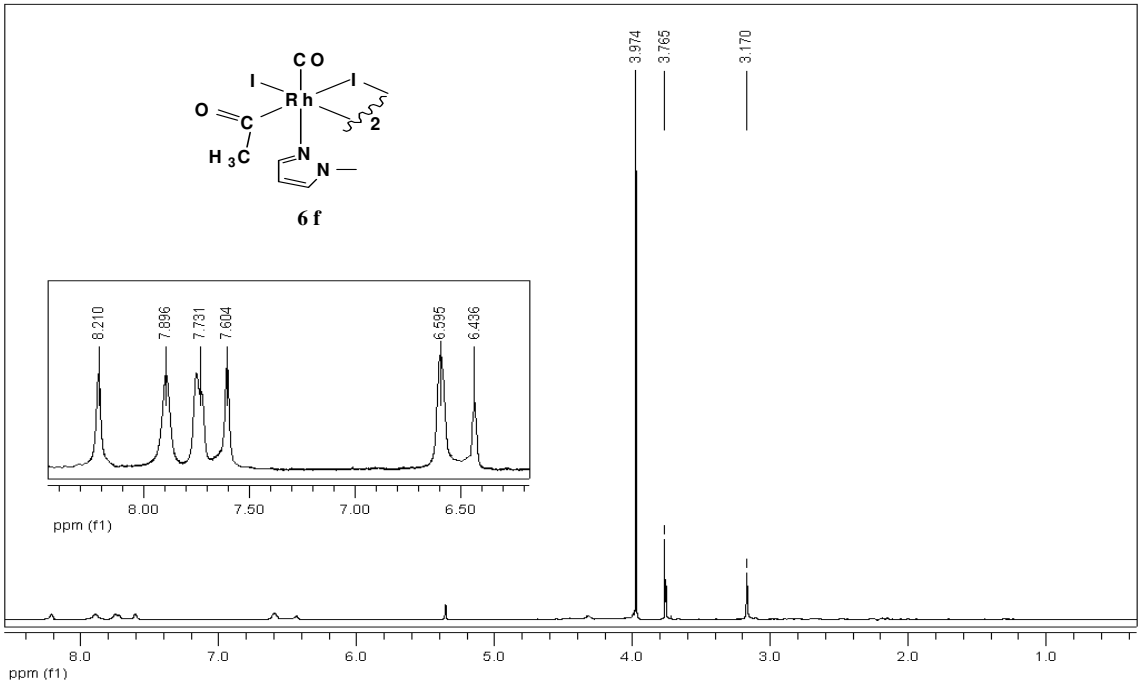

Figure 7. ^{1}H NMR spectrum of **6f** in the 1.00-9.00 ppm region at 298 K in CD_2Cl_2.

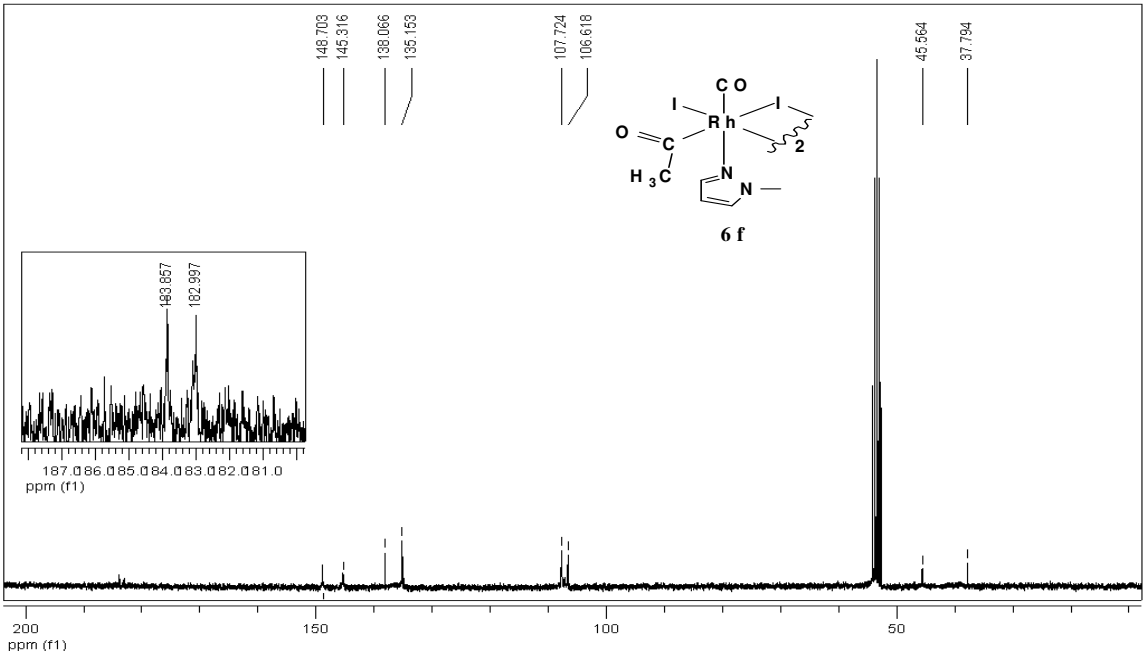

Figure 8. $^{13}C\{^{1}H\}$ NMR spectrum of **6f** at 298 K in CD_2Cl_2. $-CH_3CO$ signals were not detected.

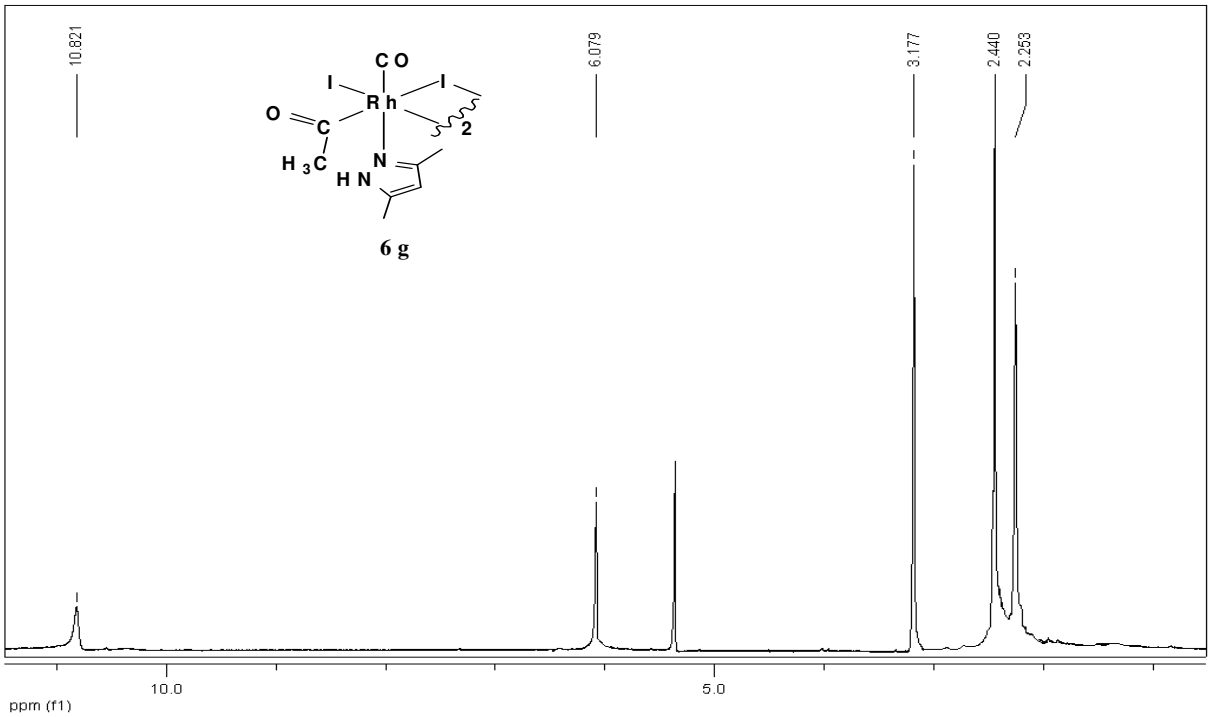

Figure 9. ^{1}H NMR spectrum of **6g** in the 1.00-11.00 ppm region at 298 K in CD_2Cl_2.

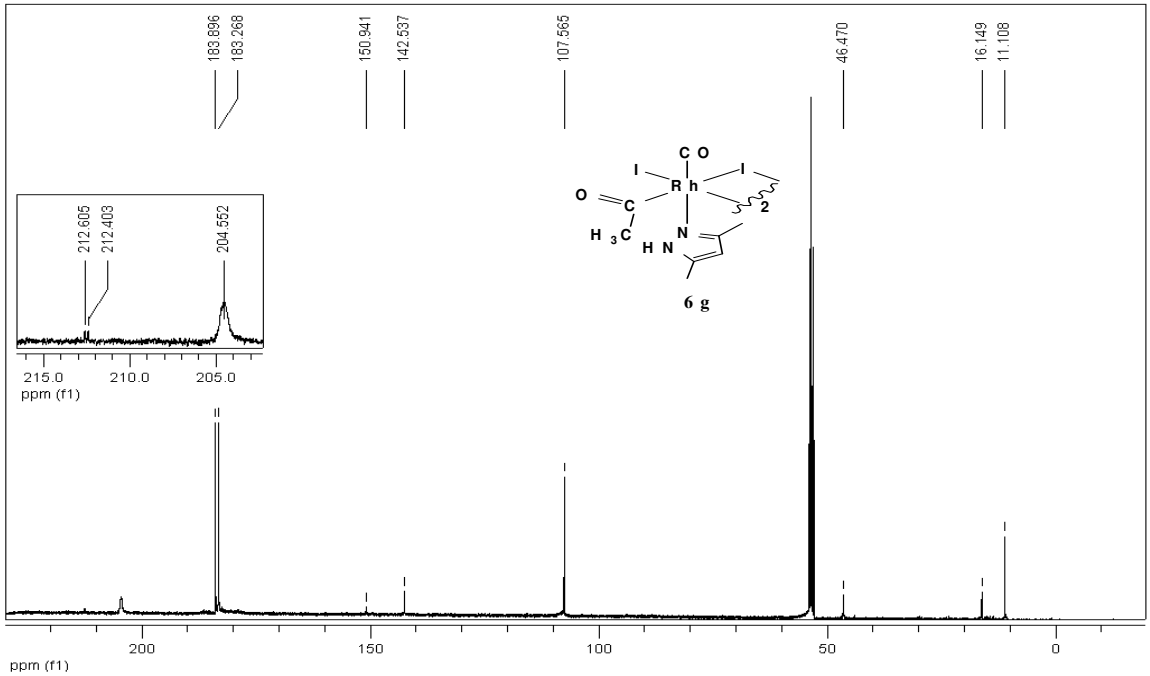

Figure 10. $^{13}C\{^{1}H\}$ NMR spectrum of **6g** at 298 K in CD_2Cl_2.

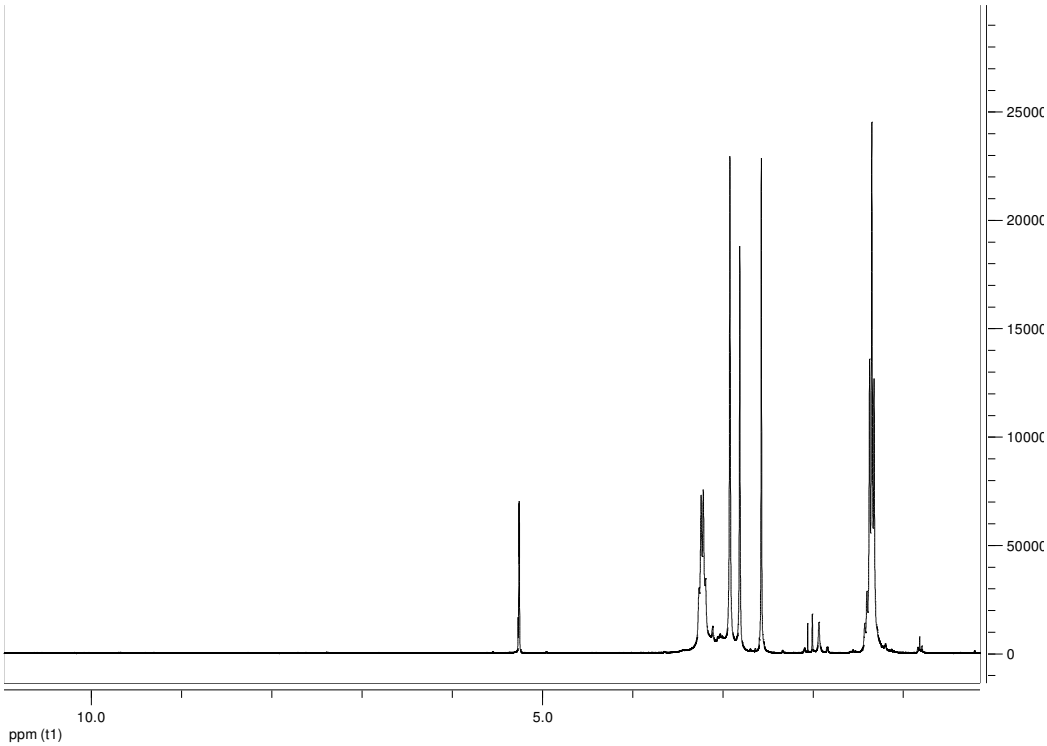

Figure 11. ^{1}H NMR spectrum of **6h** at 298 K in CD_2Cl_2.

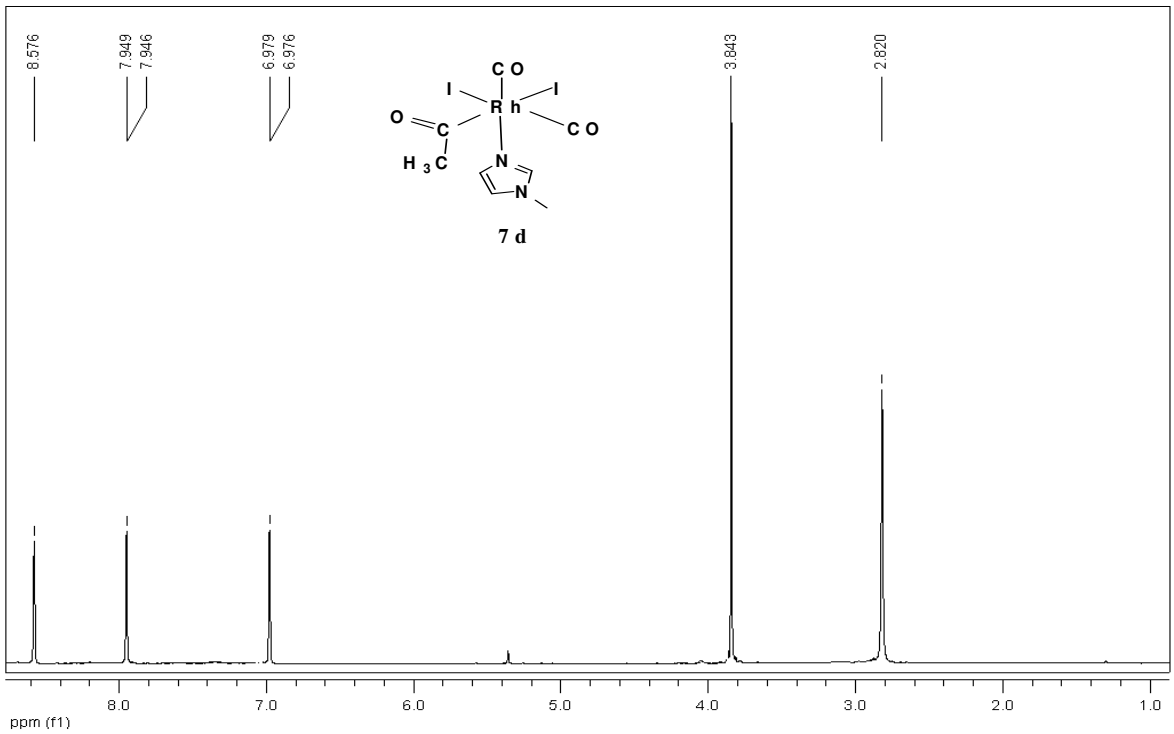

Figure 12. ^{1}H NMR spectrum of **7d** in the 1.00-8.50 ppm region at 298 K in CD_2Cl_2.

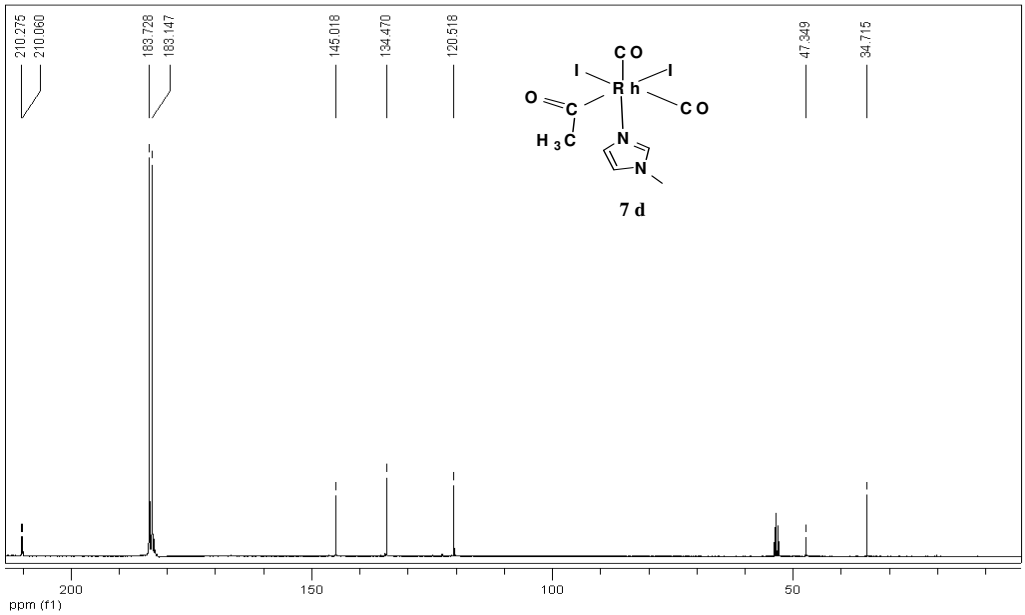

Figure 13. $^{13}C\{^{1}H\}$ NMR spectrum of **7d** at 298 K in CD_2Cl_2.

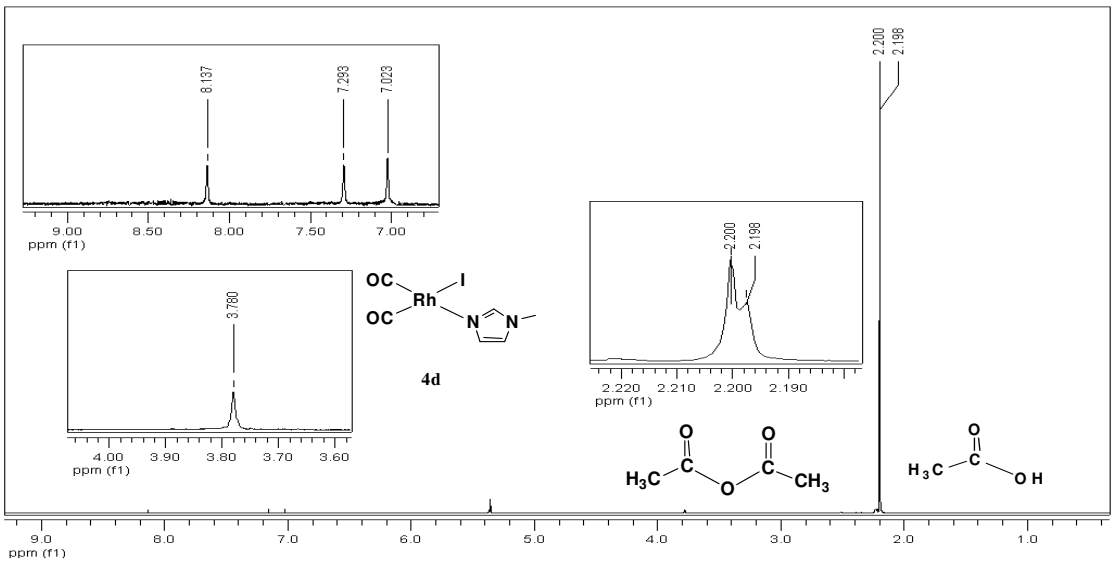

Figure 14. ^{1}H NMR spectrum in the 1.00-9.00 ppm region at 298 K in CD_2Cl_2: Under ^{13}CO atm during 36 hours, occurs reductive elimination of **7d** affording **4d**, acetic anhydride δ (2.200) and acetic acid δ (2.198).

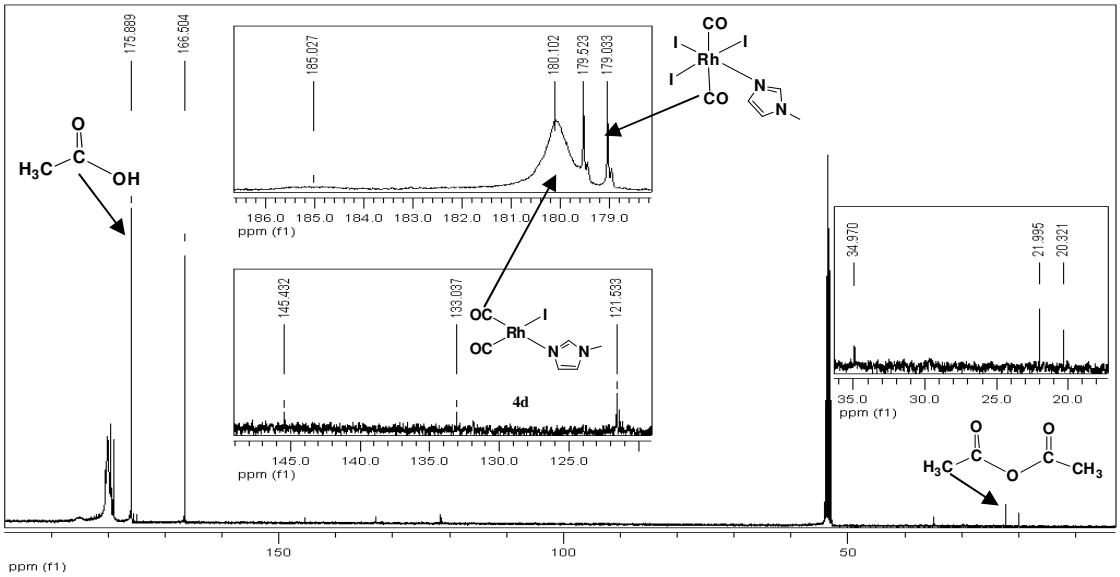

Figure 15. ^{13}C{^{1}H} NMR spectrum in the 10.0-190.0 ppm region at 298 K in CD_2Cl_2: Under ^{13}CO atm during 36 hours, occurs reductive elimination of **7d** affording **4d**.

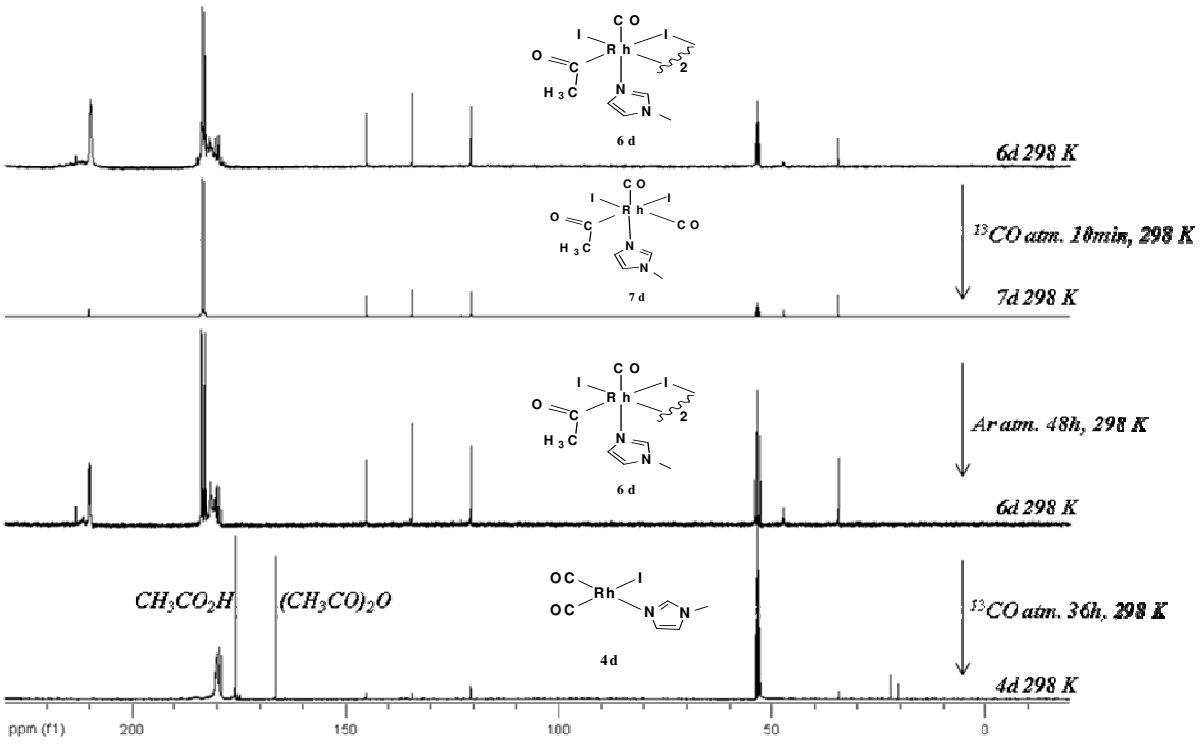

Figure 16. $^{13}C\{^{1}H\}$ NMR stacked spectra of **6d-7d-6d-4d** at 298 K in CD_2Cl_2.

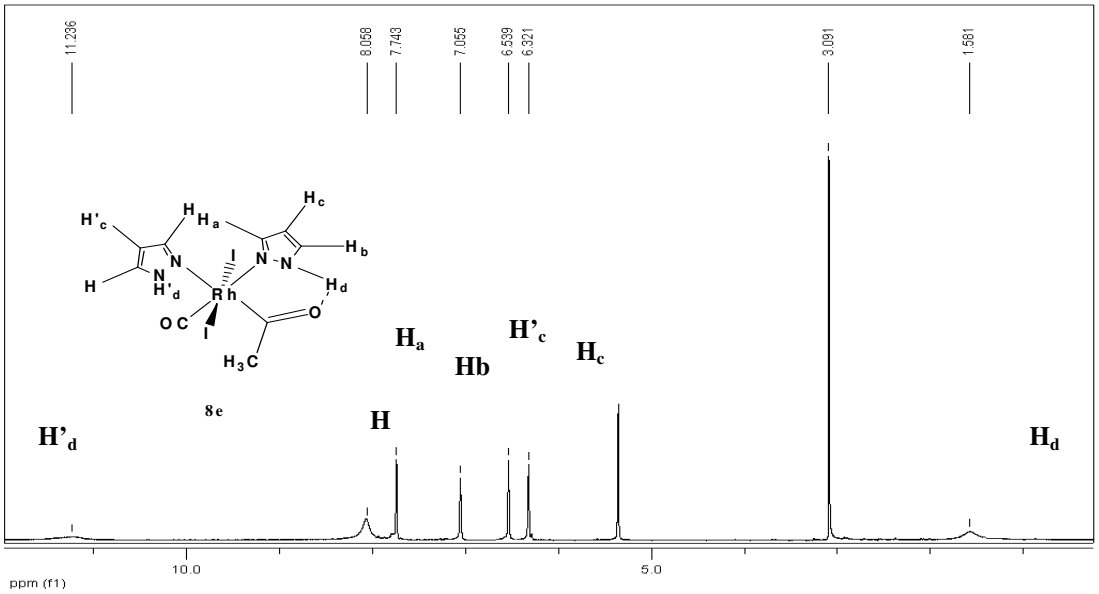

Figure 17. ^{1}H NMR spectrum of **8e** in the 1.00-12.00 ppm region at 298 K in CD_2Cl_2.

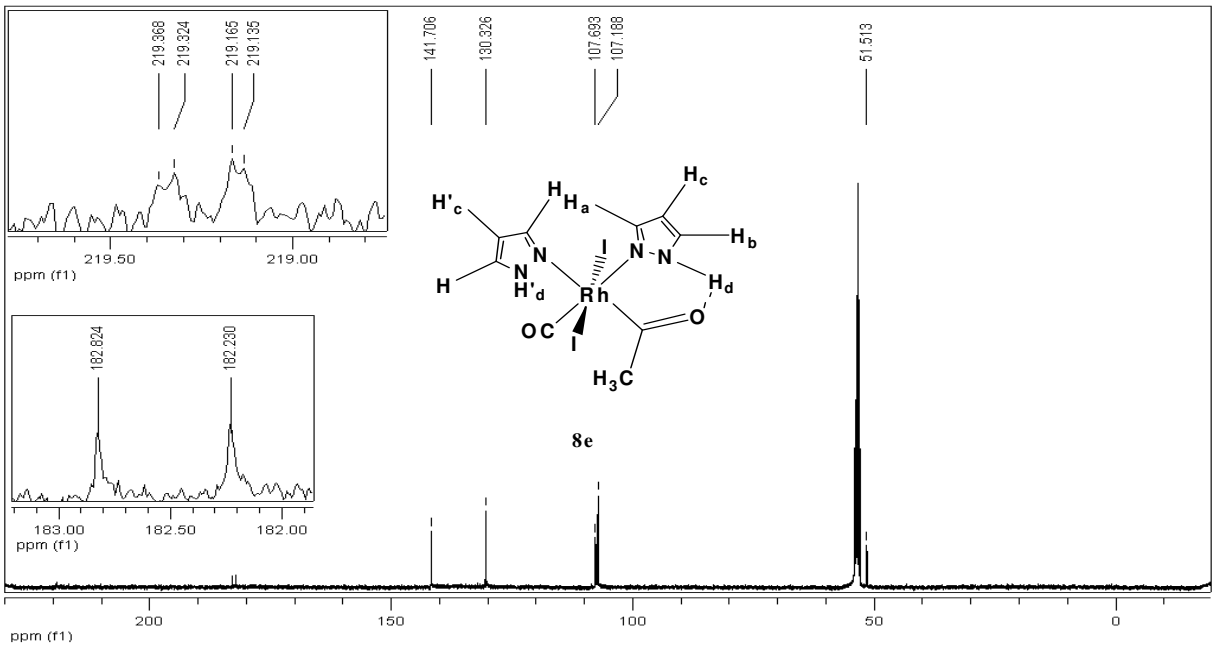

Figure 18. $^{13}C\{^{1}H\}$ NMR spectrum of **8e** at 298 K in CD_2Cl_2.

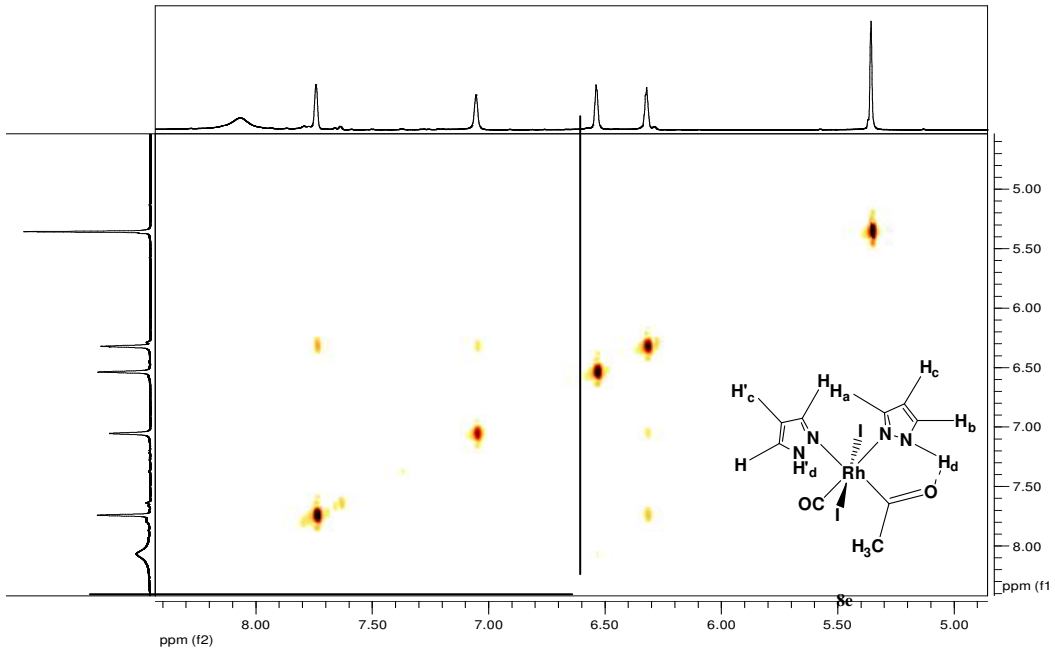

Figure 19. 2D ^{1}H-^{1}H COSY NMR spectrum of **8e** in the 5.00-9.00 ppm region at 298 K in CD_2Cl_2.

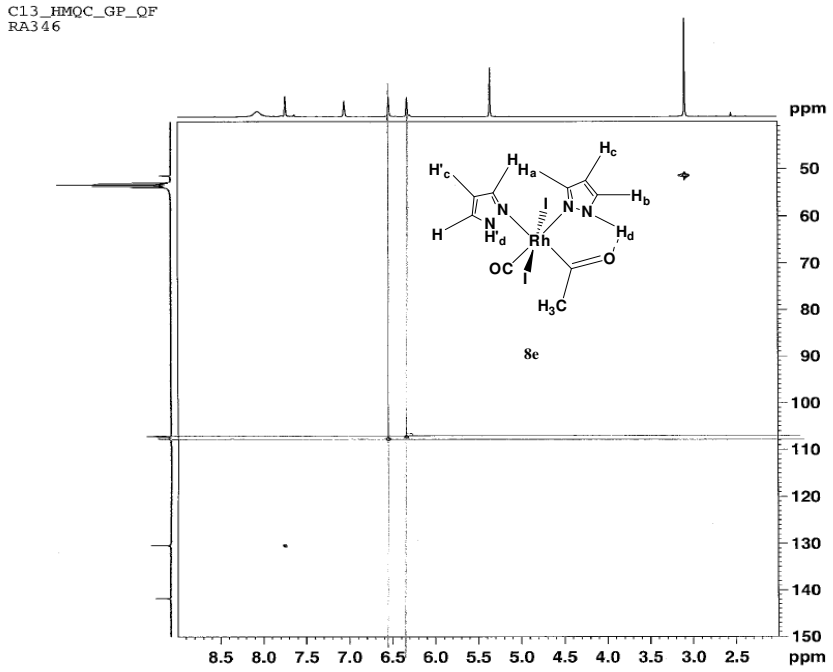

Figure 20. 2D ^{1}H-^{13}C HMQC NMR spectrum of **8e** at 298 K in CD_2Cl_2.